# Synthesis of Complex Polyester-Architectures and their Crystallization.

# Dissertation

zur Erlangung des Doktorgrades der Naturwissenschaften
(Dr. rer. nat.)

der

Naturwissenschaftlichen Fakultät II
Chemie, Physik und Mathematik

der Martin-Luther-Universität
Halle-Wittenberg

vorgelegt von

Herrn **Ajay Kasegaonkar**

geb. am 20. October 1983 in Tuljapur, India

Betreuer: Prof. Dr. Wolfgang H. Binder
Gutachter: Prof. Dr. Wolfgang H. Binder
Gutachter: Prof. Dr. Rainer Jordan
Datum der Verteidigung: 14.9.2017

# Abstract

In this thesis, the synthesis and different crystallization behaviour of star shaped supramolecular PCL-PIB copolymers as well as photocleavable star shaped polymers are targeted.

The synthesis supramolecular block copolymer is based on thymine–triazine interaction between of PCL and PIB respectively. The different molecular weights of star shaped PCL's are synthesized by ring opening polymerization of ε-caprolactone and functionalized them with thymine moiety. The crystallization behaviours of pseudo block copolymers are compared with linear block copolymers of similar molecular weights via DSC technique. Finally the morphologies of the synthesized pseudo block copolymers are studied via SAXS technique.

In second part of the thesis, we report the synthesis and different crystallization behaviour of linear- and star- PCL's containing photo-cleavable linkers (5-hydroxy-2-nitro benzaldehyde), subsequently modulated by photochemical switching. Basis is the attachment of a photo-cleavable moiety close to the star-core of a three-arm star poly(caprolactone), so that the crystallization behaviour can be modulated via a photochemical stimulus. Initially, a three arm photo-cleavable initiator was synthesized for ring opening polymerization of ε-caprolactone i.e. for synthesis of star shaped photo-cleavable polymers. The polymerization of Ɛ-caprolactone via this initiator and stannous octanoate catalyst resulted in the synthesis of different star shaped three arm photo-cleavable poly(ε-caprolactone)s with molecular weights ranging from 14.5 kDa to 38.4 kDa. Their structure is confirmed by 1H NMR and ESI-TOF MS, proving the true star-structure and the successful initiation at all three initiating centers. Via kinetic photo-degradation studies monitored by GPC the successful cleavage of the arms from the central core can be proven. Polymers before and after photo-cleavage displayed significant changes in their crystallization behaviour, therefore it is a photo-triggered crystallization-behavior of PCL-polymers. Thus the confinement exerted by the star-polymer is removed via the photo-irradiation, thus enabling photo-switching of crystallization as shown via DSC techniques.

## Index

**Chapter 1: Introduction……..……1**

1.1 Theories of polymer Crystallization ……..1

1.2 Crystallization of linear and multiarm block copolymers…….……..11

1.2.1 Crystallization in linear block copolymers……...…….....12

1.2.2 Crystallization in star polymers……..……16

1.2.3 Crystallization in multi-armed copolymers……..……19

1.3 Crystallization in supramolecular polymers……21

**Chapter 2: Aim……..…….24**

**Chapter 3: Concept……..…….…26**

3.1 Supramolecular star shaped block copolymers …….…...26

3.2 Photo-cleavable star shaped polymer……. ……..……..27

**Chapter 4: Synthesis of Supramolecular Star shaped block copolymers……..……31**

4.1 Synthesis of thymine functionalized poly(Ɛ-caprolactones)…….32

4.2 Synthesis of triazine functionalized PIB…….……...4

4.3 Synthesis of hydrogen bonded star shaped PCL-PIB block copolymers……..46

4.4 Synthesis of supramolecular star poly(Ɛ-caprolactone) network……54

**Chapter 5: Star shaped photo-cleavable initiators……..……58**

5.1 Photochemical reactions…….…….58

Photocleavable polymers…….…….……61

5.2 Three arm photo-cleavable initiator…….….……..64

5.3 Six arm photo-cleavable initiator…….……68

**Chapter 6: Synthesis of photo-cleavable star-shaped poly(Ɛ-caprolactones)…..……75**

6.1 Ring opening polymerization of Ɛ-caprolactone by using the three arm photo-cleavable initiator…….……...…75

6.2 Photo degradation of star-shaped poly(Ɛ-caprolactone)…….……...79

6.3 DSC study of star-shaped photo-cleavable polymers before and after photo-cleavage.85

**Chapter 7: Experimental……..……87**

**Chapter 8: Summary……..…95**

**References……...101**

**Appendix……I**

**Acknowledgement……...……XI**

**List of publications……..……XII**

**Curriculum vitae……..……XIII**

# Abbreviations

| | |
|---|---|
| AFM | Atomic force microscopy |
| BCP | Blockcopolymer |
| DIPEA | *N,N*-Diisopropylethylamine |
| DMF | Dimethylformamide |
| DCC | N,N'Dicyclohexylcarbodiimide |
| DCM | Dichloromethane |
| DLS | Dynamic light scattering |
| DMAP | 4-Dimet hylaminopyridine |
| DMF | Dimethylformamide |
| DP | Degree of polymerization |
| DMSO | Dimethylsulfoxide |
| DSC | Differential scanning calorimetry |
| ESI MS | Electrospray Ionisation Mass spectrometry |
| FTIR | Fourier Transform Infra-red spectroscopy |
| GPC | Gel permeation chromatography |
| $\Delta H_m$ | Melting enthalpy |
| HPLC | High Pressure Liquid Chromatography |
| $M_n$ | Number average molecular weight |
| $M_w$ | Mass average molecular weight |
| NMR | Nuclear magnetic resonance |
| PDI | Polydispersity index |
| PCL | Poly(ε-caprolactone) |

| | |
|---|---|
| PIB | Polyisobutylene |
| PLLA | Poly-L-lactide |
| ROP | Ring opening polymerization |
| SAXS | small angle x-ray scattering |
| SPBCP | Supramolecular Pseudo-Block copolymer |
| TGA | Thermo gravimetric analysis |
| THF | Tetrahydrofuran |
| TLC | Thin layer chromatography |
| $T_c$ | Crystallization temperature |
| $T_g$ | Glass transition temperature |
| $T_m$ | Melting temperature |

# Chapter 1: Introduction

**Polymer crystallization:**

Crystallization is a case of phase transition which determines the final properties of many technologically relevant systems, e.g. semicrystalline polymers, metals, ceramics, pigments, pharmaceuticals, minerals, etc.[1] The mechanical properties of a polymer are dependent on the presence of crystals within it. Thermoplastic polymers crystallize to some extent; this takes place when the molten polymer is cooled below the melting point of crystalline phase. Polymers crystallize from their molten state at temperatures much lower than their thermodynamic melting temperatures; this supercooling is one of the major differences that distinguish polymers from other substances. There are basically two ways to understand the polymer crystallization. The first one is via the structural and morphological perspective in which resulting polymer crystal structure and morphology give the information about crystal growth processes. The other approach is based on the results observed via *in situ* scattering experiments during crystallization.[1,2] For crystallization, the polymer chains must partially disentangle from each other and forego conformational entropy to fit into a crystal phase, flexible polymer chains fold upon themselves to form a crystal. In melt crystallized structures, thin lamellar polymer crystals together with entangled noncrystalline layers give rise to semicrystalline polymer state.[1-4] Crystallization mechanism of a polymer is dependent on crystallization temperature as well as the initial state of the sample. The structure and properties of semicrystalline polymers can be studied by using different experimental techniques, scientific disciplines and theoretical approaches. All properties of polymers are dependent on molecular morphology as well as the crystallization mechanism. The information about the crystallization mechanism is obtained by crystallization kinetics. For interpretation of kinetics, it is necessary to establish the equilibrium requirements.[5,6]

## 1.1 Theories of Polymers crystallization:

When structural regularity present within the polymer chains and there is presence of molecular symmetry, the polymer crystallization occurs. The polymer crystallization takes place well below the melting temperature and at a specific rate of temperature; if cooling is very slow, then at certain temperature infinitely large crystals exist but it is not the case that all polymers are able to crystallize.[7] Even if a polymer do crystallize at any rate, the degree of crystallinity developed is less than 100%. Due to presence of long chains of molecules, the concept of crystallinity in polymers is slightly different than that in low molecular weight substances. A complete parallel alignment is not possible in case of polymers, instead of

that; small crystalline domains formation takes place and these crystalline domains are the clusters of chain segments.[7,8]

**Thermodynamics of polymer crystallization:**

The Gibbs free energy *G* of any system is related to enthalpy *H* and entropy *S* by the equation,

$$G=H-TS$$

where *T* is the thermodynamic temperature and the system is in equilibrium when *G* is minimum. When compared with completely extended chains, entangled chains in a polymer melt give higher entropy due the number of conformations available to a coil. The higher value of *S* leads to a lower value of *G*.[9,10] Now, if the melt is cooled below the melting temperature $T_m$ of the polymer, crystallization may occur. A high degree of ordering in polymer crystals shows reduction in *S*. If the magnitude of the enthalpy change, $\Delta H_m$ is higher than that of the product of the melting temperature and entropy change ($T_m \Delta S_m$), crystallization will be favored thermodynamically due to the lower value of G. In case of rapid cooling of polymer melt, crystallization is controlled by kinetics. It is also possible to cool the melt of crystallizable polymers so rapidly that crystallization is completely absent and an amorphous polymer results, in this case crystallization can be induced by annealing the amorphous polymer in between $T_g$ & $T_m$. [10]

**Fringed micelle model:**

Semicrystalline polymers are consisting of the crystallites embedded in an amorphous matrix; this led to the Fringed micelle model of polymers (Fig. 1(A)). The fringed micelle model was proposed by Herrmann, Gerngross and Abitz[11] in 1930 to explain the structure of gelatin afterwards it was applied to natural rubber. According to this model, there is presence of fibrillar crystallites which can grow parallel and perpendicular to chain axes. The size of crystalline regions is much smaller than the length of polymer chains; the micelles or crystallites are surrounded by amorphous network.[12,13] The crystalline regions are made up of from parallel aligned polymeric chains, whereas the amorphous regions are consisting of disordered chains. Every polymeric chain passes alternately through crystalline and amorphous region. The crystallization with highly stretched rubber can be explained well with this mode at the same time it is unable to explain spherulites and lamellar single crystals.[11-14]

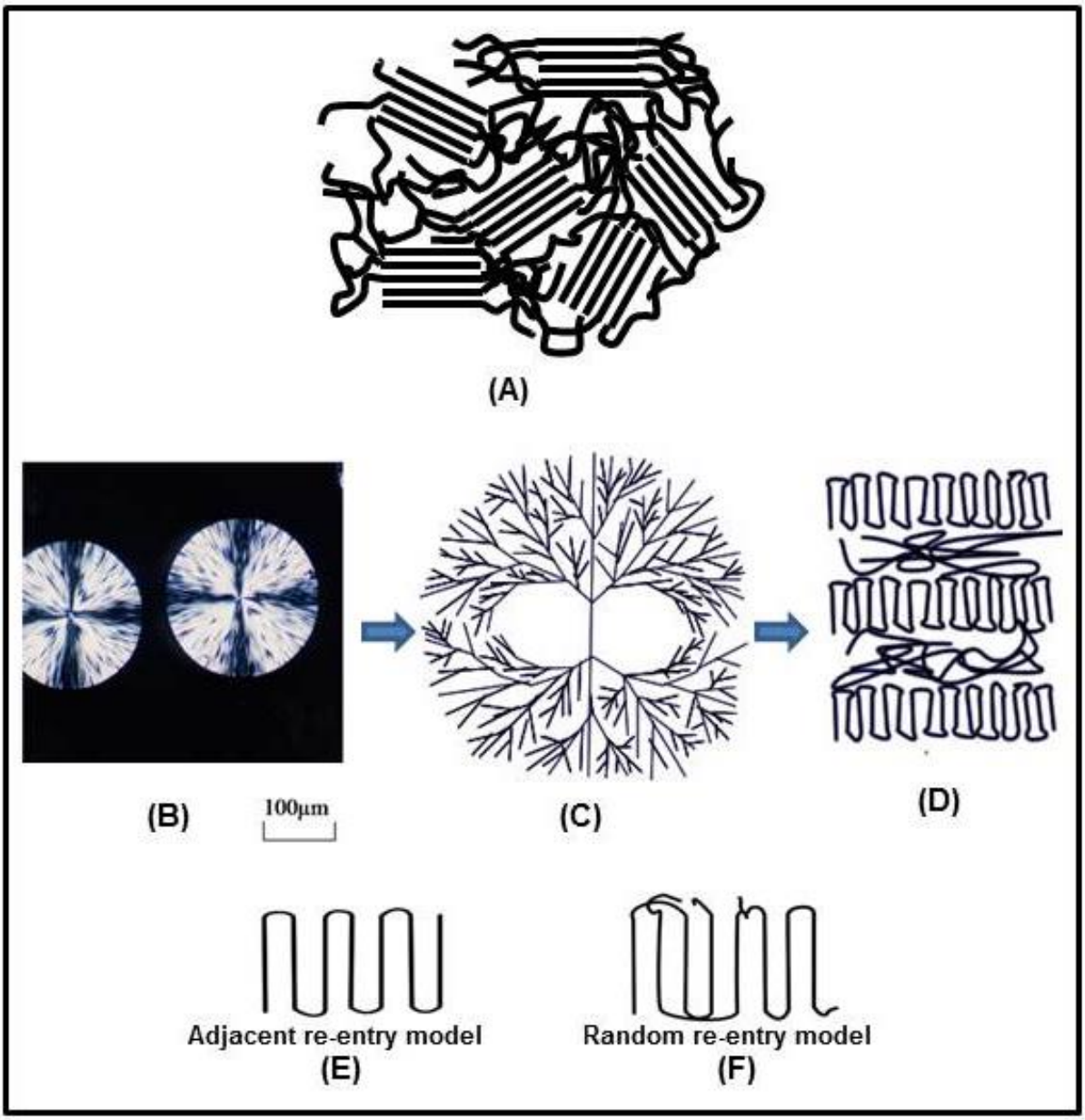


**Fig.1.1: Schematic of crystallization in semicrystalline polymer: (A)Fringed micelle model, (B) POM image of PLLA[15], (C)structure of spherulite, (D) Lamella, (E) Adjacent re-entry model, (F) Random re-entry model.**

## Spherulites:

Semicrystalline polymers exhibit different characteristic features, on different length scales. After the Fringed micelle model, a study of thin layers of polymers crystallized between glass plates was carried out. The observation of those layers in a polarized light microscopy suggested that the crystalline forms of linear polymers were spherulitic (Bunn and Alcock 1945).[16] The optical micrographs of a semicrystalline polymer show a spherical object called spherulites (Fig. 1(B)), which appear somewhere in the view field and then grow in size. This process is called as crystallization by nucleation and growth of spherulites. Spherulites

are composed of ribbon like chain folded lamellar crystals that radiate from their centres. The structure of these spherulites results from a repeated branching and splaying of the crystal lamellae. The radial growth rate of a spherulite is identical with the lateral growth rate of the constituent lamellar crystallites. Lamellar crystals act as building blocks to assemble into spherulites.[17,18] In 1957, Keller developed a model to describe the chain folding lamellar nature of the single crystals. In 1957 Fischer showed that crystallites in melt grown spherulites are having lamellar morphology instead of fibrillar (Fig. 1(D)).[12,17,19,20]

**Lamellar model**

Polycrystalline polymers are more appropriately termed as semicrystalline polymers due to the quite large region between crystalline domains. Polymer chains are much longer compared to the crystalline regions in semicrystalline polymers i.e. crystallites which have size of several hundred angstroms. Polymer chains can fold in a regular fashion called lamellae. To achieve polymer crystallization it is necessary to get rid of the chain entanglements of the melt which cannot be resolved within the short time available. The entangled chains get shifted into the amorphous intercrystalline regions. As the crystal thickness is smaller compared to the chain length, respective chain returns into the same or the adjacent crystal after an excursion into the amorphous region, the crystalline layers are therefore named as 'folded chain crystals'.[21,22]

The chain-folded structure can be discussed in brief by using random re-entry (switchboard) or adjacent re-entry models (Fig. 1(E) & Fig. 1(F)), both of these theories describe the lamellar growth of crystals. In case of cooling from polymer melt, the lamellar crystallites formation with amorphous interface is the basic characteristics but the structure and surface characteristics of these lamellas mainly differ according to the way the chains enter and leave the lamellar region.[23] A model, in which a molecule leaves and reenters the crystal randomly, is called the **switchboard model or random reentry model**. In case of the **adjacent reentry model**, molecules leave and reenter in adjacent positions. The adjacent reentry model is consisting of either 'sharp, regular and tight folds', or 'loose, irregular and of variable length'. A crystallite with regularly folded, smoothly surfaced interface with adjacent re-entry of chains, but with some loose folding and emergent chain ends or cilia that results in the formation of disordered surface.[10,22 23,24]

## 1.1.1 Various models of crystallization process:

1. **Hoffman-Lauritzen model:**

   There are two principle types of theory have been put forward to understand the growth of lamellae i.e. thermodynamic and kinetic theories.

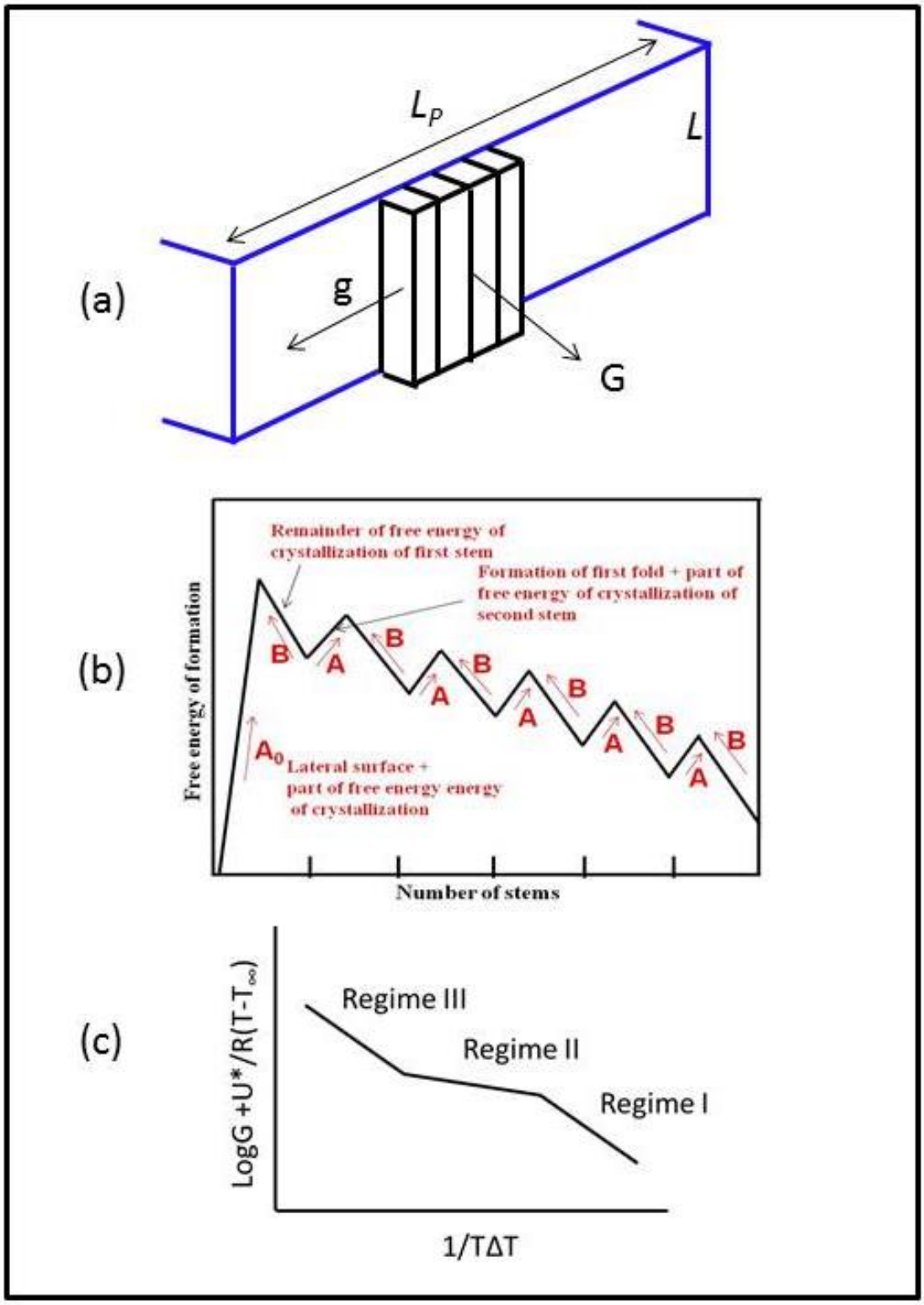


**FIGURE 1.2: (a) A growing crystal lamella as described by the Hoffman and Lauritzen theory[21] The plate-like crystallite (the thickness here is denoted L, the width $L_p$ is assumed as constant) extends in one lateral direction only with a growth rate G. The attachment of further stems subsequent to the nucleation step (with rate g) is treated as a rapid process (g>>G). (b) Free energy evolution of formation of a chain folded nucleus.[25] (c) Regimes where the stem gets attached to the growing lamellae.**

In case of thermal equilibrium, the Gibbs free energy of the conformation and packing of molecules within the crystal should be minimum. The thermodynamic theories, for very long molecules, shows that the fold period observed at a particular temperature $T_c$ of crystallization corresponds to a true minimum in the Gibbs free energy density of the crystal at $T_c$, provided that all contributions to the free energy including thermal vibrations are properly accounted for.[12] These theories are rejected on the basis that any minimum in the free energy at a particular fold length is likely to be broad and shallow compared to the free energy of crystallization, so that equilibrium would not be reached within the usual crystallization times. More recent theories are kinetic theories suggesting that the observed fold length is close to that for which rate of crystallization is highest. The first version of kinetic theory was presented by Hoffman and Lauritzen known as Hoffman-Lauritzen theory.[12,21] The theory explains the linear growth rate G of spherulites or axialites as a function of the degree of supercooling. Theory pays particular attention to the energetic of the chain folded nuclei formation, the fold period i.e. thickness of the crystals decreasing with undercooling i.e. at higher temperatures while the rate of primary crystallization increases with decreasing temperature especially at low undercooling. The linear growth rate of spherulites was determined by using polarized light microscopy, the photomicrographs showed that the linear increase of the spherulite radii with respect to time while cooling from the temperature above the melting point.[12,21,26]

According to Hoffman-Lauritzen model, the nucleus forms and spreads by addition and removal of the polymer chains. Nucleation which is a result of gain in bulk free energy and loss of energy, required to create new crystal or surface. In this model, polymer molecules are assumed to attach growth front in term of stems, each of length comparable to the lamellar thickness $L$.[12] The first step is assumed to be associated with nucleation. The barrier for this step arises from a combination of gain in bulk free energy in the formation of parallelepiped stems and the cost in free energy to make additional surfaces (Fig. 1.2(b)). Due to the largest energy barrier, this step is called the rate determining step, the magnitude of this step increases with increase in lamella thickness. In the Fig. 1.2(b), A is the rate of deposition of the stem on the growth front while B is the removal of the stem from the growth front. The overall rate of crystal growth is the result of A and B. The theory describes three regimes where the stem gets attached to the growing lamellae in different ways. In regime I, secondary nucleation controls the growth of crystals, while in regime III, it is controlled by multiple nucleation. The regime II is intermediate where the growth of crystal is faster than in the regime I but slower than in regime III (Fig. 1.2(c)). It is also important to note that this theory considers the attachment of the stem on the substrate as one step and

does not consider the entropic effect of nucleation which has been included in modified versions of this theory later. [12,21,25]

The Hoffman-Lauritzen growth rate of polymer crystals is given by,

$$G= G_o\exp[-U^*/R(T-T_\infty)]\exp[-A/T(\Delta T)f]$$

Where, $G_o$ is pre-exponential factor, U* is universal constant characteristic of the activation energy of chain motion in the melt, T is crystallization temperature,R is the gas constant, $T_\infty$ is the theoretical temperature at which all motion associated with viscous flow, A is nucleation parameter, $\Delta T=T^\circ_m-T$ where $T^\circ_m$ is the equilibrium melting temperature and $f=2T/(T^\circ_m+T)$.[27,28]

Hoffman-Lauritzen theory concludes that the minimum thickness of the thermodynamically stable lamella is $2\sigma/\Delta F$, where σ is the fold surface energy and ΔF is the gain in free energy density. The theory also concludes the Arrhenius relationship of the temperature with the growth rate of lamellae. [12,29,30]

## 2. Sadler-Gilmer model

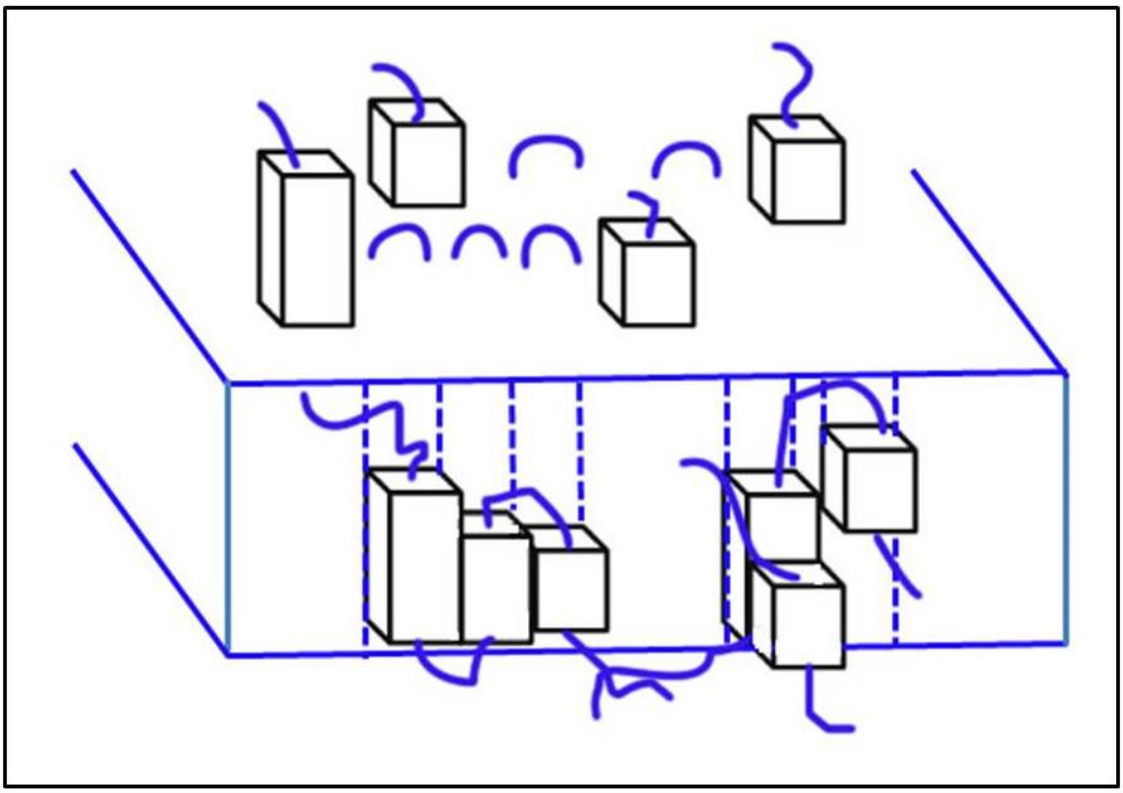

**FIGURE 1.3: Sadler-Gilmer's model of roughening[12]**

Initially Sadler reported that the free energy barrier might be entropic rather than enthalpic in nature. Afterwards Sadler and Gilmer explained the theory being called as Sadler-Gilmer theory. **Sadler-Gilmer theory,** i.e. entropic theory explains the crystallization behavior of small molecules.[12]

At temperatures higher than the roughening temperature, microscopically rough and macroscopically round surfaces are generated; at temperature below roughening temperature growth occurs through invariantly faceted surfaces, the stems shorter than stable stem size can be attached to the growth front due to the thermal roughening. If the absorption energy of the stem on to the surface is less than *KT* roughening takes place. Also, if only a part of the stem rather than whole stem adds to the surface and remainder then collapses behind it then roughening takes place.[12,31,32]

**3. Strobl's model:**

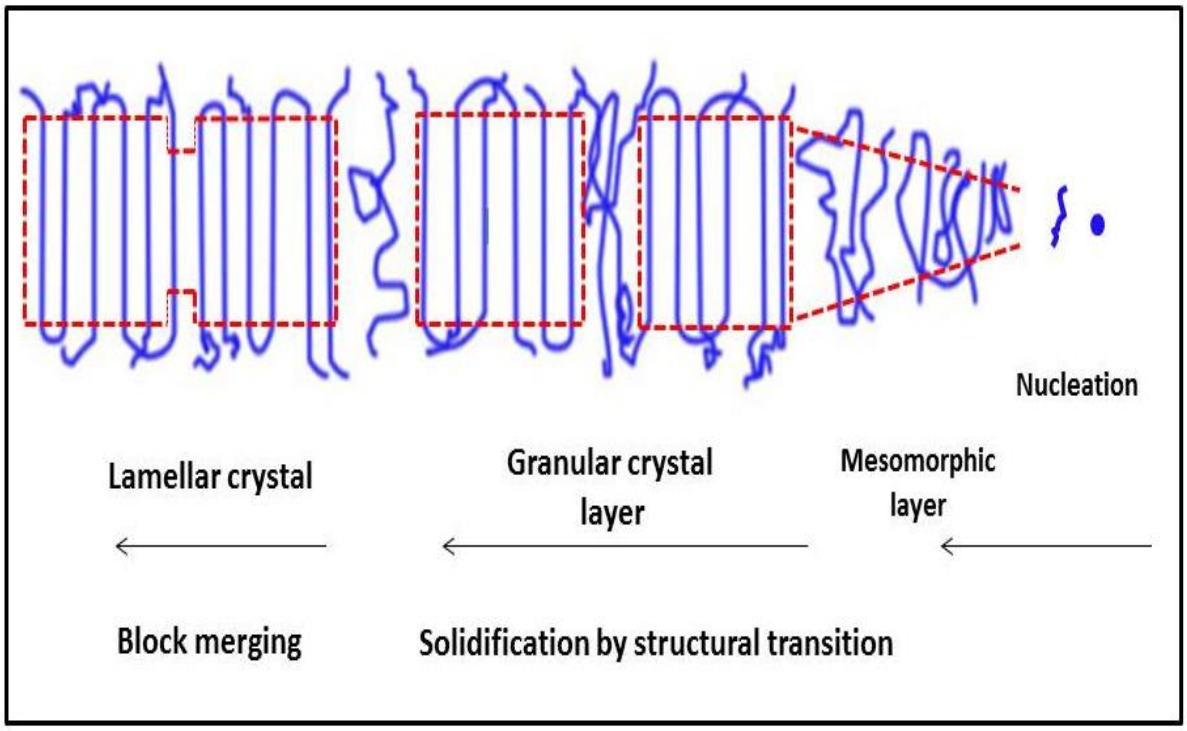


**FIGURE 1.4: Strobl's model[21]**

Strobl and co-workers have studied the crystallization mechanism morphologically, showed a major route for melt crystallization. According to Strobl's model, in all processes of polymer crystallization, a mesomorphic precursor phase is first formed before the crystallization phase. Blocks of this mesomorphic state then attach to the growth front. Whether such mesomorphic phases are stable intermediates before the formation of

crystalline phase and whether critical chain stiffness is required for such mesomorphic phases, is not yet completely understood.[2,6,21]

### 1.1.2 Nucleation mechanism and crystallization kinetics:

Nucleation is the process in which formation of new phases begins. For crystallization process the free energy barrier must be overcome to start growth of nuclei, whereas density fluctuations help for this process and proceed for a stable stage and ordered regions of critical size i.e. primary nuclei, the process is called primary nucleation. The process of formation of embryonic crystallites which further grows to form crystal, is called nucleation.[33] The primary nuclei are those which initiate crystal growth in a polymer melt containing no crystals. The further propagation i.e. growth of a polymer crystal on a smooth crystal surface called secondary nucleation whereas tertiary nucleation is the attachment of molecular segments to growing crystals. It is the process in which crystal thickening together with formation of subsidiary crystal lamellae takes place.[34,35] Nucleation also classified on the basis of the mechanism and origin of nuclei formation. Homogeneous nucleation is the process in which nuclei formation takes place in a chemically homogeneous space containing no foreign surfaces, whereas heterogeneous nucleation takes place in the presence of foreign surfaces e.g. nucleating agents or other solid surfaces.[33,34] Thermal and athermal nucleation are time dependent processes, thermal nucleation occurs throughout the crystallization and in athermal nucleation all crystals get started to grow at the same time and the resultant spherulites are of similar sizes. Homogeneous nucleation is thermal whereas heterogeneous nucleation can be thermal or athermal but mostly thermal. Another type of nucleation is self-nucleation, in this process an originally crystalline polymer sample is melted and due to some reasons nuclei of melted crystals are preserved in the melt beyond melting temperature, when these samples are cooled, the preserve nuclei initiate the crystallization process. [33,34,36]

Avrami parameters are useful to explain the nature of the crystallization process. Crystallization rate constant *k* is dependent on crystallization temperature and takes both nucleation and crystal growth rates into account.

In case of homopolymers melt where crystal growth advances over a macroscopic scale, both nucleation and crystallization takes place simultaneously during the crystallization. The Avrami equation describes the development of crystallinity at a given temperature,

$$x_c(t)=1-\exp(-kt^n)$$

Where $x_c(t)$ is the normalized degree of crystallinity at time t and n is the Avrami exponent relating to nucleation mechanism as well as growth geometry.

Half times of crystallization $t_{1/2}$ can be given by the equation,

$$t_{1/2} = (0.693/k)^{1/n}$$

The avrami exponent n indicates the crystal growth mechanism, the function of time dependence of nucleation and the number of dimensions in which growth takes place, but it is not a function of the amount of nucleation.[36] Crystal growth can be rod-, disc- or sphere like in one, two and three dimensions respectively. Exponents 3 or 4 indicate instantaneous or sporadic nucleation of 3D spherulites, respectively. Exponent of 2 indicates a disc like growth, whereas exponent of 1 indicate instantaneous nucleation of rod shaped crystals. Avrami equation explains the crystal growth and the type of nucleation during polymer crystallization but it is applicable where the volume does not change, however this is not the case in polymer crystallization and assumes constant type of crystal growth or nucleation which is not possible in each case.[36-38]

**Table 1.1: Avrami exponents (n) for various types of crystal growth geometries.[36]**

| Avrami exponent (n) | Type of crystal growth and nucleation expected |
|---|---|
| 3+1 | Spherulitic growth from sporadic nuclei |
| 3+0 | Spherulitic growth from instantaneous nuclei |
| 2+1 | Disk-like growth from sporadic nuclei |
| 2+0 | Disk-like growth from instantaneous nuclei |
| 1+1 | Rod-like growth from sporadic nuclei |
| 1+0 | Rod-like growth from instantaneous nuclei |

In microphase separated melt of block copolymers where the crystal growth is strongly restricted by the nano-scaled continuity, once a nucleus formed in the microdomain, growth of the nucleus is limited to a very short range which completes before a new nucleus formation takes place in the microdomain. It implies that crystallization is isolated within

individual microdomains and the crystallization rate is proportional to the material not yet crystallized i.e the crystal growth must be instantaneous within spherical or cylindrical domains and homogeneous nucleation is the rate determining step. In this case, the rate of crystallization will be proportional to the number of microdomains that have not yet nucleated, yielding an Avrami exponent n=1 and the crystallization kinetics given by,

$$x_c(t)=1-\exp(-k_N t)$$

where $k_N$ is the nucleation rate constant, and $x_c(t)$ follow a simple exponential function instead of a sigmoidal curve.[37,39]

Earlier studies of Nojima et. al[40] on the crystallization behavior of microphase separated PCL-PB diblock copolymer by SAXS, showed that the crystallization kinetics of semicrystalline block copolymer with a rubbery amorphous phase does not differ much from that of homopolymers. Loo et.al.[41] on the basis of perturbations and crystallization kinetics, categorized the crystallization in the diblocks into breakout, templated and confined. When morphological perturbations on a large scale disrupted the melt structure producing conventional sigmoidal crystallization kinetics, called as breakout crystallization. Melt structure was retained on crystallization in case of the confined crystallization, the crystallization was initiated by homogeneous crystallization and crystallization kinetics was nonsigmoidal with n=1. The crystallization kinetics was sigmoidal with n>1 in case of the templated crystallization and overall morphology was retained after crystallization. In this case of the templated crystallization there were ‘rouge’ crystals connecting different cylinders which allow a large volume of material to be crystallized from a single nucleus and rate of crystallization was much faster than that of the confined crystallization.[37,40-42]

## 1.2 Crystallization of linear and multiarm block copolymers:

When two or more different polymer chains get connected with each other by chemical interaction to form a single molecule then resultant polymer is called block copolymer. Semicrystalline block copolymers show considerable morphological richness, arises due to microphase separation between unlike blocks in the melt, which favours the formation of nanometres length scale domains, and also due to the crystallization of one block, which favours the formation of alternating amorphous and crystalline layers. When block interaction strength ($\chi N$) is larger and the melt is microphase separated, in that case depending on the block segregation strength, different morphologies including breakout, templated and confined crystallization may be observed. From the viewpoint of polymer nanotechnology Crystallization of long chains confined in isolated nanodomains is an interesting research subject.[41,43]

There are various types of block copolymers dependent on their number of the number of constituent polymer chains as well their arrangement or architecture, for example, linear diblock (AB), cyclic diblock (AB), triblock (ABA), and star diblocks (AB)n or linear ABC, ACB, and BAC triblocks or three-armed stars where A, B, C are distinct monomers. [44]

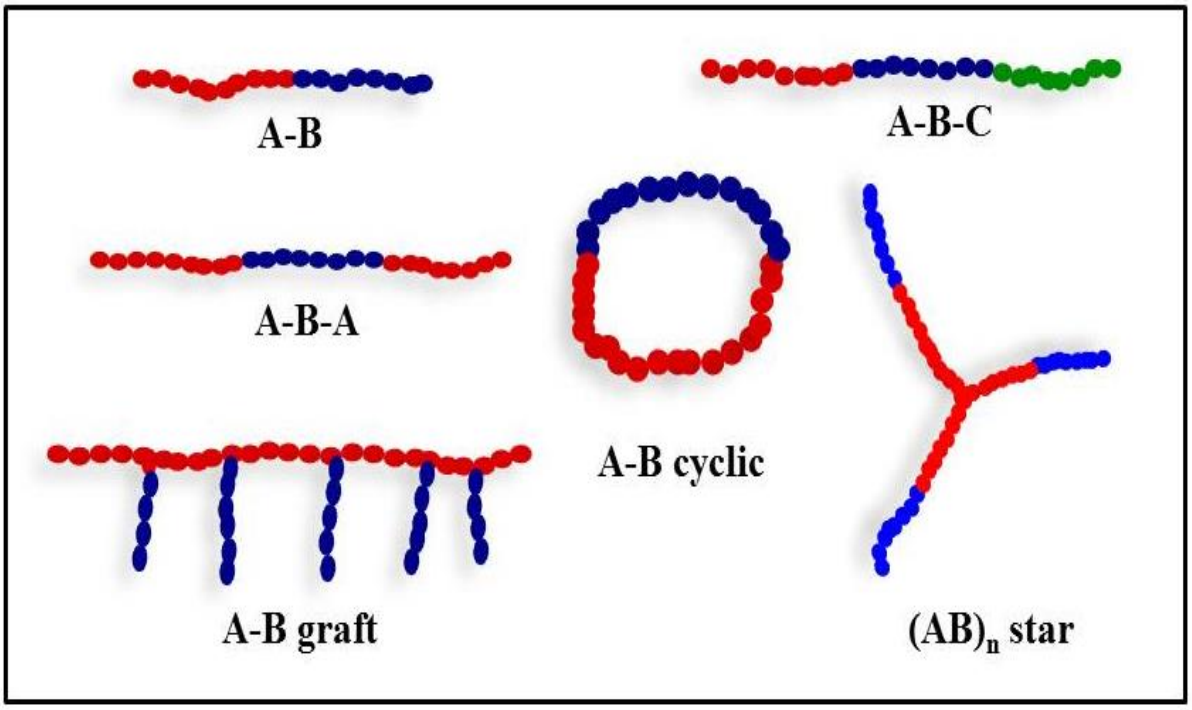


**FIGURE 1.5: Block copolymers and their architectures**

## 1.2.1 Crystallization in linear block copolymers

The structural and mechanical properties of a crystalline homopolymer can be modified by attaching a noncrystalline block to it.[45,46] Microphase separation and crystallization are the key steps in the structural development of semicrystalline block copolymers.[39] In case of homopolymers crystallization takes place via extended conformation or kinetically controlled chain folding. In case of block copolymers, equilibrium chain folding occurs and non-crystallizable block controls the equilibrium number of folds. Structural changes in block copolymers containing crystallizable component, in particular chain folding, resulting from crystallization compete with those occurring due to microphase separation i.e. the final morphology after crystallization depends on whether the sample is cooled from a microphase separated melt or crystallizes from a homogeneous melt or solution. There are three key transition temperatures, which decides the final morphology of the semicrystalline block copolymers: the order disorder transition temperature ($T_{ODT}$), the crystallization temperature of the crystallizable block ($T_c$) and the glass transition temperature of the amorphous block ($T_g$).[34,39] Block copolymers consisting of two or more different homopolymer subunits, in general the different chemical blocks have repulsive interaction.

The effective repulsion and the bonding constraint between the blocks forms the various ordered structures i.e. microphase separation depends on block ratio and the temperature. When homogeneous molten blocks of a diblock copolymer transform into heterogeneous microphases, it is called as order disorder transition.[10,34,39]

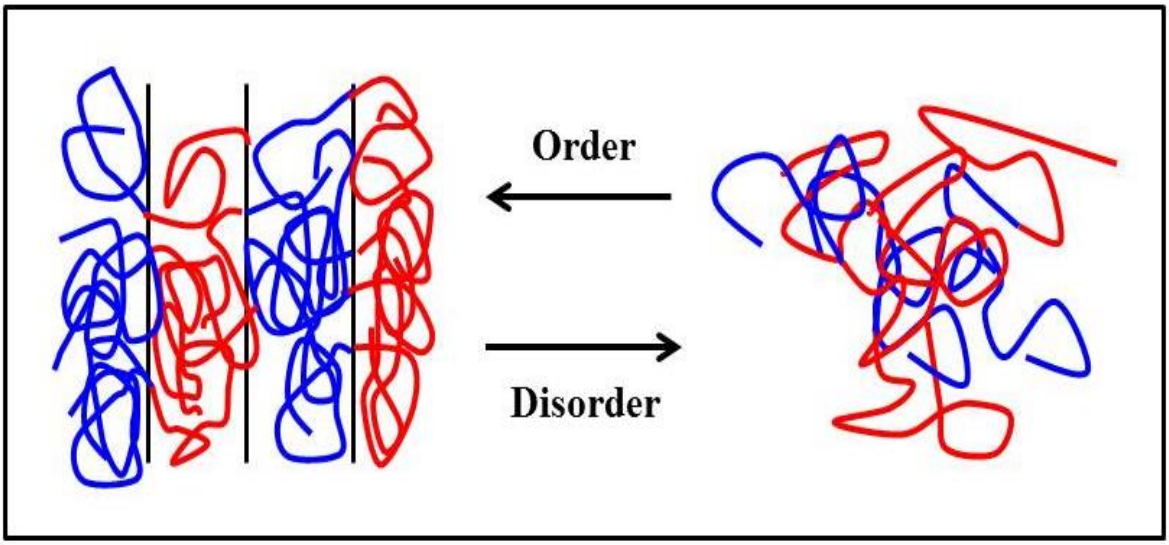


**FIGURE 1.6: Order disorder transition in block copolymers[10].**

There are five different scenarios depending on the $T_c$, $T_g$ & $T_{ODT}$ of semicrystalline block copolymers are discussed below.

In case of homogeneous melt ($T_{ODT}<T_c>T_g$) microphase separation is driven by crystallization if $T_g$ of the amorphous block is lower than $T_c$ of crystallizable block, results in lamellar morphology and spherulites depending on the composition. For a weakly segregated system with soft confinement ($T_{ODT}>T_c>T_g$), crystallization often occurs with little morphological constraint, enabling a breakout from the ordered melt structure and crystallization overwrites previous melt structure and results in lamellar structure and spherulites depending on the composition, whereas in case of weakly segregated system with hard confinement, ($T_{ODT}>T_c<T_g$), the crystallization of crystallizable block overwhelm the microphase segregation because of the weak segregation strength. When a system is strongly segregated with soft confinement ($T_{ODT}>T_c>T_g$), the crystallization can confined within spherical, cylindrical or lamellar microdomains whereas a strictly confined crystallization get observed in a strongly segregated with hard confinement ($T_{ODT}>T_c<T_g$).[37,39]

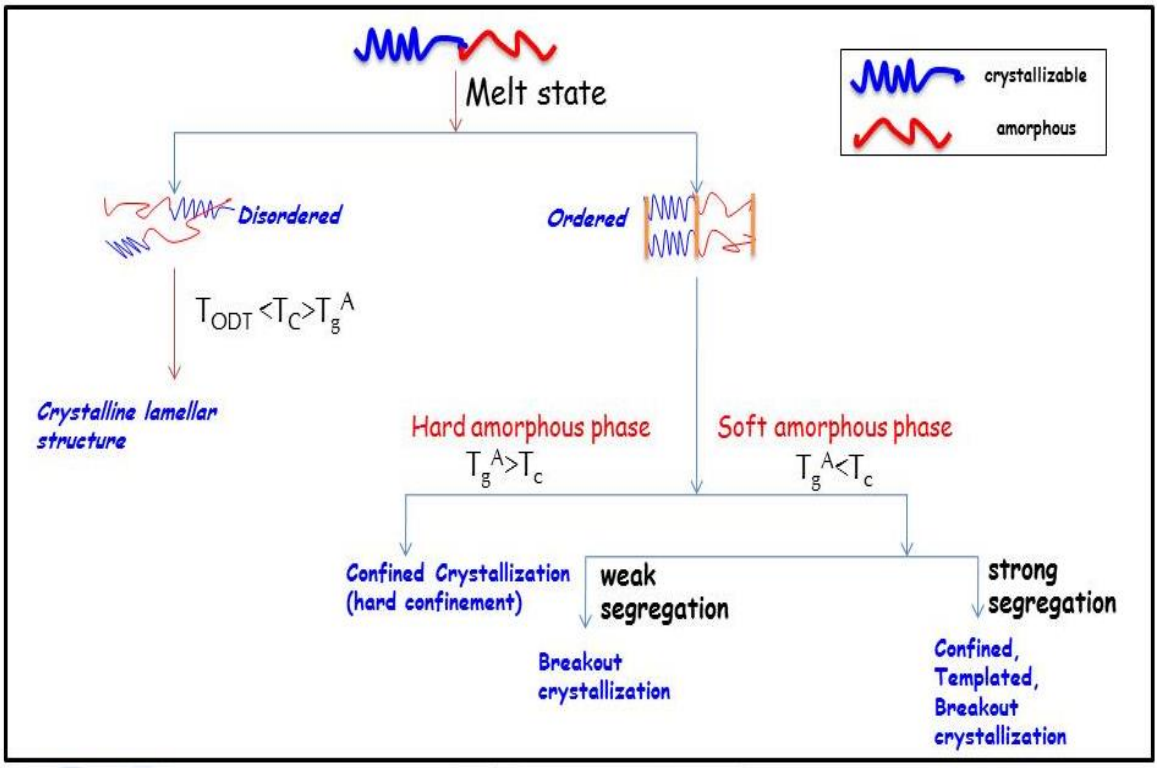


**Fig. 1.7: $T_c$, $T_g$ & $T_{ODT}$ dependent crystallization scenarios of semicrystalline block copolymers.**

Small angle X-ray scattering SAXS is an important tool for the investigation of the morphology of semicrystalline block copolymers at the level of microphase separated structure while wide angle X-ray scattering WAXS is used to probe the structure at the length scale of the crystal unit cell. In SAXS patterns, the abscissa is wave vector $q=4\pi\sin\theta/\lambda$ where $2\theta$ is the scattering angle and $\lambda$ is the wavelength. Furthermore, in SAXS, scattering density correlation function enables to determine the thickness of the crystalline region. SAXS has been employed to study the crystallization of poly(ε-caprolactone) in poly(ε-caprolactone)-poly(butadiene) diblock copolymers; the melting temperature of PCL in the diblock copolymer was much lower in comparison with that of homopolymer. A sample with an order-disorder temperature less than melting temperature, i.e. $T_{ODT}<T_m$ quenched directly from disordered melt did not show sharp diffraction peaks i.e. crystallization took place directly from homogeneous melt. Another sample with $T_{ODT} \sim T_m$ quenched from homogeneous melt, microphase separation preceded crystallization but the ordered morphology was destroyed by crystallization.[34]

If A & B are two different monomers, then χAB is an interaction parameter which gives the thermodynamic interaction between A & B, this parameter is inversely proportional to temperature. The onset of an ordered mesophase from a homogeneous melt is dependent on the product χN (N is the polymerization index) and *f*, the fraction of monomers A. When

the incompatibility of different chemical blocks (χN) becomes sufficient, the segments segregate into the domains forming periodically ordered microstructures. When the product χN exceeds 10.5, molecular segments in diblock copolymer self-assemble to form microphase structure. The segregated domains can form various morphologies like lamellae, hexagonally packed cylinders, body-centered-cubic (BCC) spheres, and the bicontinuous networked gyroids. The size and morphology of the microdomains can be controlled by variation in molecular weight, molecular architecture, molecular structure, segregation strength and composition.[47-51]

**Orientation of folded chains:**

The properties of semicrystalline homopolymers can be modified by the formation of their block copolymers. Crystallization in homopolymers creates a kinetically controlled chain folding whereas equilibrium chain folding can occur while crystallization in semicrystalline block copolymers, these number of folds are being controlled by the size of the second-non-crystallizable block. The introduction of amorphous block helps to modify the mechanical and thermal properties of semicrystalline block copolymer. Structural changes in block copolymers or final morphology is dependent on whether the sample is cooled from microphase separated melt or crystallized from homogeneous melt or solution.[34]

Molecular weight and cooling rate of polymer melt control the Morphology and the speed of chain diffusion. Lateron, morphology and the speed of chain diffusion decides the orientation of crystalline stems with respect to the interface of the microstructure in block copolymers. In case of homopolymers, folding of chains occurs in a way that stems are always perpendicular to the lamellar interface, whereas in case of block copolymers, a parallel orientation was observed in crystallization from a lamellar melt phase and perpendicular folding was observed in a cylindrical microstructure.[52]

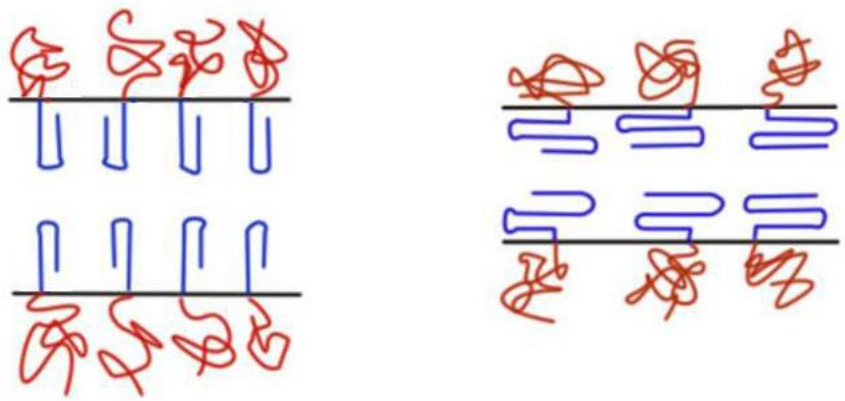

**FIGURE 1.8: Perpendicular and parallel chain folding[52]**

## 1.2.2 Crystallization in star polymers:

The most obvious characteristics of a polymer are the shape of its molecules and the skeletal structure i.e. molecular architecture. A polymer can be linear, star shaped, branched, hyperbranched, cyclic, ladder like, comb shaped, cross-linked, etc. The molecular architecture is important for various properties of polymer e.g. viscosity, thermal stability, crystallinity, etc.[25] Short chain branches reduce the crystallinity while long chain branches affect the rheological properties. Star and hyperbranched polymers have different viscosity than their linear analogue whereas ladder polymers exhibit high strength and thermal stability.[53,54] In case of star shaped polymers, the crystallisable linear chains are generally fixed at a certain point i.e. at the central core. This central core restricts the crystallization of star shaped polymers because of steric constrain and the crystallization in star shaped polymers has been discussed by various authors till now. The crystallization behaviour of star shaped polymers is dependent on their architecture, number of arms as well as on the molecular weight of the polymer.[53-56]

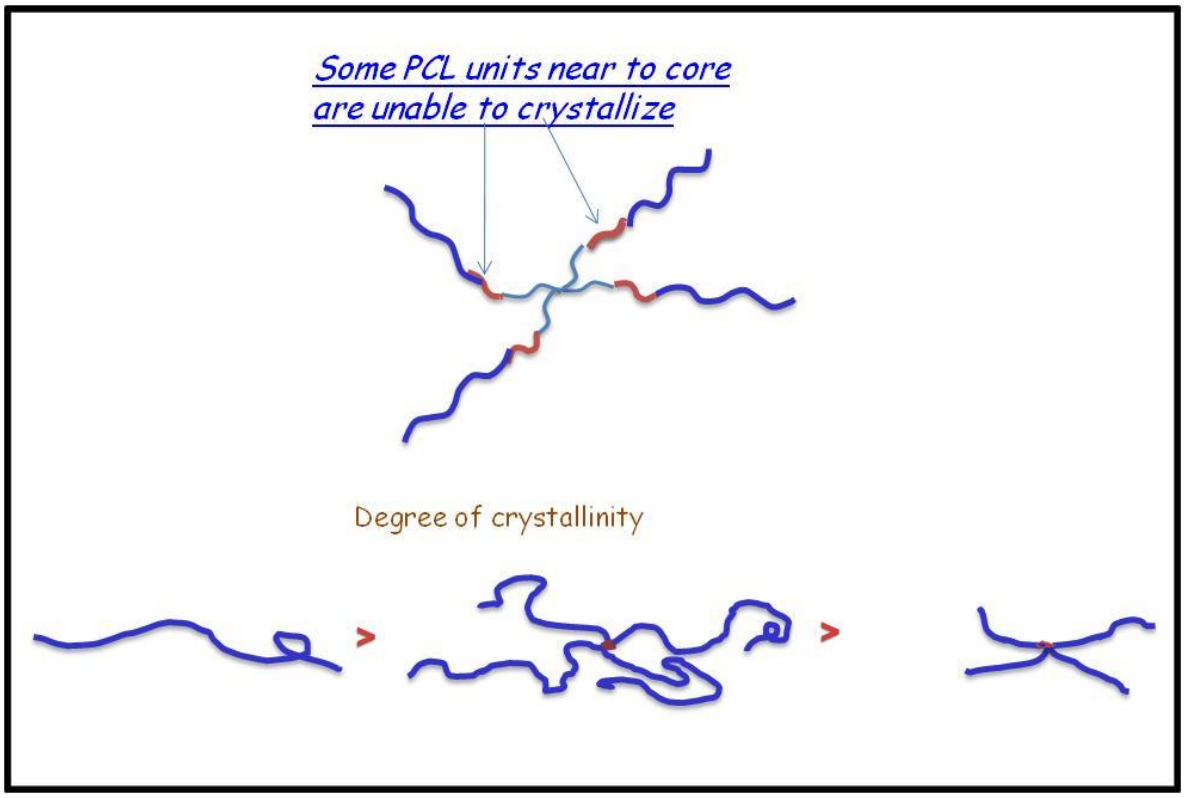


**FIGURE 1.9: Schematic diagram for crystallization in star shaped polymers.**

Risch et.al[57] studied the different crystallization behaviours of linear and star shaped Polyamide-6. The crystallization half-times of star-branched nylon-6 as a function of *super-cooling* were reduced compared to those of linear nylon-6 of comparable molecular weight

whereas the general spherulitic superstructure appeared unaffected by increasing branch-point functionality up to six.[54,57]

In case of star shaped polymers, the diffusion of the branch chain is low and the chain density is high because one chain end of branched polymers is bound.[58] The comparison of star and linear polymers has been studied and it is observed that the star polymer has generated more number of spherulites. On the other hand, the spherulite growth of the star polymer is slower than that of the linear; this is caused by the differences in the chain density and diffusion rate, respectively.[59] The melting point, the crystallization temperature and $X_c$ of the star polymers increases with increasing molecular weight. Also the crystallization rate of star shaped polymers was slower than that of the linear polymers. The comparison of the crystallization behaviour of linear-, 3 arm-, 4 arm- and 6 arm- polymers with equivalent molecular weight showed that the degree of crystallinity decreases with increase in arm numbers. This is due to a large number of free chain ends disrupt the fold pattern of the crystals during crystallization. The effect of arm number on melting temperatures and $X_c$ of star shaped polymer with equivalent molecular weight is found to be negligible. [58,60-63] The star architecture greatly reduces the crystallization rate when arms are short, the star polymers with short arms are difficult to nucleate but when the arms are long enough to interact with each other, the star architecture favours the nucleation.[64]

The X-ray diffraction pattern and crystal unit cell were almost the same for the star as well as the linear poly(ε-caprolactone). The crystal rearrangement tendency was less pronounced in star polymers in comparison with that of linear polymers. The star polymers based on hyperbranched core showed a larger depression in PCL crystallinity in comparison with the star polymers based on dendrimer and Dendron cores.[54]

The crystallization behaviour of various star polyesters with crystallisable PCL arms has been reported.[54,56,61,65,66] In case of hyperbranched polymers- the crystallization behaviour, thermal properties and morphology changes with respect to molecular weights as well as degree of branching. The heterogeneous branching points in HPCL's are expected to hinder the polymer chains from packing regularly for the effective crystallization.[54] In comparison with linear poly(ε-caprolactone) samples, the hyperbranched polymer demonstrated lower melting temperature and melting enthalpy as well. The WAXS analysis also confirms that the degree of crystallization of polyesters decreases with increase in degree of branching.[67]

The study of crystallization kinetics of star-shaped polylactides (PLLAs) by means of isothermal and nonisothermal crystallization was reported.[68] The study shows that, Avrami exponent (n) values of isothermal crystallization were independent of the isothermal crystallization temperature $T_c$ for different series of star-shaped PLLAs. Whereas the, the

values of Avrami exponent n were strongly dependent on the arm numbers of star-shaped structures, the more arms of a star-shaped PLLA were reduced the isothermal crystallization rate. In case of the nonisothermal crystallization kinetics for the star-shaped PLLAs, the increased activation energies of the star shaped polymers, indicates much decreased crystallizabilities of star-shaped PLLAs with more arms. The melting temperature, the crystallization temperature and the degree of crystallinity of these poly(L-lactide) polymers decreased with an increasing number of arms of the polymer. The isothermal crystallization rate constant (*K*) of these poly(L-lactide) polymers decreased with increasing arm numbers of polymeric sample. Linear polymers presented spherulites with good morphology and apparent Maltese cross patterns, but the unclear Maltese cross patterns and imperfect crystallization were observed for the star-shaped four and six arm polymers. [68,69] A detail investigation on the effect of architecture on physical properties of PLLA, was reported by Kim et. al.[70] In dynamic crystallization, the linear PLLA showed longer induction time and longer overall crystallization time, in comparison with the star shaped PLLA. Both linear and star architectures showed the same crystal structure in wide angle X-ray diffractometer analysis.

Table 1.2: Effect of arm numbers of polymers on values of Avrami exponent (*n*)[69,71]

| Sr. No. | Polymer | $M_n$(GPC) | $M_w/M_n$ | *n* |
|---|---|---|---|---|
| 1 | LPCL-1 | 5980 | 1.57 | 2.2 |
| 2 | 2LPCL-1 | 5190 | 1.12 | 2.4 |
| 3 | 4sPCL-1 | 6900 | 1.07 | 3.0 |
| 4 | 6s-PCL-1 | 7160 | 1.05 | 2.7 |
| 5 | LPCL-4 | ----- | ----- | 1.8 |
| 6 | 2LPCL-4 | 20730 | 1.53 | 1.8 |
| 7 | 4sPCL-4 | 18830 | 1.34 | 2.3 |
| 8 | 6sPCL-4 | 17110 | 1.07 | 2.5 |
| 9 | LPLLA | 6780 | 1.11 | 2.74 |
| 10 | 2LPLLA | 9550 | 1.11 | 2.62 |
| 11 | 4sPLLA | 13250 | 1.05 | 2.29 |
| 12 | 6sPLLA | 12700 | 1.10 | 2.31 |
| 13 | 6sPLLA | 14990 | 1.12 | 2.44 |
| 14 | 6sPLLA | 23360 | 1.06 | 2.52 |
| 15 | 6sPLLA | 29060 | 1.04 | 2.59 |

### 1.2.3 Crystallization in multi-armed copolymers:

The nucleation and crystallization as a function of their morphology and chemical architecture can be studied by using linear diblock and star block. Multi-armed copolymers show special crystallization properties different than the linear copolymers, including different crystallization morphologies.[47]

In case of polystyrene (PS) and PCL block copolymers, more compact morphologies were obtained in miktoarm star copolymers (with two arms of PS and two arms of PCL) than linear PS-b-PCL diblock copolymers. As a result of this, the crystallization of the PCL is much higher confined in the miktoarm stars case than in the linear diblock copolymer case [44,47,72-75] The study of crystallization behaviour and kinetics of poly-(ethylene oxide) in polystyrene/poly(ethylene oxide) heteroarm star copolymers has shown that the macromolecular architecture is an important factor that influences the crystallinity and the crystallization kinetics of the crystallizable blocks in amorphous-crystalline block copolymers. The crystallinity reduces with increase arm numbers and leads to smaller spherulites.[76]

The structure and dynamics of structure formation have been studied in model triarm star block copolymers composed of two crystallizable blocks (poly(ethylene oxide) (PEO) and poly(ε-caprolactone) (PCL)) and one amorphous block (polystyrene (PS)). Both crystallizable blocks have similar mobilities and melting temperatures. They crystallize in different unit cells (monoclinic vs orthorhombic) and show a competition. In case of higher block length ratio only the longer blocks get crystallized, in case of similar block lengths both can crystallize.[77]

Cruz and Sanchez theoretically reported the phase stability of the (AB)*n* star-block copolymers and predicted that the (AB)*n* star-block copolymer forms a core–shell structure (self-micellization) as arm number *n* gets large values.[78,79]

The crystalline morphologies of star shaped poly(Ɛ-caprolactone)-b-poly(lactide) was also discussed where the authors observed that, the macromolecular mobility of inner PCL blocks was spatially restricted by the outer PLLA block, the crystallization of outer PLLA block dominates over the crystallization of inner PCL core. The polarized optical micrographs indicates that the size of the spherulites of star shaped PCL-b-PLLA is much smaller than that of the star shaped poly(ε-caprolactone), whereas the growth rate of spherulites increases with increasing PLLA block length. The spherulitic diameter of these block copolymer increases linearly with increasing isothermal crystallization time.[80]

The ordered microphase separated morphologies for simple diblock copolymers are quite different than those of star shaped block copolymers. Sanchez et. al[79,81] were reported the

microphase separation in star shaped polymers. The comparison between microphase separation in $A_nB_n$ star shaped polymers and $(AB)_n$ star shaped polymers is well described.

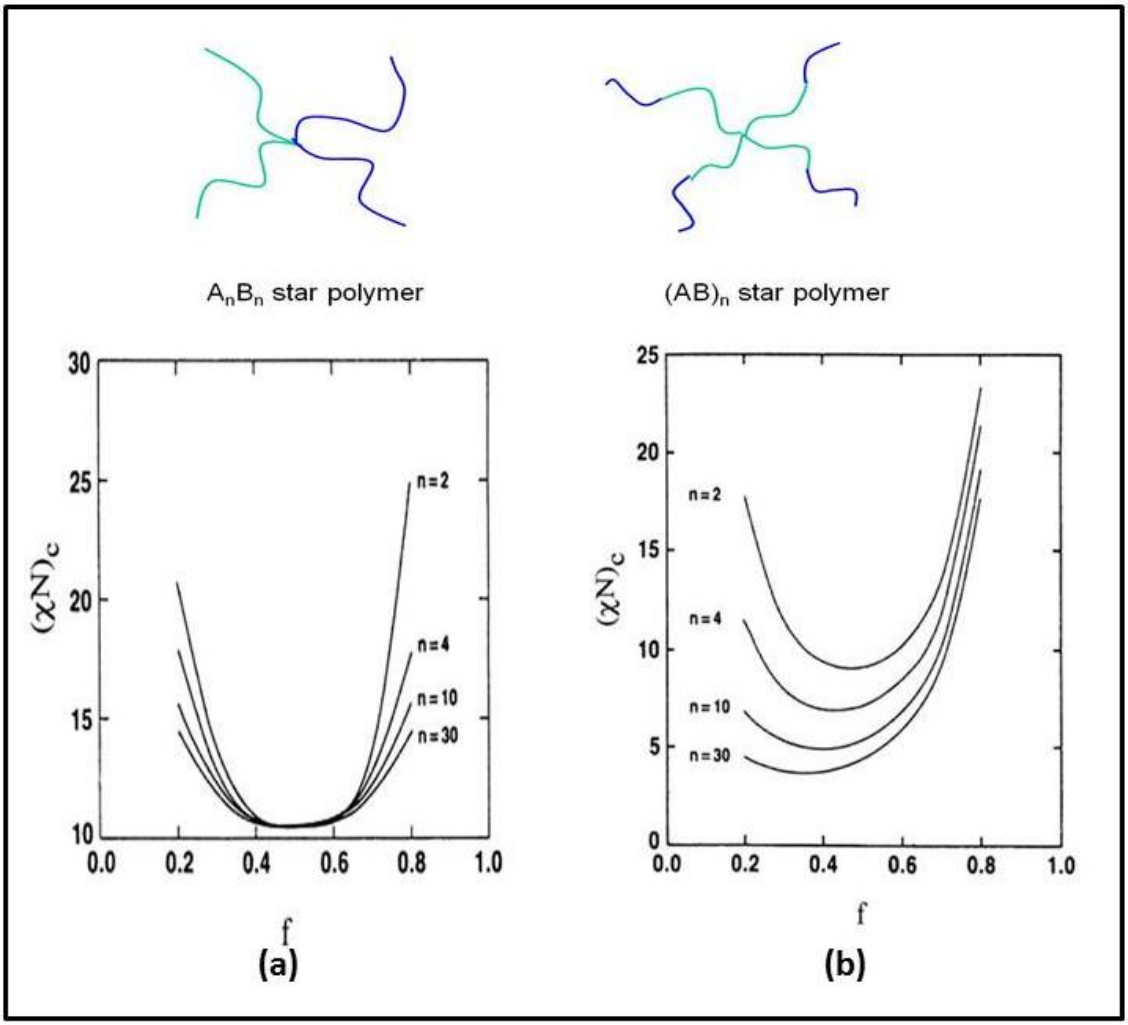


**FIGURE 1.10: Microphase separation in a) $A_nB_n$ and b) $(AB)_n$ type star shaped polymers[81]**

In case of $A_nB_n$ type star polymers, the $(\chi N)_c$ is independent on the number of arms and is always equal to 10.5, but in case of $(AB)_n$ type star polymers $(\chi N)_c$ is dependent on number of arms. As the arm number of $(AB)_n$ type star polymer increases , the star block copolymers start to form the core and shell structure. The core consists of A block and shell consists of B block. The increase in arm numbers of star polymers favours the microphase separation. Hence the microphase separation in $(AB)_n$ type star polymers is much easier than $A_nB_n$ type star shaped polymers.(fig. 1.10)

S. Uchida et al.[82] reported the synthesis and and microphase separation in $(AB)_n$ type star shaped polystyrene-*b*-polyisoprene block copolymer. The star block copolymers with various no. of arms, i.e. in the range of 7 to 77 were studied in detail. The transmission

electron microscopy (TEM) and small-angle X-ray scattering (SAXS) showed that the ordered structure of star polymers with the number of arms less than 77 were having the lamellar morphology with the periodic distances same like the linear diblock copolymers.

## 1.3 Crystallization in supramolecular polymers

The stress relaxation in conventional polymers occurs via reptation — a snakelike movement of the polymeric chains, in the same way stress relaxation in supramolecular polymers also occurs by reptation, at the same time supramolecular chains can release strain by breaking and then recombining their weak supramolecular interaction. This procedure is temperature dependent, chains become shorter at higher temperature (opened state or partially opened state), which increases the movement of chains, reduces viscosities, sometimes shows liquid like behaviour. Hydrogen bonding controls various properties of polymers such as crystallization, packing, and morphology. [83,84]

**ODT** is the temperature where the phase separated domains of a phase separated block copolymer melt begin mixing.[85,86] In case of supramolecular block copolymers, hydrogen bonding interactions often control miscibility. Supramolecular block copolymers represent a versatile platform to generate functional nanostructures without going through complex synthesis.[87] The thermo-reversible hydrogen bonding interactions play an important role in the ODT.[84,88]

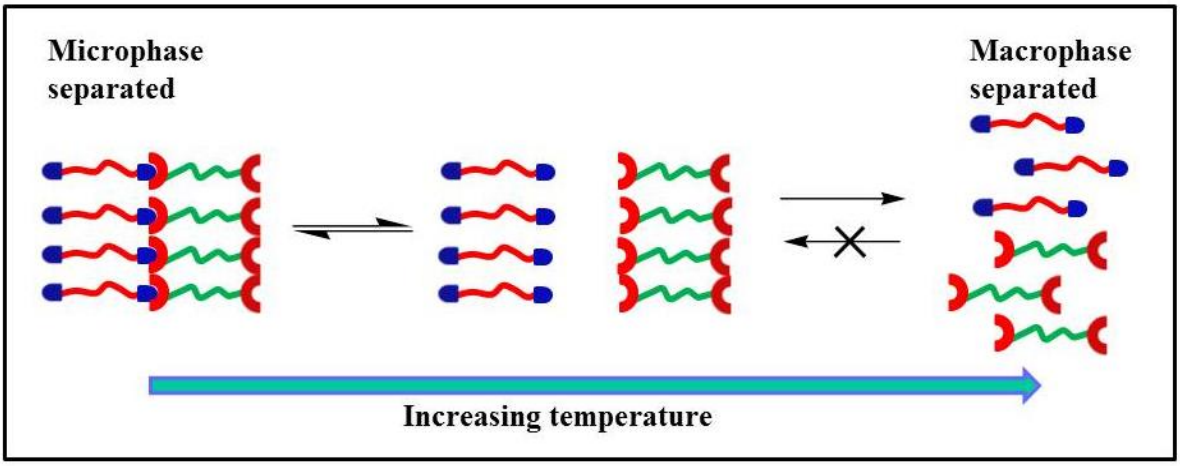


**FIGURE 1.11: Microphase and macrophase separation in Supramolecular block copolymers[88]**

### Linear pseudo block copolymers:

The crystallization in pseudo-BCP's consisting of a crystallizable PCL block and an amorphous PIB block both held together by hydrogen bonding are described by Binder et. al. Avrami exponent observed for these pseudo-BCP's were close to three, indicative of unrestricted crystal growth. Nonisothermal DSC measurements displayed a strong decrease of $T_c$ values of supramolecular mixtures in comparison to PCL homopolymer.[89,90]

In case of PCL-PS pseudo BCP's, the crystallization of PCL chains was confined in hard PS barrier.[91]

Multiple hydrogen-bonded (MHB) polymers, such as poly(styrene) (PS), poly(isoprene) (PI), and microphase separated PS-b-PI block copolymers were shown 100 times higher melt viscosity at a constant shear rate than those without multiple hydrogen bonding.[92] Stadler et al.[93] was reported microphase separated poly(isoprene)-*b*-poly(1,3-butadiene) diblock copolymers with random hydrogen bonds based on phenylurazole. In this case hydrogen bonding induced microphase separation in an originally miscible block copolymer and it formed a thermoreversible network structure.

**Stacked supramolecular polymers:**

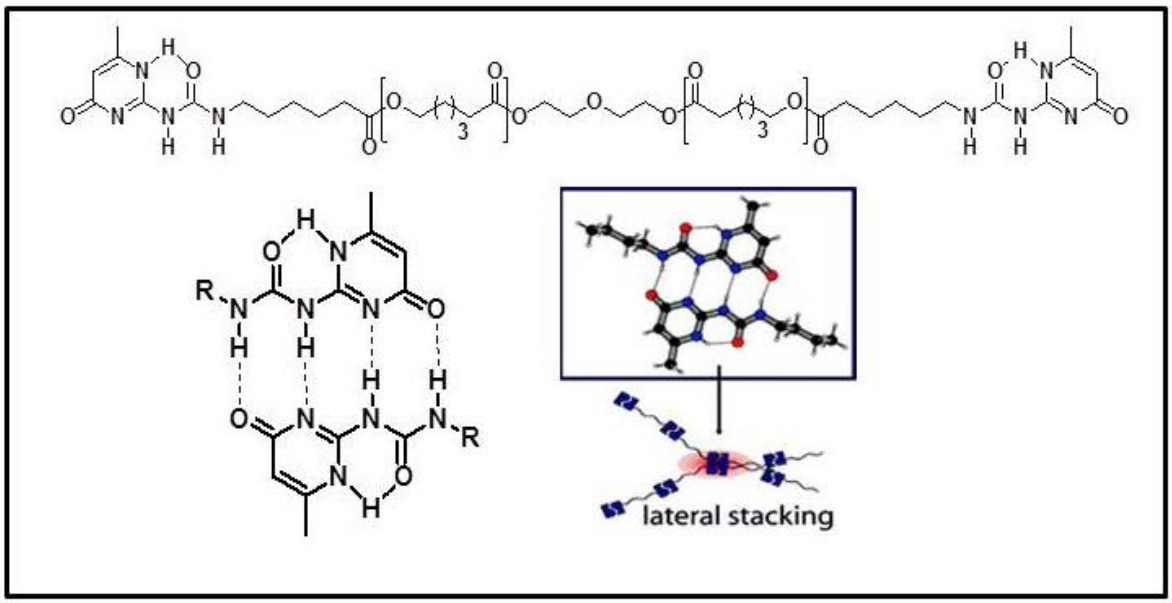


**FIGURE 1.12: Lateral stacking of Ureidopyrimidinone functionalized supramolecular PCL[94]**

Sijbesma et. al. studied the crystallization behaviour of stacked Ureidopyrimidinone functionalized supramolecular polymers. They observed that crystallization temperatures of stacked i.e. Upy functionalized polymers were found to be much lower than PCL homopolymers indicate that UPy moieties decreased the rate of crystallization of the PCL backbones.[94]

Furthermore, they also studied the crystallization in supramolecular copolymers of ε-caprolactone and δ-valerolactone and compared it with PCL, PVL and p(CL-*co*-VL). The traditional polymers PCL, PVL and p(CL-*co*-VL) shown melting temperatures 53$^{o}$C, 55$^{o}$C and 15$^{o}$C respectively whereas p(CL-co-VL)diUPy displayed two melting temperatures due to microphase separation of UPy moieties and polymer part. Whereas, the hydrogen bonded p(CL-co33%VL)diUPy displayed only one higher melting temperature at 73 $^{o}$C, as a result of the enhanced UPy crystallite formation.[95]

**Supramolecular codendrimer:**

An order-to-disorder transition in a block codendrimer caused by Intermolecular Hydrogen Bonds was studied by Wang et. al. The FT-IR data shown that the intermolecular hydrogen bonds cause a molecular segregation and gives rise to a layered structure in an amphiphilic block codendrimer of PBE and PMPA (*g*3-PBE-*b*-*g3*-PMPA-$(OH)_8$. The SAXS diffraction patterns showed the presence of a layered structure at a temperature range below 50 °C and the ODT occurred at 50°C.[96] There are several supramolecular BCP observed to undergo thermally induced, nonreversible order−order transitions (OOTs), resulting in several well-defined morphologies. The nonreversible OOTs show the importance of intermolecular interactions on the overall phase behavior of the supramolecule.[87]

## 2. Aim

The molecular architecture of a specific polymer is an important property which affects the crystallisation behaviour of that polymer; therefore it is interesting to study the crystallization behaviour of a star shaped polymer via its block copolymer formation as well as via changing its architecture through photocleavage.

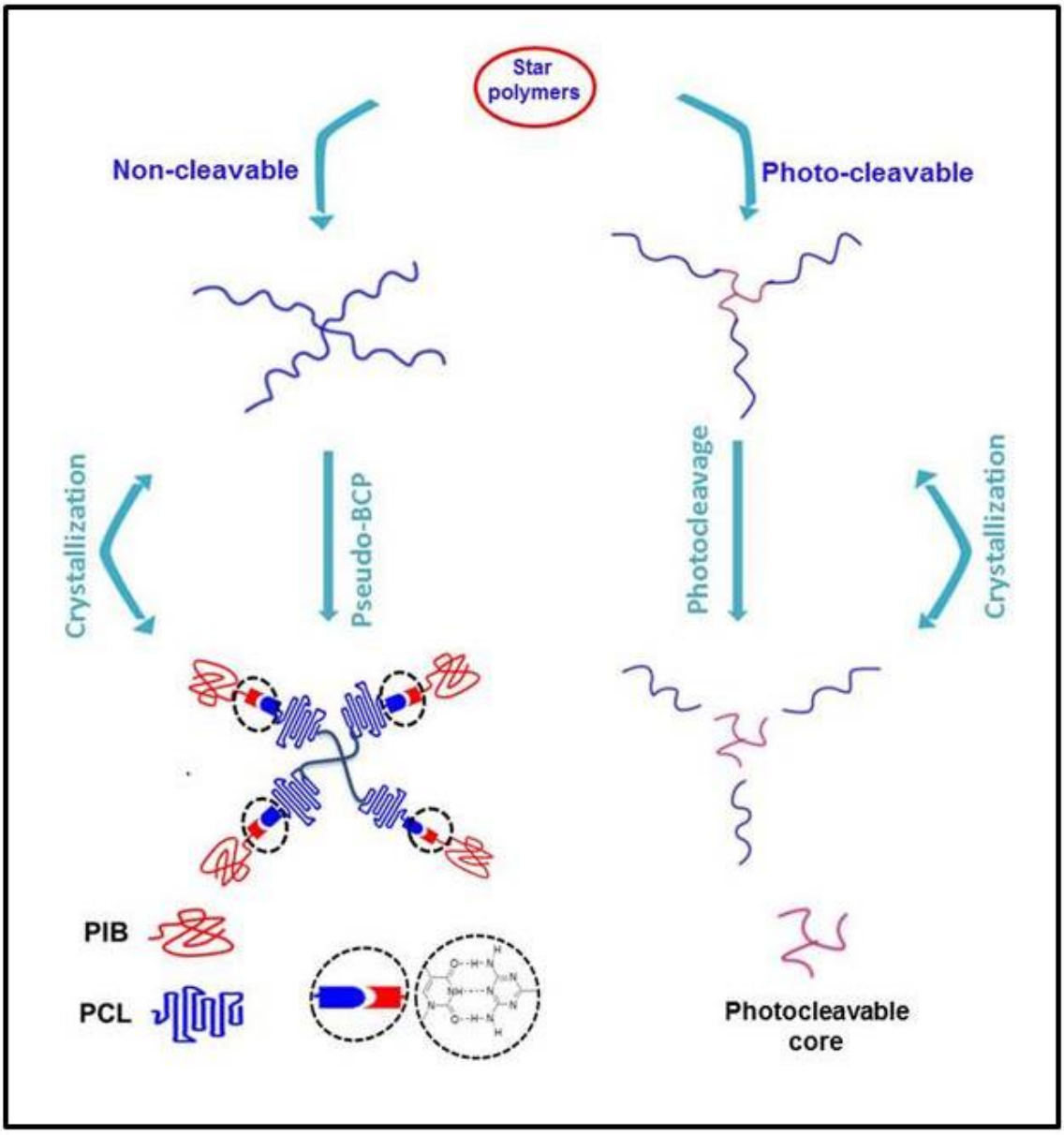


**FIGURE 2.1: Crystallization in star polymers (A) connected to an amorphous block via supramolecular bonds (B) via photo-cleavable segment**

The crystallinity and the thermal properties of semicrystalline homopolymers can be modified by synthesizing their block copolymer with amorphous homopolymers. In this work, we aim to modify the crystallization behaviour of a star shaped semicrystalline polymer by connecting an amorphous block e.g. PIB via supramolecular interaction. Also, it is

interesting for us, to synthesize photo-switchable star shaped polymers and to study the crystallinity changes in the photo-cleavable star shaped polymers i.e. star shaped poly(Ɛ-caprolactone). For this purpose, the multivalent photo-cleavable initiators having ability to initiate ring opening polymerization of Ɛ-caprolactone should be synthesized, and used for the synthesis the star shaped photo-cleavable poly(Ɛ-caprolactone).

# 3. Concept

## 3.1. Supramolecular star shaped block copolymers

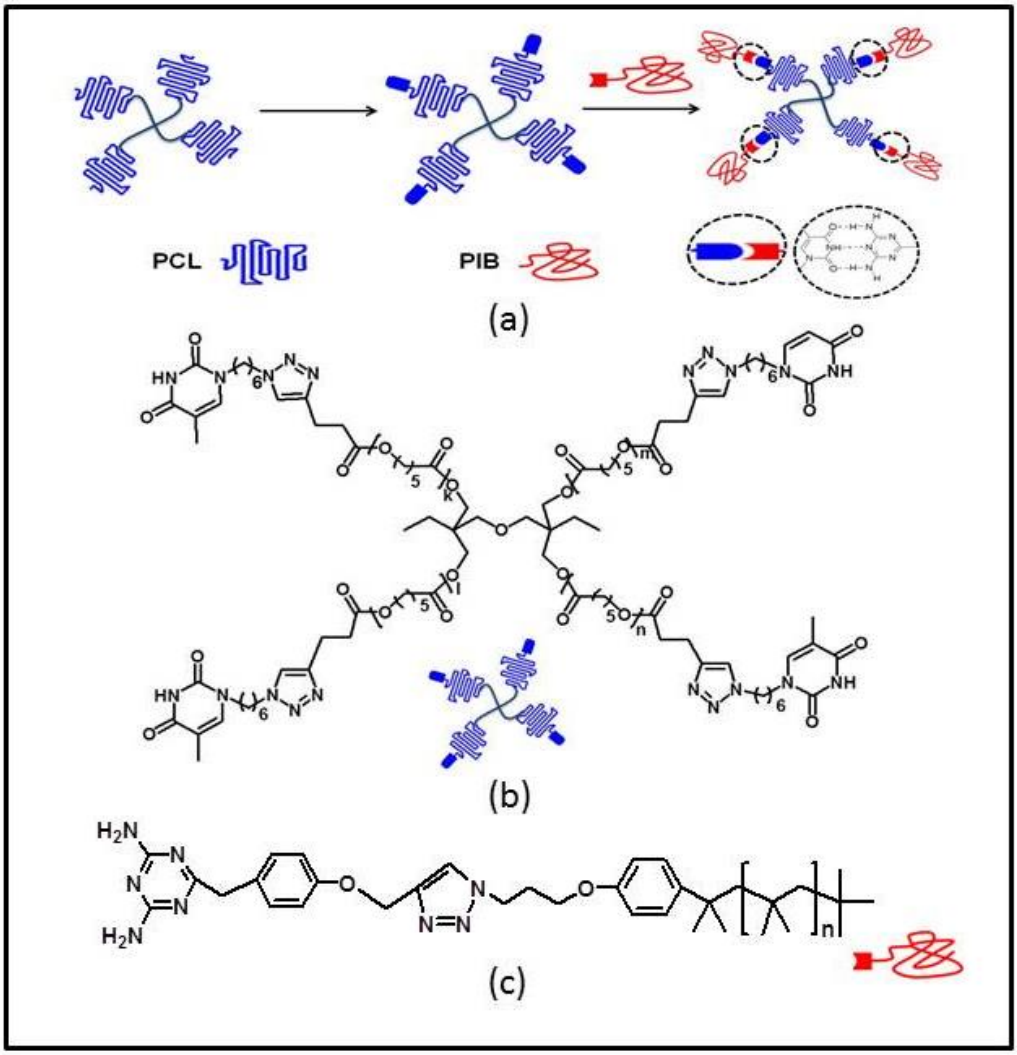


**Fig. 3.1 (a) Schematic illustration for synthesis of star shaped supramolecular block copolymer (b) Thymine functionalized star shaped poly(Ɛ-caprolactone) (c) Structure of triazine functionalized poly(isobutylene).**

The Fig. 3.1 indicates the route to synthesize star shaped SPCL-PIB supramolecular block copolymer; the blocks will be connected by thymine-triazine interaction. The three step synthesis can be achieved via synthesis of hydroxyl functionalized SPCL, alkyne functionalized SPCL and thymine functionalized SPCL respectively.

The hydroxyl functionalized star shaped PCL will be treated with pentynoic acid to get alkyne functionalized star shaped PCL by using esterification reaction. Furthermore alkyne functionalized PCL will be reacted with thymine azide by using copper(I)-catalyzed azide alkyne cycloaddition (***CuAAC***) . At the same time synthesis of 2,4-Diaminotriazin-functionalized PIB will be carried out by polymerization of isobutylene and end group modification afterwards. The synthesized samples must have a high purity, since the

impurities and non-functionalized polymer chains avoids the formation of hydrogen bonds between the two blocks. In addition to this, Impurities can as nuclei to initiate the crystallization.

The preparation of supramolecular pseudo - block copolymers (SPBCP) will be carried out by dissolving the two homopolymer blocks in a solvent, mixing, evaporation of the solvent and annealing the samples to favour the formation of hydrogen bonds. The SPBCP can form either an ordered (micro phase-separated) or a disordered-macro-separated structure. These studies will provide information about the properties of the crystallization barrier (PIB). The crystallization behaviour of SPBCP and pure homopolymer are to be investigated and compared with isothermal and non-isothermal conditions.

It is also interesting to prepare supramolecular networks of star shaped PCL (Fig. 3.2) with help of a di-triazine connector and to study their properties by using DSC and SAXS.

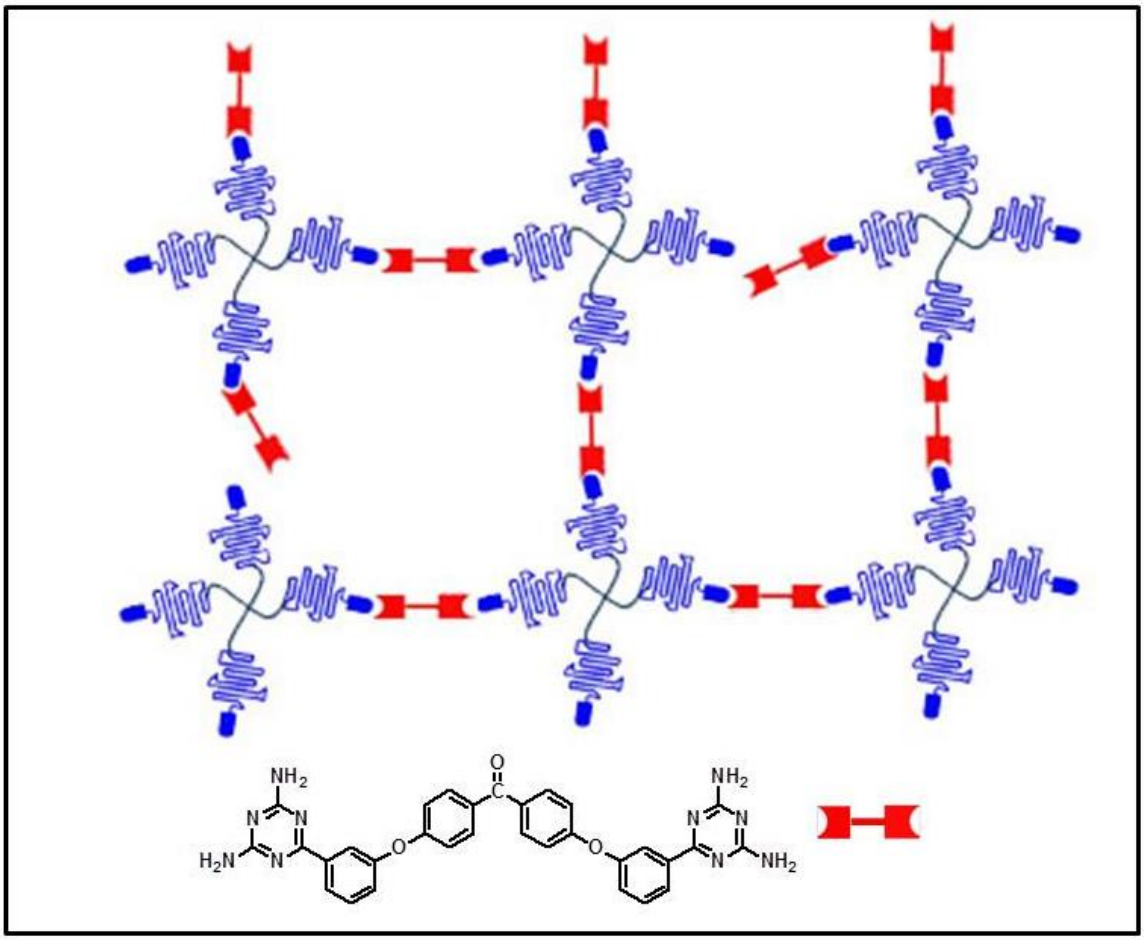


**Figure 3.2: Supramolecular SPCL network.**

### 3.2 Photo-cleavable star shaped polymers

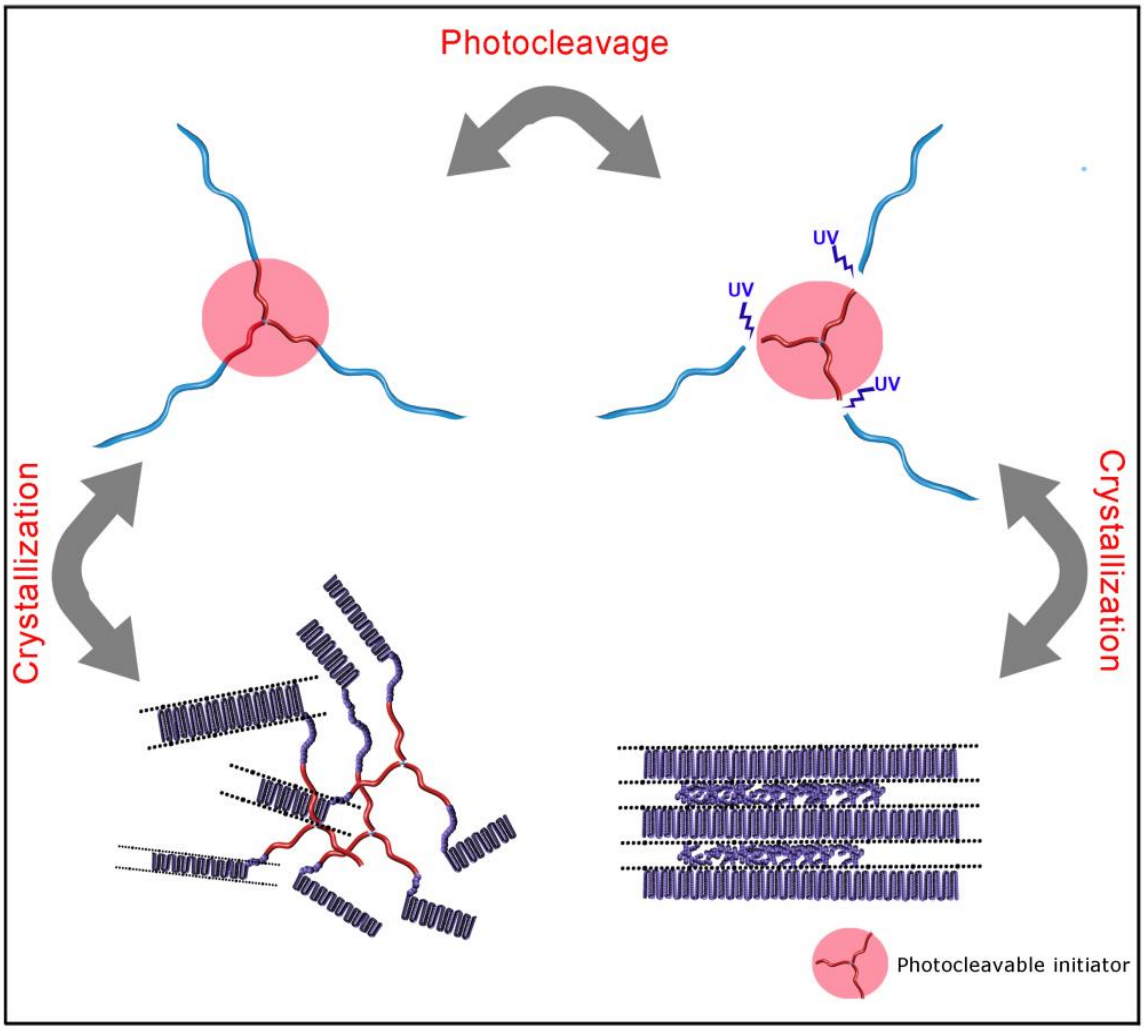


**FIGURE 3.3: Schematic representation of concept of star shaped photo-cleavable polymers**

The figure 3.3 shows the schematic representation of our concept i.e. photocleavage of star shaped polymers and their crystallization behaviour. For this purpose, the synthesis of trivalent and hexavalent photo-cleavable initiators are planned. The *o*-nitrobenzyl groups are easily photo-cleavable moieties therefore 2-nitro,5-hydroxy benzaldehyde was selected to attach on the cynuric chloride as well as hexachlorophosphazene. For example, the trivalent initiator will be synthesized via a two-step reaction, the first step should be the synthesis of trivalent aldehyde and the second step will be the reduction of aldehyde groups to get trivalent alcohol, reducing agent must be specific for aldehyde group and should not affect the nitro group.

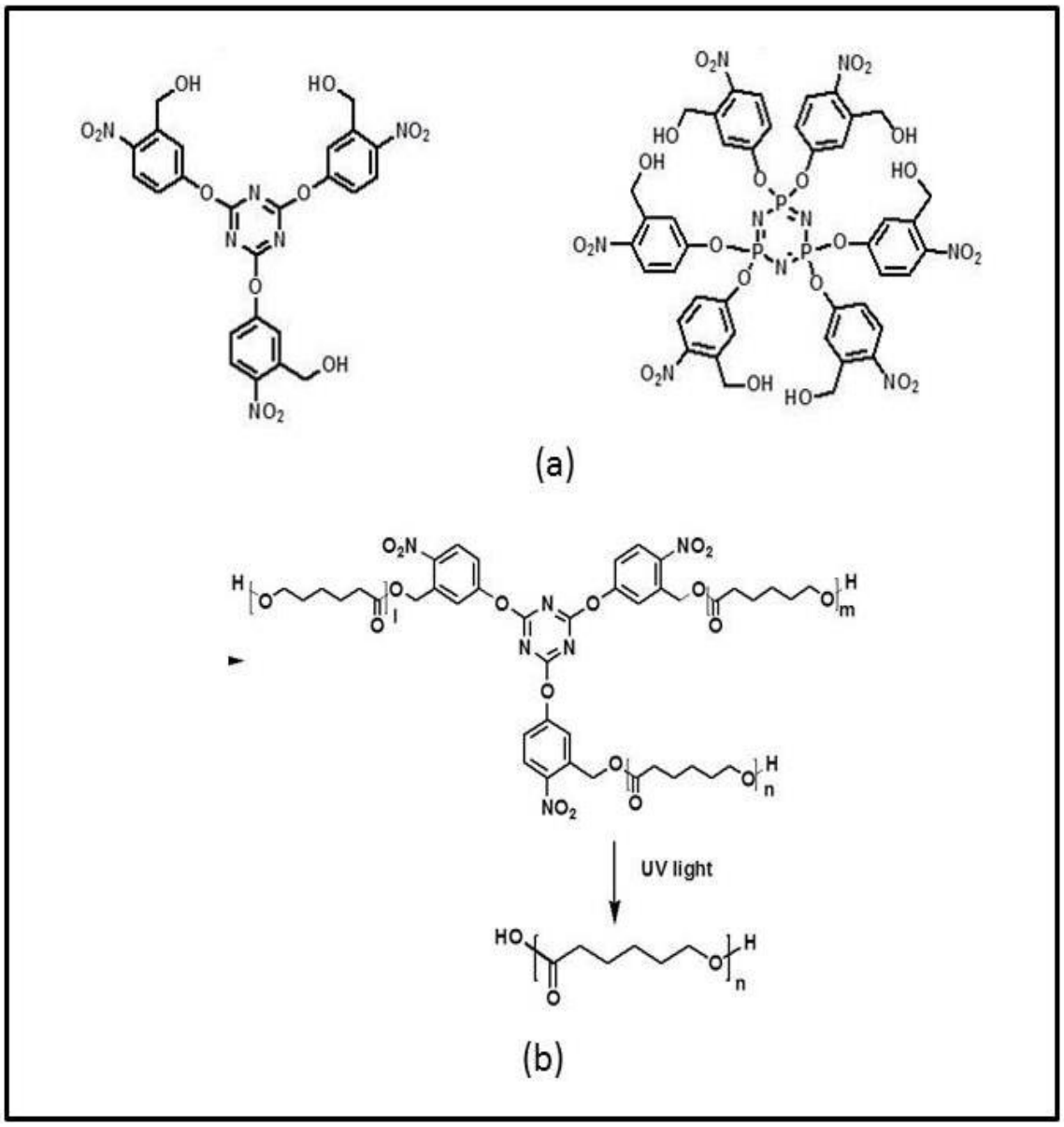


**FIGURE 3.4: (a)Schematic illustration of multivalent photo-cleavable initiator synthesis (b) Schematic illustration of photo-cleavage of star polymer.**

After confirming the structure of photo-cleavable initiator by various characterization techniques like $^{1}$H-NMR, $^{13}$C-NMR, ESI-TOF-MS, $^{31}$P-NMR, it can be used for ring opening polymerization of cyclic esters e.g. Ɛ-caprolactone or L-lactide. Thereafter, the ring opening polymerization Ɛ-caprolactone will be carried out by using trivalent photo-cleavable initiator in presence of $Sn(oct)_2$ to obtain the three arm star shaped photo-cleavable poly(Ɛ-caprolactone). The structure of the synthesized polymer will be characterized by $^{1}$H-NMR, GPC and ESI-TOF-MS.

As the ONB linker between central core and polymer chains is photo-cleavable, the star architecture of the synthesized polymer will be switched to the linear architecture by

irradiation of UV-light. Furthermore the crystallinity changes of the synthesized polymer will be studied before and after photo-cleavage. The complete photo-cleavage of the star shaped poly(ε-caprolactone) can be confirmed by GPC, HPLC, ESI-TOF-MS, etc.

# 4. Synthesis of Supramolecular Star shaped block copolymers

The numbers of star shaped block copolymers are reported till now in the literature having various applications due to their architecture. The covalently bonded star-shaped poly(ε-caprolactone)-*b*-poly(oligo(ethyleneglycol)methacrylate),[$PCL_a$-*b*-$POEGMA_b$]$_4$,[97] star shaped (Polycaprolactone-poly(ethylene glycol) monomethyl ether) star[PCL-mPEG]$_4$ and Star(Polycaprolactone -poly(2-ethyl-2-oxazoline) star[PCL-PEtOx][98], s(PEG-PCL)$_4$[99], disulfide-centered star-shaped poly(ε-benzyloxycarbonyl-L-lysine)-*b*-poly(ethylene oxide) block copolymers (i.e., $A_2B_4$ type Cy-PZlys-*b*-PEO)[100], star shaped poly(ε-caprolactone) and poly(ethyl ethylene phosphate)[101] , four-armed star-shaped poly(ethylene glycol)-b-poly(ε-caprolactone) block copolymer (sPCL-b-PEG-GA)[102], star-shaped 8 arms PEG-*b*-PLLA block copolymer[103] are having application in pharmaceutical fields like drug delivery systems and implantation. Compared to linear polymers with the same molecular weight, star-shaped polymers have the superiority of drug loading and delivery[102]. Five arm Star-shaped poly(ethylene oxide)-block-poly(tert-butyl acrylate) block copolymers[104], star-shaped copolymers containing poly (styrene) (PS) and poly(γ-benzyl-L-glutamate) (PBLG)[105], poly(ethylene oxide)- block-poly(-caprolactone) (PEO-b-PCL) star-block copolymers,[106] star-shaped poly(ethylene oxide)-b-poly(ε-caprolactone)[107] have applications in nanotechnology field. All these BCPs are synthesized by various techniques like copper-catalyzed azide-alkyne cycloaddition (CuAAC), ring-opening polymerization and thiol-yne chemistry, atom transfer radical polymerization, condensation reaction, etc.

The poly(isobutylene) is a soft rubbery solid, having a low glass transition temperature ($T_g$ = −70º C), low specific thermal conductivity, low water permeability, and high dielectric strength. Low Mn PIBs are useful as lubricants, additives, and viscosity modifiers whereas high $M_n$ PIBs include sealants, and adhesives.[14] Poly(isobutylene) (PIB) is a commercially important due to its thermal stability, good flexibility at ambient temperature, and impermeability to gases.[108] Linear triblock copolymer (PC1-PIB-PC1) was reported by Storey et. al.[109] Synthesis and crystallization of PCL-PIB pseudo block copolymers is reported by Ostas et. al.[89,90].

Therefore, to understand the effect of architecture in supramolecular BCP, we decided to synthesize star shaped PCL-PIB supramolecular BCP with PCL core and PIB shell. Therefore it was necessary to introduce supramolecular moieties on both PCL and PIB chains. For this purpose the synthetic way planned to attach thymine moiety on four arms of PCL core. Triazine functionalized PIB was synthesized as reported in literature[89]. Furthermore, after coonecting these blocks by supramolecular interaction, the crystallization

study was carried out by using DSC analysis and phase separation by using SAXS analysis.

## 4.1 Synthesis of thymine functionalized poly(Ɛ-caprolactones)

The synthesis of thymine functionlized SPCL was carried out via a three-step synthesis. The first step is to synthesize hydroxyl functionalized star PCL.

### 4.1.2 Synthesis of star shaped poly(Ɛ-caprolactones):

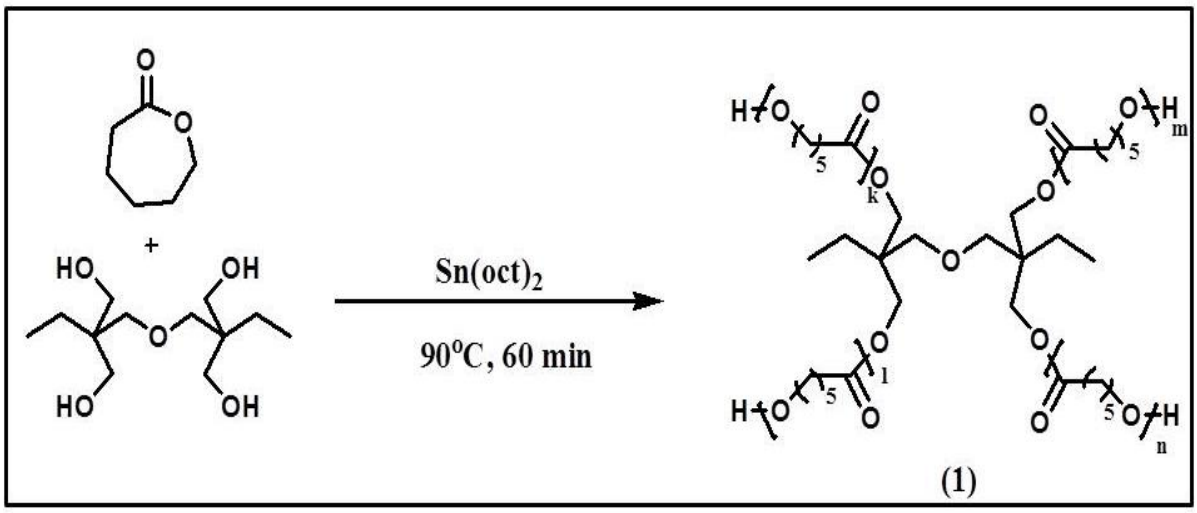


**Scheme 4.1: Synthesis of star shaped poly poly(Ɛ-caprolactone)(1)**

Ring opening polymerization of Ɛ-caprolactones by using multivalent alcohol as initiator in presence of catalyst is a well-known method to prepare star shaped poly(Ɛ-caprolactones). There are various synthetic mechanism are reported for ROP of Ɛ-caprolactone which includes anionic polymerization, cationic polymerization, organocatalytic polymerization or co-ordination insertion polymerization. For ROP of lactones the commonly used coordination insertion initiators are alkoxides of the metals with d-orbitals e.g. Al or Sn alkoxides. The coordination of metal-alkoxide with a carboxy group of monomer takes place, this nucleophiilic attack cleaves the CO-O linkage of monomer with simultaneous insertion into metal-alkoxide bond and repetitions of this process results in synthesis of polyester with hydroxyl end group.[110]

As traces of moisture can initiate or terminate the polymerization, the reaction was carried out in extremely dry condition. Schlenk flask used for polymerization was dried by three ‘heating and argon cycles’ and then all materials were added inside glove-box. Pentaerythritol and ditrimethylol propane are four arm initiators commercially available for polymerization of lactones. To avoid steric hindrance and to successfully initiate all four PCL chains, Ditrimethylol propane was used as a four arm initiator instead of pentaerythritol.

Stannous octanoate was used as catalyst for ring opening polymerization. Hence the polymerization of Ɛ-caprolactone was carried out in presence of ditrimethylol propane as a initiator and $Sn(oct)_2$ as a catalyst (Scheme 4.1). The structure of above synthesized star shaped poly(Ɛ-caprolactone) was confirmed by using $^1$H-NMR and ESI-TOF-MS analysis.

**Table 4.1: Polymerization data of star shaped poly (Ɛ-caprolactone)**

| Sr. No. | Polymer code | Catalyst | $M_n$(GPC)[a] g/mol | PDI[a] | $M_n$(NMR)[b] g/mol | $M_n$(GPC)[c] g/mol | $M_n$ (each arm) |
|---|---|---|---|---|---|---|---|
| 1 | Star[PCL-1.7k-OH]$_4$ | $Sn(oct)_2$ | 9650 | 1.18 | 7050 | 7628 | 1750 |
| 2 | Star[PCL-6k-OH]$_4$ | $Sn(oct)_2$ | 28400 | 1.16 | 22800 | 18959 | 5700 |
| 3 | Star[PCL-13k-OH]$_4$ | $Sn(oct)_2$ | 61000 | 1.2 | 52000 | 48225 | 13000 |

[a] Number average molecular weight obtained by using GPC with RI detector.
[b] Number average molecular weight calculated by using proton NMR.
[c] Number average molecular weight obtained by using GPC with LS detector.

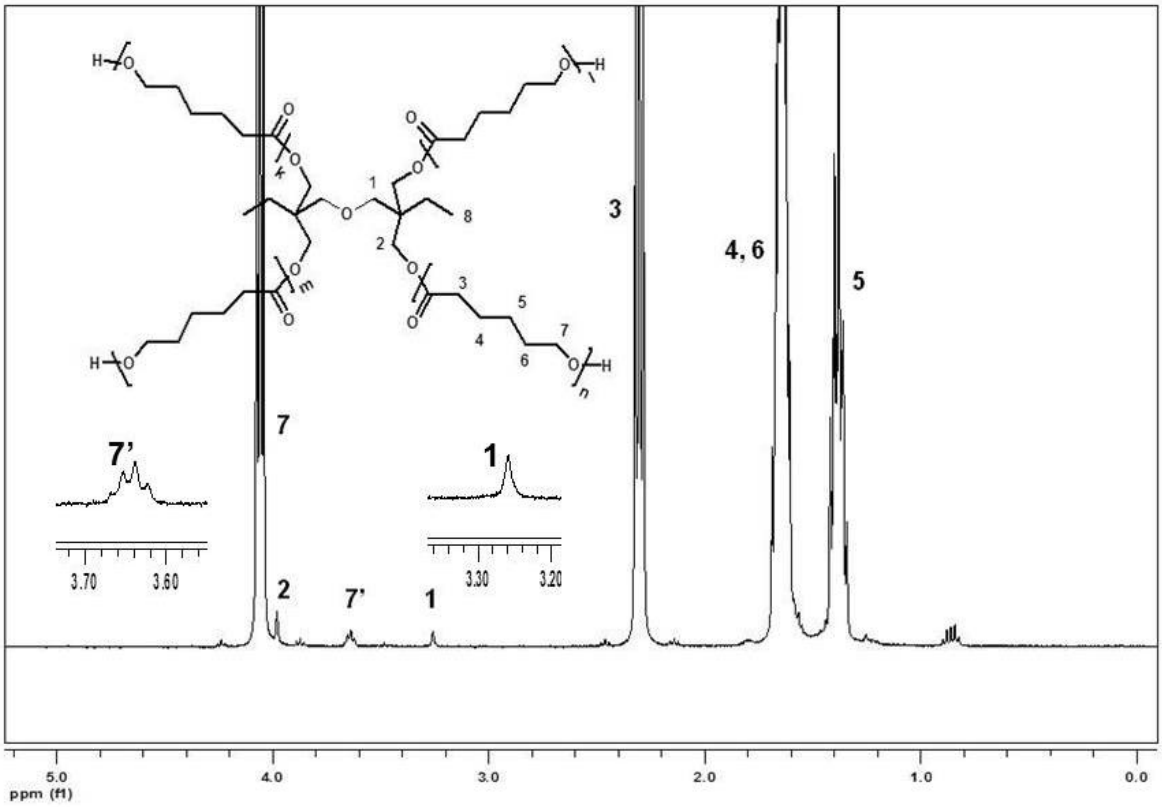


**FIGURE 4.2: $^1$H-NMR spectrum of star shaped poly(Ɛ-caprolactone)**

Fig.4.2 shows the $^1$H-NMR spectrum of star shaped PCL. In $^1$H-NMR, peak no.1 & 2 shows the presence of $CH_3$ and $CH_2$ protons of DiTMP initiator in synthesized polymer, whereas

peak no. 3 to 7 represents the PCL arms with end-group 7'. Peak no.3 is a triplet at 2.33ppm for proton of $C\underline{H}_2$-CO-O of PCL chain, peak no. 4 and 6 show multiplet at 1.68 ppm and peak no.5 is also a multiplet at 1.41 ppm, these peaks represents protons of CH2 groups of PCL chains. $^1$H-NMR measurement was carried out in $CDCl_3$ solvent.

Fig. 4.3 shows the ESI-TOF-MS spectrum of SPCL-OH, the measurement was carried out in THF/Methanol/Acetonitrile mixture. The spectrum shows different no. of series with charge order +3, +4 and +5. In fig. 4.3 the full mass spectrum and expanded region of spectrum between m/z 1480 to 1600 are shown. Also two representative simulated and measured isotopic patterns are shown in that figure. The peak at m/z=1540.65 and m/z= 1551.91 show the expected isotopic pattern for $[M+4Na]^{++}$. The ESI-TOF-MS clearly indicates the presence of four hydroxyl end groups of star shaped polymer. This analysis is also a good tool to check whether there is any presence of linear polymer chains, and the spectrum did not show any linear chain content in the polymer.

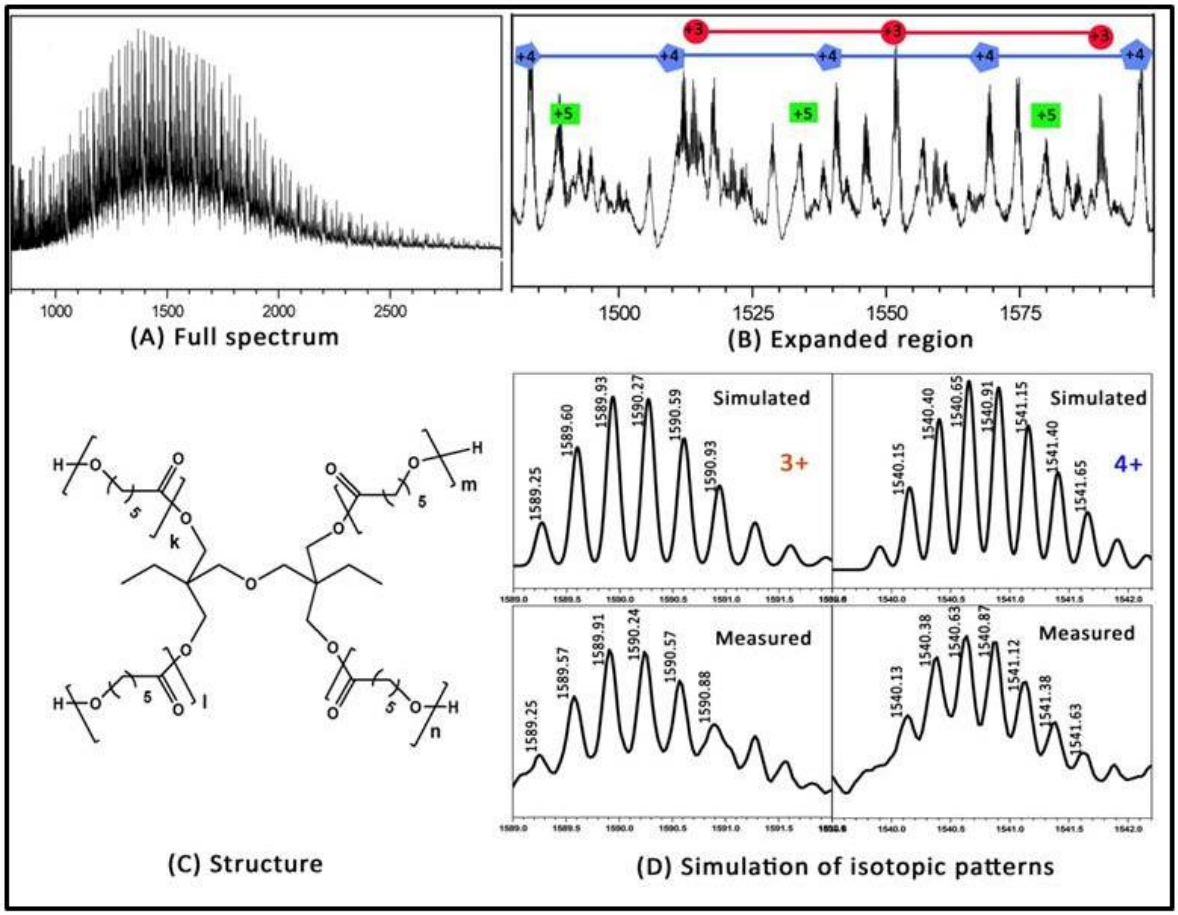


**FIGURE 4.3: ESI-TOF-MS spectrum of star shaped poly(Ɛ-caprolactone). (a) Full spectrum (b) Expansion of spectrum (c) structure (d) Isotopic pattern simulation**

### 4.1.2 Synthesis of star shaped alkyne functionalized poly(Ɛ-caprolactone)s:

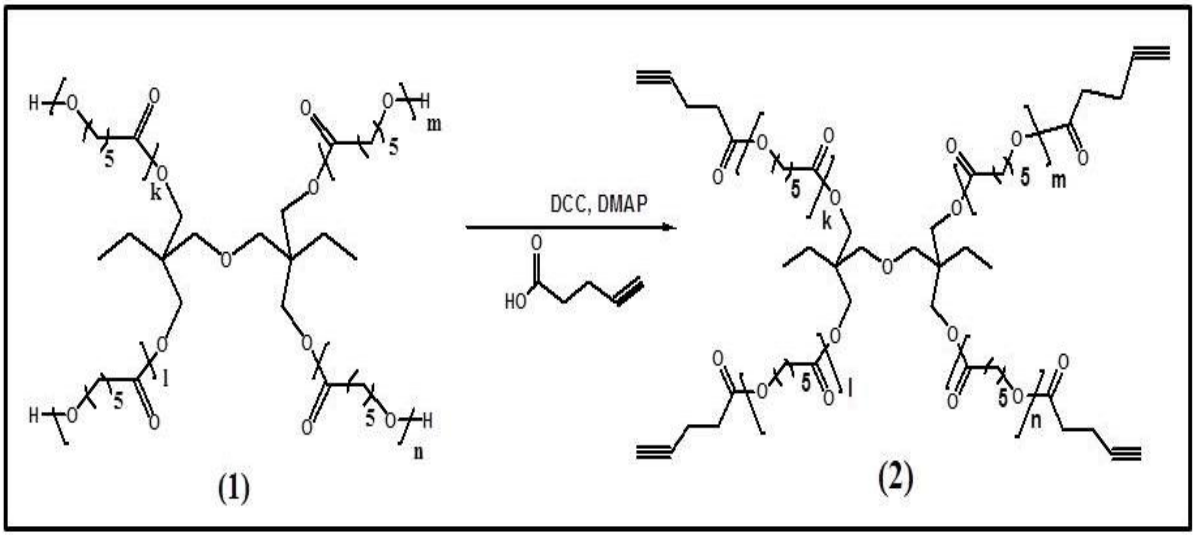


**Scheme 4.2: Synthesis of alkyne functionalized poly(Ɛ-caprolactone)(2)**

Synthesis of alkyne functionalized star shaped poly(Ɛ-caprolactone) was carried out by Steglich esterification reaction. In this reaction, esterification of alcohol end groups was carried out with carboxylic acid by using DCC & DMAP (Scheme 4.2). DCC (dicyclohexylcarbodiimide) and the carboxylic acid are able to form an *O*-acylisourea intermediate, which offers reactivity similar to the corresponding carboxylic acid anhydride, whereas DMAP acts as catalyst. Star shaped poly(Ɛ-caprolactone) on reaction with 4-pentynoic acid in presence of DCC and DMAP gives alkyne functionalized star shaped poly(Ɛ-caprolactone)**(2)**.

The structure of the purified compound is confirmed by $^{1}$H-NMR analysis (fig. 4.4); measurement was carried out in $CDCl_3$. In comparison with $^{1}$H-NMR of hydroxyl functionalized star shaped poly(Ɛ-caprolactone), absence of triplet at 3.67 ppm in $^{1}$H-NMR of alkyne functionalized star shaped poly(Ɛ-caprolactone) indicates that all hydroxyl groups are reacted and converted to alkyne group. In addition, peak no. 1 i.e. triplet at 1.97 ppm shows the presence of alkyne groups. Multiplet at 2.52 ppm shown by peak no. 2 & 3 are for protons of –CH2 groups of pentynoic moieties. At the same time singlet at 4.01 ppm and singlet at 3.25 ppm show the presence of central core in polymeric compound, shown by peak no. 4 & 5 respectively.

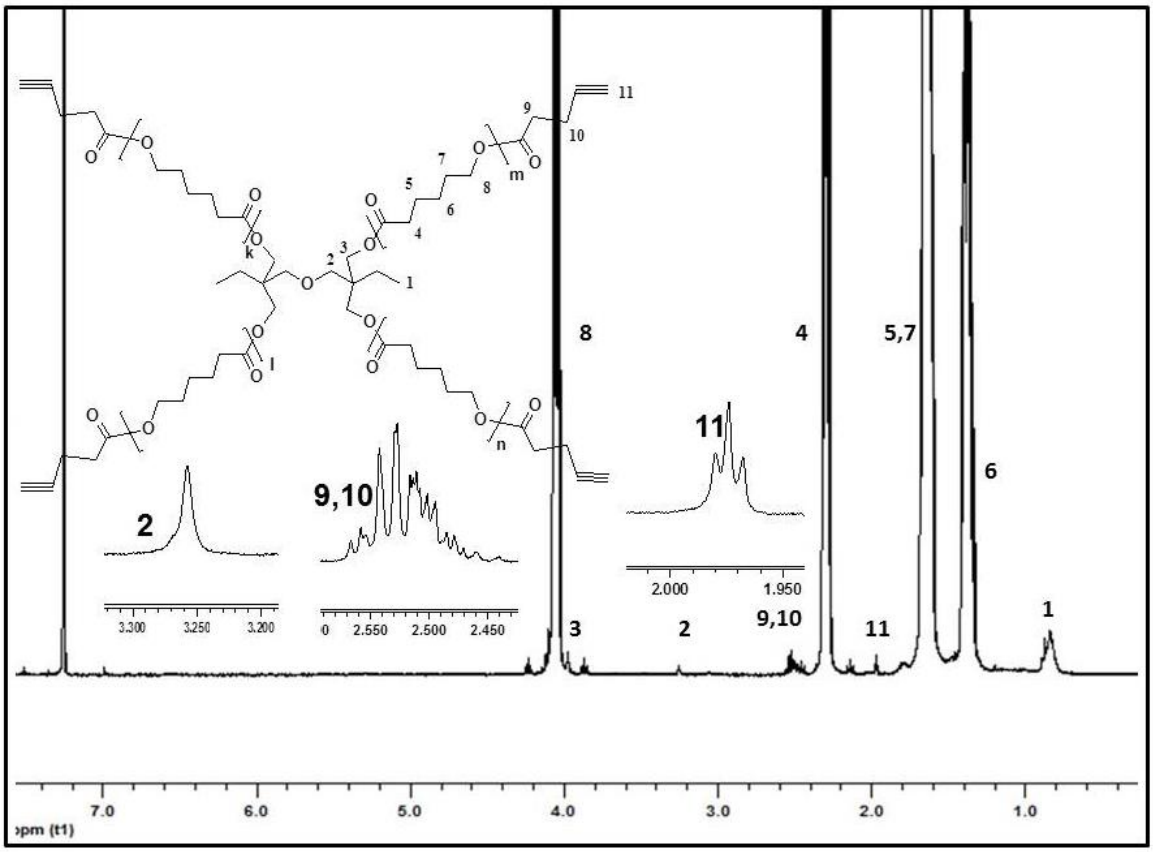


**FIGURE 4.4: $^{1}$H-NMR spectrum of alkyne functionalized star shaped poly(Ɛ-caprolactone)**

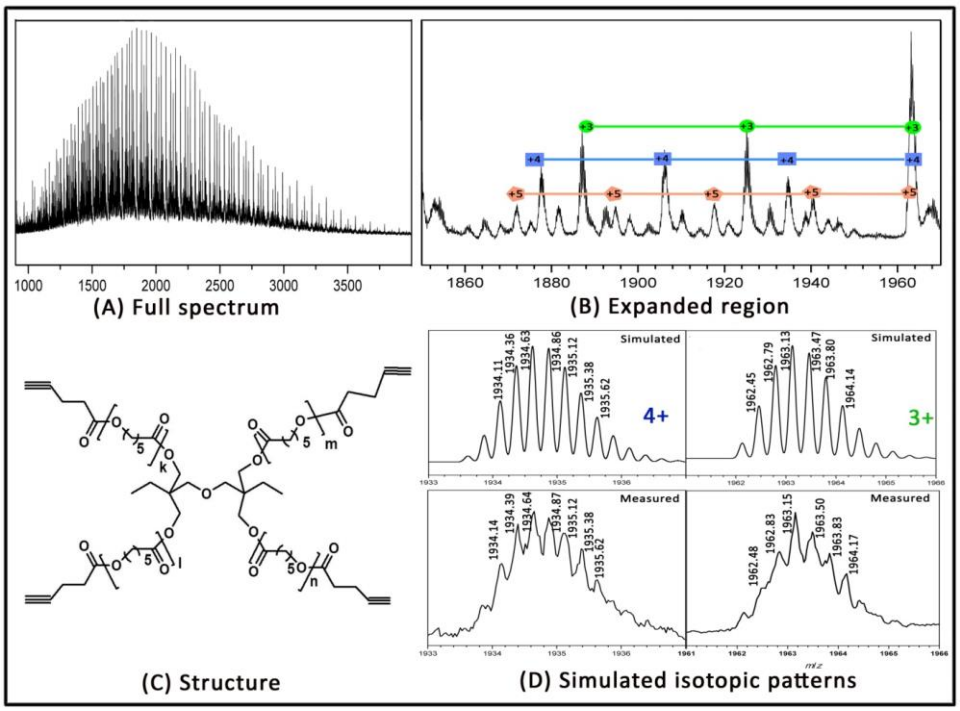


**FIGURE 4.5: ESI-TOF-MS spectrum of alkyne functionalized star shaped poly(Ɛ-caprolactone). (a) Full spectrum (b) Expansion of spectrum (c) Isotopic pattern simulation**

Furthermore after the alkyne functionalization of all four arms of the star shaped PCL is confirmed by using ESI-TOF-MS (fig. 4.5). The ESI-TOF-MS is again a good tool here to confirm the alkyne functionalization of all four chains of the star polymer. The full mass spectrum and expanded region of spectrum between m/z 1850 to 1970 are shown in the figure. The spectrum shows different no. of series with charge order +3, +4 and +5. The peak at m/z=1963.13 and m/z= 1871.88 show the expected isotopic pattern for $[M+3Na]^{3+}$ and $[M+Na]^{5+}$ respectively. The perfect fitting of measured isotopic pattern and simulation pattern clearly indicates that all four –OH groups are successfully converted into alkyne groups.

### 4.1.3 Synthesis of star shaped thymine functionalized poly(Ɛ-caprolactone)

In order to introduce a moiety capable to form hydrogen bonding, thymine group was introduced on alkyne functionalized poly(Ɛ-caprolactone) via click reaction. Click Chemistry is a reaction between azide and alkyne, these groups in presence of Cu-catalyst yield covalent product - 1,5-disubstituted 1,2,3-triazole. This process is also known as CuAAC - Cu catalysed alkyne azide cycloaddition, it proceeds with formation of a triazole by the reaction between azide and alkyne groups. The substituents do not affect the reaction and reaction can be carried out under mild conditions. [111,112]

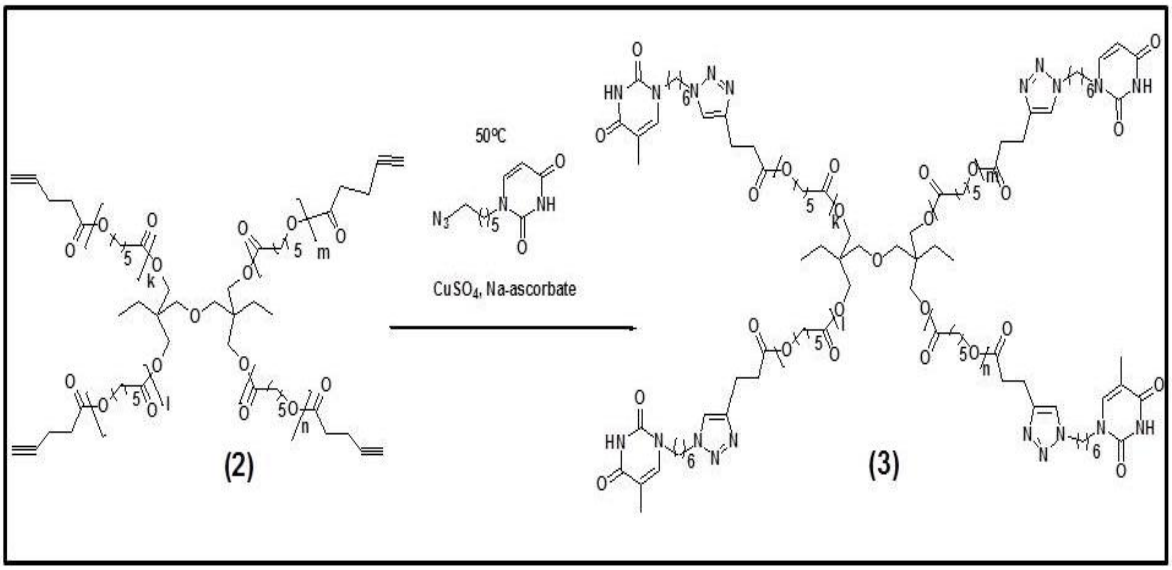


**Scheme 4.3: Synthesis of thymine functionalized star shaped poly(Ɛ-caprolactone)(3).**

In this reaction, star shaped alkyne functionalized poly(Ɛ-caprolactone) reacts with 1-(6-Azidohexyl) Thymine in presence of cupric sulphate pentahydrate and (+)-sodium-L-ascorbate, the reaction takes place at 58°C for 20 hrs in DMF. This reaction mixture was later on passed through basic alumina to remove Cu-catalyst and then precipitated in cold

methanol. The purity of synthesized product was confirmed by 1H-NMR analysis and ESI-TOF-MS analysis (Scheme 4.3).

$^1$H-NMR measurement of purified star shaped thymine functionalized poly(Ɛ-caprolactone) was carried out in $CDCl_3$ solvent (Fig. 4.7). The singlet at 3.25ppm and singlet at 4.01ppm are the peaks due to -$CH_2$ protons in central core. There is small shift in peak no. 4 & 5 i.e. –$CH_2$ of thymine functionalized SPCL in comparison with those of alkyne functionalized SPCL i.e. overlapped peaks at 2.52 shifts to two different triplets at 2.72ppm and 3.03 ppm respectively. Singlet at 6.96 ppm i.e. peak no. 5 clearly confirms the successful click reaction, which represents proton in triazole ring. Furthermore, three singlet's i.e. peak no. 9,10 and 11 at 7.33 ppm, 1.91 ppm and 8.02 ppm respectively indicates the presence of thymine ring in polymer chain.

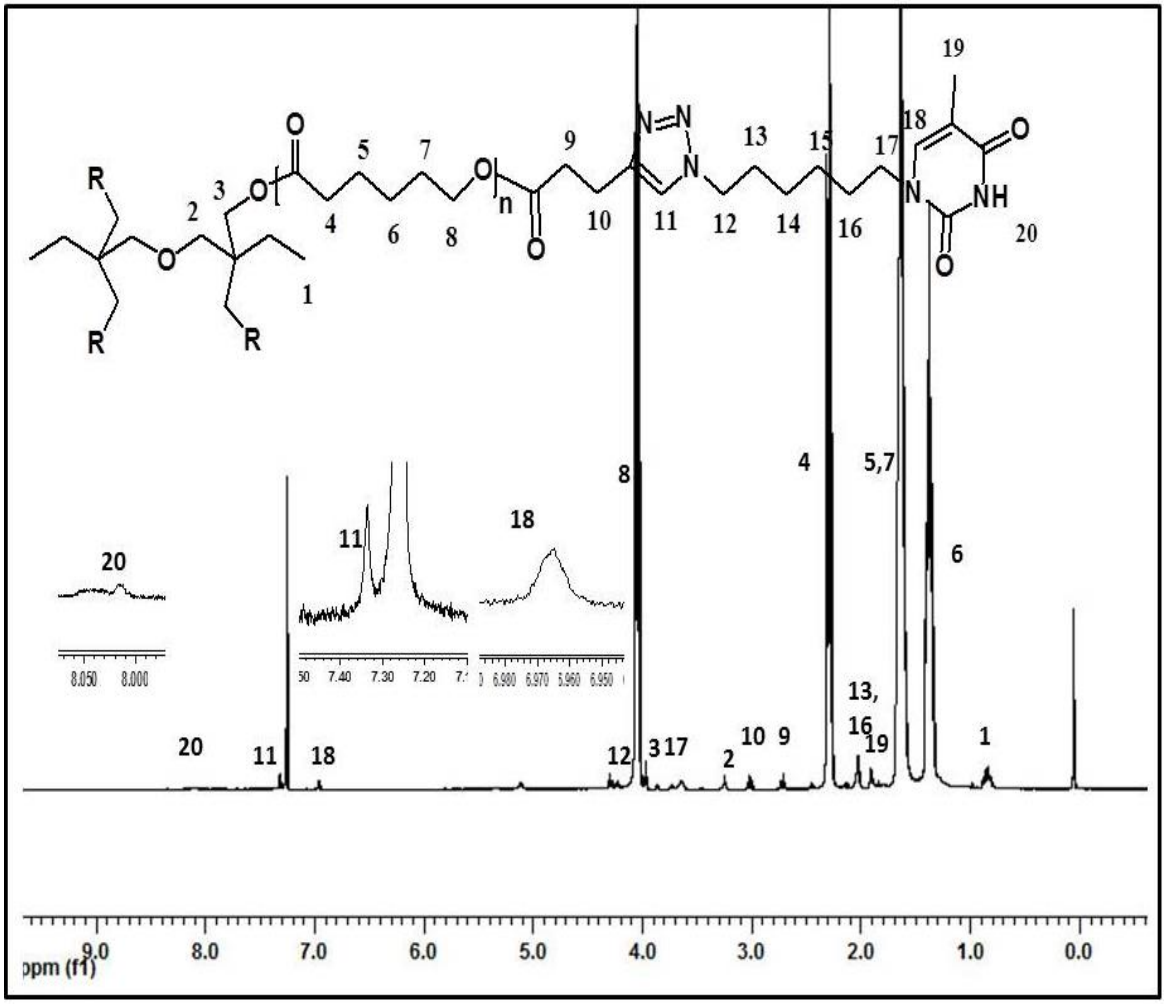


**FIGURE 4.7: $^1$H-NMR spectrum of thymine functionalized star shaped poly(Ɛ-caprolactone)**

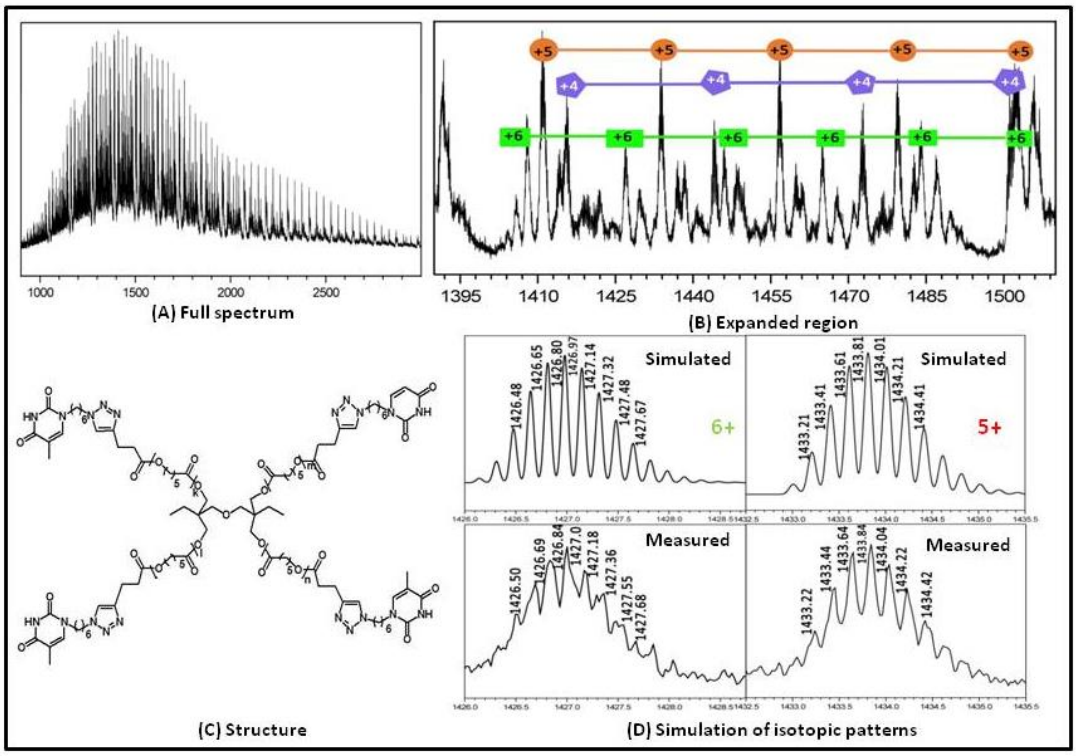


**FIGURE 4.8: ESI-TOF-MS spectrum of thymine functionalized star shaped poly(Ɛ-caprolactone). (a) Full spectrum (b) Expansion of spectrum (c) Isotopic pattern simulation**

Finally, ESI-TOF-MS confirmed the success of click reaction and the thymine functionalization of all four alkyne groups (fig 4.8). The figure also shows a expanded region of m/z 1390 to 1510. A series of five time charged mass is shown in the fig.4.8, which shows five different peaks in the equivalent distance of monomer mass i.e distance of 114 in case PCL with 1456.65, 1478.48 and 1502.10 are for $[M+Na]^{5+}$, the peak at m/z 1407.96 is for $[M+Na]^{6+}$. As there are different no. of charges i.e. +3, +4, +5, +6 etc are present, many peaks are getting overlapped on each other.

### 4.1.4 Polymerization and functionalization data of star shaped poly(Ɛ-caprolactone):

The polymerization data and stepwise changes in molecular weight of the star shaped polymers are summarized in table 4.2. The three different molecular weights of thymine functionalized star shaped PCL in range of 6000 g/mol to 51000 g/mol were synthesized. The molecular weight of Star[PCL-1.7k-OH]$_4$ (7050g/mol) remains almost constant after alkyne (7700g/mol) as well as thymine (6950g/mol) functionalization. In the similar way molecular weights of Star[PCL-6k-OH]$_4$ (entry 4 to 6) and Star[PCL-13k-OH]$_4$ (entry 7 to 9) remains almost constant after alkyne and thymine functionalization respectively. All the

synthesized star poly(Ɛ-caprolactone)s were in good polydispersity range (in between 1.1 to 1.3).

**Table 4.2: Polymerization and functionalization data of star shaped poly(Ɛ-caprolactone)s**

| Sr. No. | Polymer code | $M_n$(GPC)[a] g/mol | PDI[a] | $M_n$(NMR)[b] g/mol | $M_n$(each arm) |
|---|---|---|---|---|---|
| 1 | Star[PCL-1.7k-OH]$_4$ **(1)** | 9650 | 1.18 | 7050 | 1750 |
| 2 | Star[PCL-1.7k-Alk]$_4$ **(2)** | 10400 | 1.14 | 7700 | 1925 |
| 3 | Star[PCL-1.7k-Thy]$_4$ **(3)** | 9300 | 1.15 | 8150 | 2035 |
| 4 | Star[PCL-6k-OH]$_4$ **(1)** | 28400 | 1.16 | 22800 | 5700 |
| 5 | Star[PCL-6k-Alk]$_4$ **(2)** | 30100 | 1.17 | 22950 | 5737 |
| 6 | Star[PCL-6k-Thy]$_4$ **(3)** | 30300 | 1.13 | 24000 | 6000 |
| 7 | Star[PCL-13k-OH]$_4$ **(1)** | 61000 | 1.2 | 52000 | 13000 |
| 8 | Star[PCL-13k-Alk]$_4$ **(2)** | 62000 | 1.3 | 52500 | 13125 |
| 9 | Star[PCL-13k-Thy]$_4$ **(3)** | 61400 | 1.3 | 53200 | 12975 |

a: $M_n$ calculated by using GPC calibrated by polystyrene (RI detector).

b: Number average molecular weight calculated by using proton NMR

### 4.1.5 Comparison between hydrodynamic volume of linear and star shaped PCL:

The comparison of hydrodynamic volumes of star shaped PCL and linear PCL's is shown in fig. 4.9. The hydrodynamic volumes of the star PCL's were found to be smaller than equivalent linear PCL's, whereas hydrodynamic volumes of star PCL's were increased after thymine functionalization. The hydrodynamic volumes of the polymers were calculated by

using GPC with LS detector. The molecular weights obtained by using LS detector of Star[PCL-6k-OH]$_4$ **(1),** Star[PCL-1.7k-Alk]$_4$ **(2),** Star[PCL-6k-Thy]$_4$ **(3)** are 7628g/mol, 9620g/mol and 13141g/mol respectively. Also the molecular weights of Star[PCL-6k-OH]$_4$ , Star[PCL-6k-Alk]$_4$, Star[PCL-6k-Thy]$_4$ are 18959g/mol, 22800g/mol, 28040g/mol respectively.

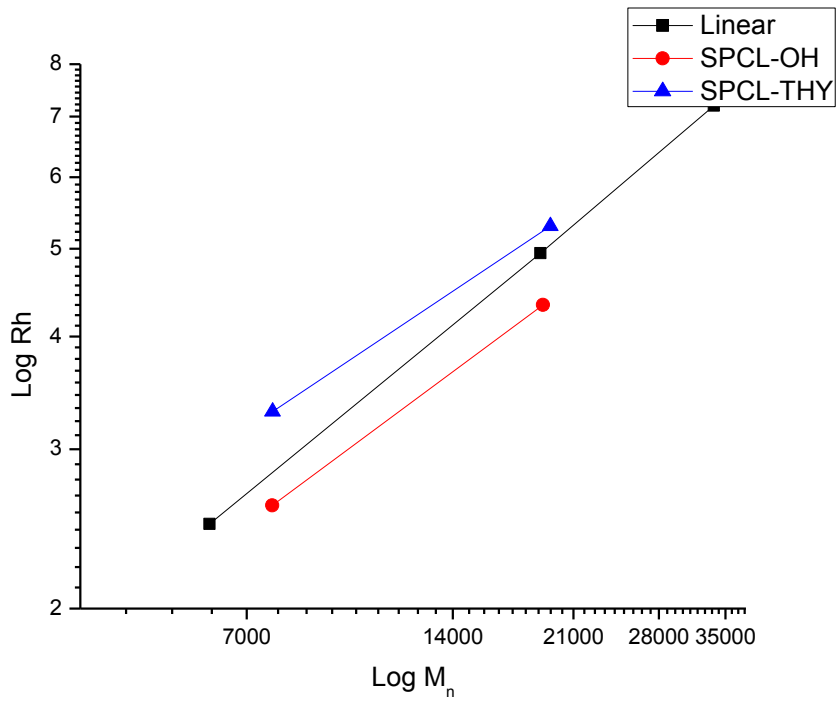


**FIGURE 4.9: Graph showing comparison between hydrodynamic radius v/s molecular weight of linear and star shaped PCL.**

### 4.1.6 Thermal analysis of hydroxy-, alkyne-, thymine- functionalized star PCL's

To understand the changes in the thermal properties during all three synthetic steps of thymine functionalization of star shaped PCL, DSC analysis of hydroxyl-, alkyne-, thymine-functionalized star PCL was carried out. The thermal analysis data of star shaped PCL's has been summarized in Table 4.3. The melting temperature $T_m$ of hydroxyl functionalized star PCL remains almost constant after alkyne as well as thymine functionalization, however there was a considerable change in the crystallization temperature of hydroxy- star PCL after alkyne and thymine functionalization i.e. $T_c$ get reduced after alkyne and thymine functionalization respectively. In case of Star[PCL-1.7k]$_4$, from (entry 1 to 3) the crystallization temperature reduced from 24.1$^o$C to 9.9$^o$C which is a large shift. In the similar way from sr. no. 4 to 6, the $T_c$ of Star[PCL-6k]$_4$ get reduced from 34.0$^o$C to 30.3$^o$C. The results indicate that effect of alkyne and thymine moieties was lower in high molecular weight star PCL in comparison with that of low molecular weight star PCL. The similar trend

was observed in case of melting enthalpies or crystallinity, in case of low molecular weight alkyne and thymine functionalized polymers there is sharp reduction in $\Delta H_m$ and $\%X_m$ was observed however a very small effect was observed in case of high molecular weight polymers (Fig 4.10).

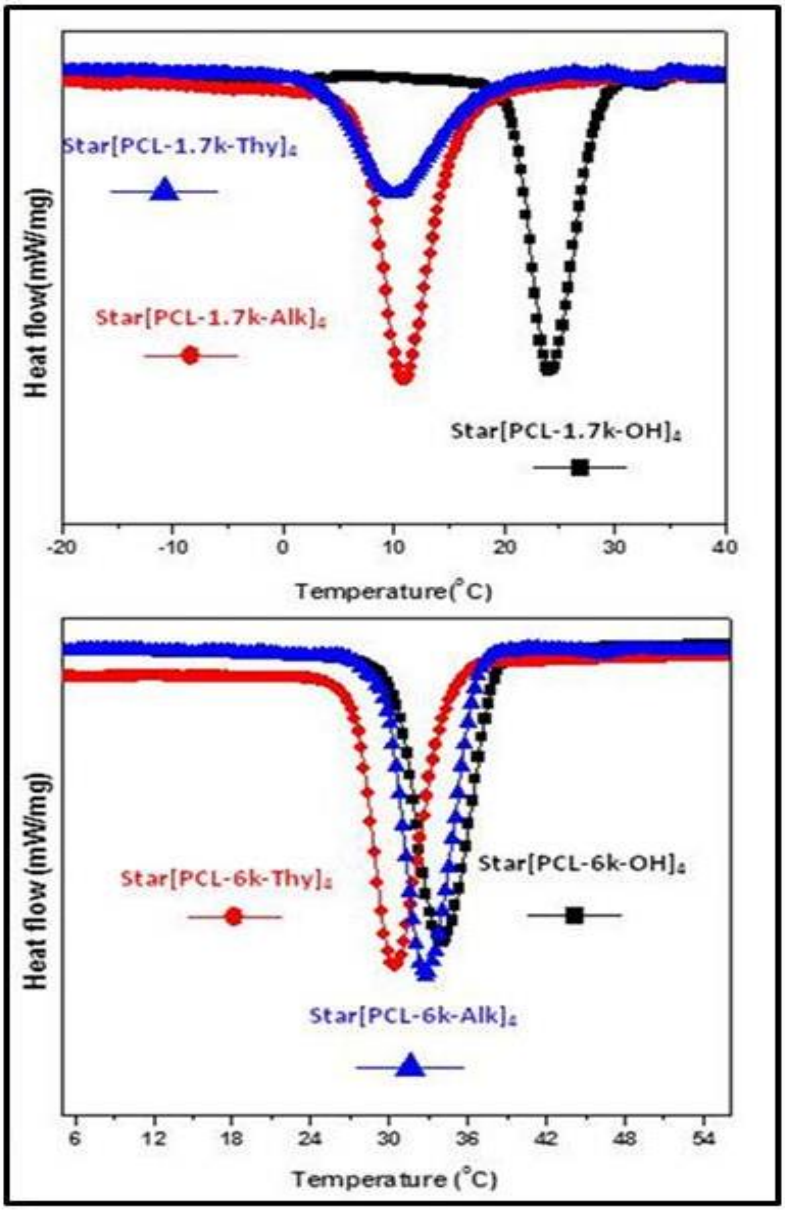


**FIGURE 4.10: DSC thermograms of star shaped poly(Ɛ-caprolactone)s. a) Cooling curves of** Star[PCL-1.7k-OH]$_4$ **(1),** Star[PCL-1.7k-Alk]$_4$ **(2),** Star[PCL-1.7k-Thy]$_4$ **(3). b) Cooling curves of** Star[PCL-6k-OH]$_4$ **(1),** Star[PCL-6k-Alk]$_4$ **(2),** Star[PCL-6k-Thy]$_4$ **(3).**

### 4.1.7 thymine- functionalized star PCL's vs. thymine functionalized linear PCL's

To understand the effect of architecture in case of thymine functionalized poly(Ɛ-caprolactone)s, we compared the thermal properties of linear thymine functionalized PCL

with equivalent total molecular weight of star thymine functionalized PCL, the $T_c$ of star PCL was less than the linear PCL; the similar thing was observed when the linear thymine functionalized PCL was compared with thymine functionalized star PCL having equivalent arm length (Table 4.3). The overall comparison of linear and star shaped PCL also indicates that the % crystallinity was much lower in case of thymine functionalized star shaped PCL. For comparison study of star and linear architecture, the crystallization data of linear PCL was used from literature reported earlier by Binder et. al.[89], those results are used here for comparison

**TABLE 4.3: Thermal analysis of hydroxy-, alkyne-, thymine- functionalized star PCL's and thymine functionalized linear PCL's**

| Sr. No. | Polymer code | $T_m$ ($^oC$) | $\Delta H_m$[a] J/g | $T_c$ ($^oC$) | $\Delta H_c$[b] J/g | $\%X_m$ |
|---|---|---|---|---|---|---|
| 1 | Star[PCL-1.7k-OH]$_4$ **(1)** | 48.2 | 65.0 | 24.1 | 67.0 | 44.5 |
| 2 | Star[PCL-1.7k-Alk]$_4$ **(2)** | 41.8,49.0 | 59.0 | 10.9 | 62.1 | 40.4 |
| 3 | Star[PCL-1.7k-Thy]$_4$ **(3)** | 47.19 | 51.0 | 9.9 | 49.5 | 33.9 |
| 4 | Star[PCL-6k-OH]$_4$ **(1)** | 56.27 | 67.2 | 34.0 | 73.7 | 50.5 |
| 5 | Star[PCL-6k-Alk]$_4$ **(2)** | 55.51 | 62.7 | 32.8 | 71.6 | 49.0 |
| 6 | Star[PCL-6k-Thy]$_4$ **(3)** | 55.06 | 55.0 | 30.3 | 62.0 | 42.5 |
| 7 | LPCL-4.5k-Thy[d] | 55.00 | 82.0 | 36.0 | -- | 58.7 |
| 8 | LPCL-8.8k-Thy[d] | 57.00 | 82.0 | 38.0 | -- | 58.7 |

a: melting enthalpy of the polymer calculated from second heating run.

b: crystallization enthalpy of the polymer in the cooling run.

c: $X_c = (\Delta H_m/\Delta H_m^o)100$; $\Delta H_m^o = 139.6$ J/g

d: linear PCL (ref. ) $M_n$(LPCL-1): 4457g/mol and $M_n$(LPCL-2): 8795 g/mol.

## 4.2 Synthesis of triazine functionalized PIB:

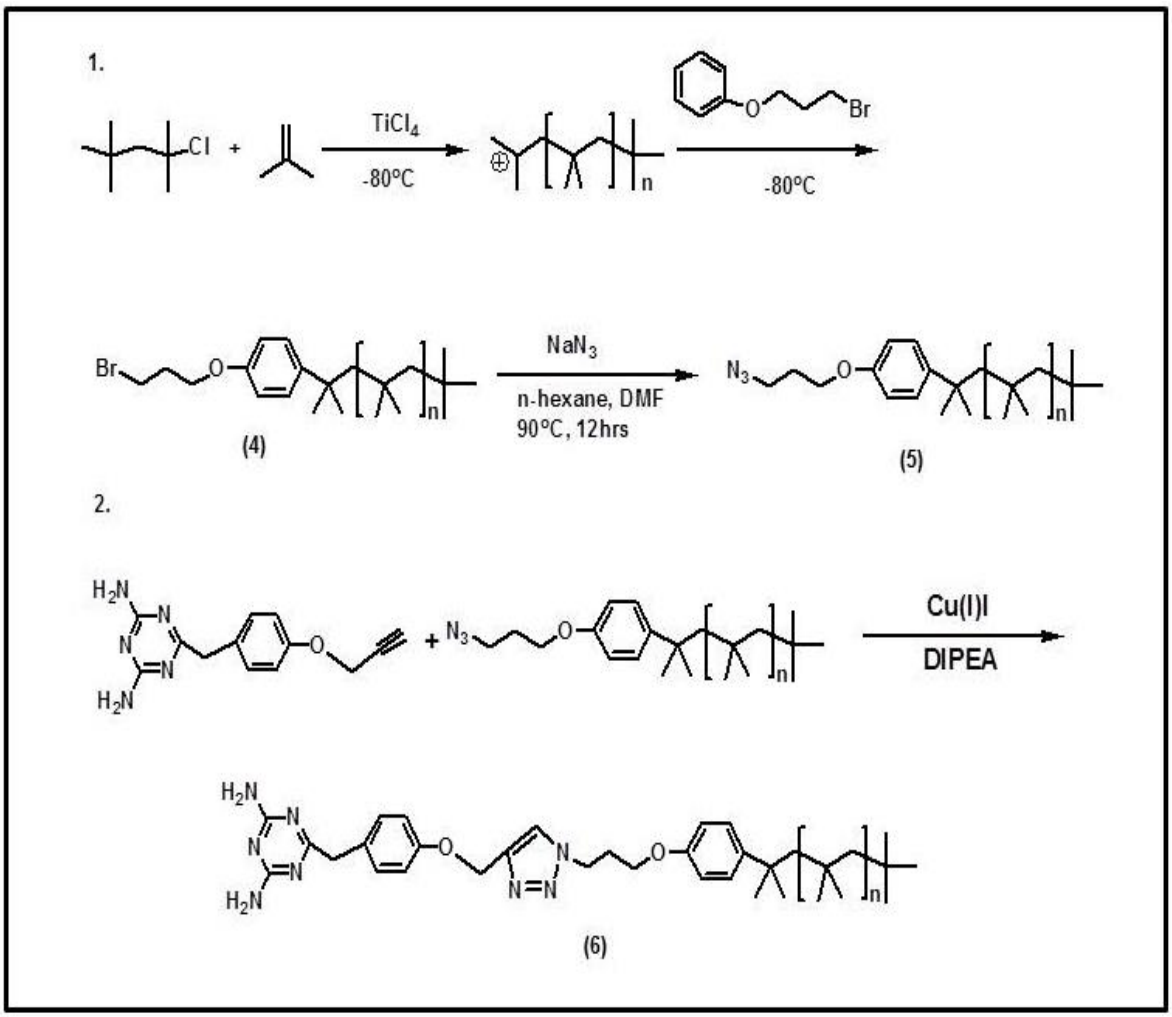


**SCHEME 4.4: Synthesis of triazine functionalized poly(isobutylene) from isobutylene by living carbocationic polymerization.**

The polyisobutylene polymer was selected as soft amorphous block and the triazine functionalized polyisobutylene was prepared through a three step reaction set. Kennedy et. al. has described the synthesis of allyl functionalized PIB. The method used for synthesis was living carbocationic polymerization by using 2-chloro-2,4,4-trimethylpentane/$TiCl_4$ as an initiating system for the polymerization of isobutylene. Quenching with 1-bromo-3-phenoxy propane (BPP) gives the bromo-functionalized PIB chain. The polymerization was carried out at -80$^o$C followed by quenching in same pot at the same temperature. Finally methanol was added to the reaction system to deactivate the $TiCl_4$. After distilling out the solvents from reaction system the product was precipitated in hexane/methanol solvent mixture to remove the unreacted BPP. Furthermore, the conversion of bromo functionalized PIB into azide functionalized PIB was carried out by SN2 reaction with $NaN_3$ (Scheme 4.4).

**Table 4.4 : Polymerization data of poly(isobutylene)**

| Sr. No. | Polymer code | $M_n$(Calc.) g/mol | $M_n$(NMR) g/mol | $M_n$(GPC) g/mol | PDI |
|---|---|---|---|---|---|
| 1 | PIB-3k | 2500 | 2700 | 2600 | 1.2 |
| 2 | PIB-8k | 8000 | 7800 | 7600 | 1.2 |
| 3 | PIB-11k | 12000 | 11500 | 11000 | 1.4 |

Furthermore the triazine group was mounted on PIB chain by Copper-Catalyzed Azide-Alkyne Cycloaddition (CuAAC). The CuAAC reaction between azide functionalized PIB and alkyne functionalized triazine was carried out by using Cu(I)Br as catalyst and DIPEA as a base in a heterogeneous solvent mixture of toluene / isopropanol / water, resulted in to synthesis of 2,6 diaminotriazine functionalized PIB in microwave radiation. The crude product was filtered through a short column of $Al_2O_3$, then unreacted PIB and the excess of 2,4 diaminotriazines were separated by column chromatography of unreacted PIB and the excess of 2,4 diaminotriazines, to obtain a pure product. The polymerization data has been summarized in the table given below and the synthesized products were characterized by $^1$H NMR and GPC.

In $^1$H-NMR (Appendix/ fig. 3)) peak numbers 11 to 15 represents the terminal triazine moiety attached to the PIB chain. The appearance of the triazole proton 10 i.e. singlet at 7.6 ppm confirmed the success of the click functionalization. The multiplet at 0.99 ppm and singlet at 1.8 ppm confirm the presence of initiator in the chain. The peak no. 3 and 4 i.e. multiplets at 1.11ppm and 1.42 ppm represent the repeating units of PIB chain. Peak at 5.04 ppm is the broad peak representing for protons of two $–NH_2$ groups of thymine groups.

## 4.3 Synthesis of hydrogen bonded star shaped PCL-PIB block copolymers:

Supramolecular chemistry is the study of systems involving aggregates of molecules or ions held together by non-covalent interactions, such as electrostatic interactions, hydrogen bonding, dispersion interactions and solvophobic effects. Architecture play important role in crystallization of a polymer. To study the effect of architecture and non-covalent interaction together, a star shaped hydrogen bonded poly(Ɛ-caprolactone)-poly(isobutylene) block copolymers prepared by the interaction of thymine functionalized SPCL and triazine functionalized PIB (Scheme 4.5).

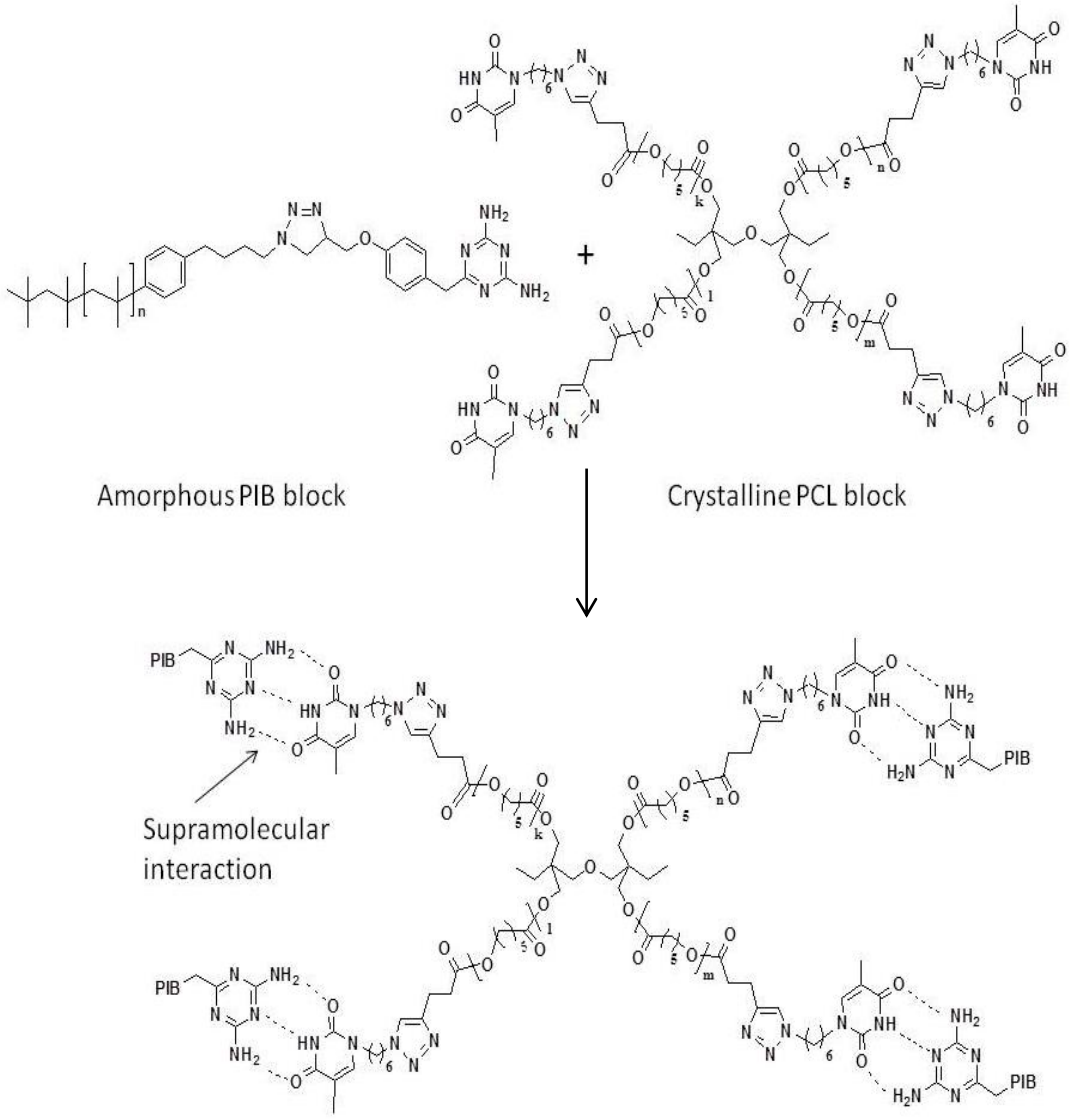


**SCHEME 4.5: Synthesis of star shaped SPCL-PIB supramolecular block copolymer**

Synthesis of supramolecular block copolymer was carried out in non-polar dichloromethane solvent, later on solvent evaporated slowly on rotary evaporator. Prepared supramolecular

BCP's were annealed at 50°C for 48 hrs. In this supramolecular-BCP two $NH_2$ groups and one N atom of triazine moiety form H-bonding with two O atoms and one NH group of thymine respectively. Hence four amorphous PIB chains get connected to one crystalline SPCL molecule by DAD-ADA non-covalent interaction. This interaction is temperature sensitive and reversible.

### 4.3.1 Thermal properties of star shaped supramolecular BCP's:

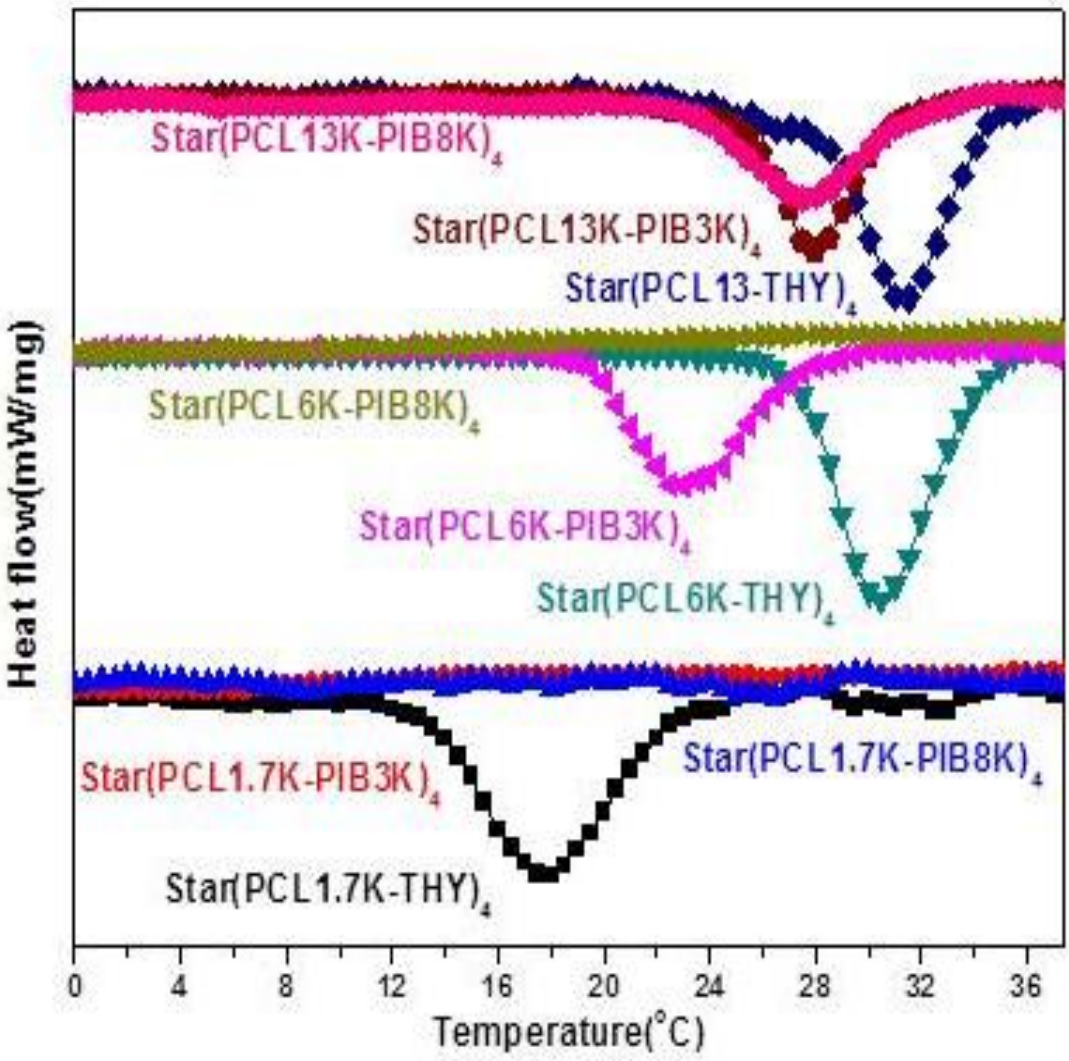


**FIGURE 4.11: Thermal analysis of star shaped SPCL-PIB supramolecular block copolymer**

In order to study the crystallization behaviour of sPCL with less mobile barrier, PIB was used as a second block connected via the thymine and the 2,4-diaminotriazine supramolecular interaction. Each molecular weight of SPCL was connected with low as well as high molecular weight of PIB to study the effect of lower segregation strength (lower $\chi N$) as well as higher segregation strength (higher $\chi N$). All the synthesized supramolecular

BCP's were annealed at 50°C for 48 hours. Modification in thermal properties of SPCL after formation of supramolecular block copolymers was studied by DSC, Fig. 4.11 shows the comparison of cooling curves of thymine functionalized SPCL with their supramolecular BCP's. The analysis shows that the cooling enthalpies (crystallinity) of supramolecular BCP's were lower than their SPCL-homopolymer counterparts. Table 4.5 contains the melting temperatures, changes in melting enthalpies, crystallization temperatures, etc. The high molecular weight star(PCL-13k-THY)$_4$ shows higher crystallinity than Star(PCL-13k-PIB-3k)$_4$, whereas crystallinity further decreases with increase in PIB block length i.e. in star(PCL-13k-PIB-8k)$_4$. In the similar way, crystallinity of Star(PCL-6k-THY)$_4$ is higher than star(PCL-6k-PIB-3k)$_4$, it disappears in case of star(PCL-6k-PIB-8k)$_4$. Crystallinity disappears in case of Star(PCL-1.7k-PIB-3k)$_4$ and Star(PCL-1.7k-PIB-8k)$_4$ whereas its counterpart Star(PCL-1.7k)$_4$ is least crystalline.

**Table 4.5: Thermal analysis of star shaped supramolecular SPCL-PIB supramolecular BCP's.**

| Sr. No. | Polymer code | $T_m$ (°C) | $\Delta H_m$ (J/g) | $T_C$ (°C) | $T_g$ (°C) | $\Delta H_c$ (J/g) |
|---|---|---|---|---|---|---|
| 1 | Star(PCL13-THY)$_4$ | 57 | 68 | 31.6 | -61.1 | 67.5 |
| 2 | Star(PCL13-PIB3K)$_4$ | 56 | 37 | 28 | --- | 43 |
| 3 | Star(PCL13-PIB8K)$_4$ | 57 | 28 | 27.5 | -67.9 | 32 |
| 4 | Star(PCL6k-THY)$_4$ | 55.06 | 55 | 30.3 | 59.1 | 66.0 |
| 5 | Star(PCL6k-PIB3k)$_4$ | 53 | 35 | 23 | -63.9 | 42 |
| 6 | Star(PCL6k-PIB8k)$_4$ | 55 | 22 | --- | -63.8 | -- |
| 7 | Star(PCL1.7k-THY) | 47.19 | 51 | 9.9 | -57.8 | 49.5 |
| 8 | Star(PCL1.7k-PIB3k)$_4$ | 45 | 7.5 | --- | -62.6 | --- |
| 9 | Star(PCL1.7k-PIB8k)$_4$ | --- | ---- | --- | -63.6 | ---- |

### Star shaped supramolecular BCP's vs. linear supramolecular BCP's:

**Table 4.6 : Comparison of linear and star architecture of supramolecular block copolymer.**

| Sr. No. | Sample | $T_m$ | $\Delta H_m$ (J/g) | $f_{PCL}$ | $T_c$ | $\Delta H_c$ (J/g) |
|---|---|---|---|---|---|---|
| 1 | Star(PCL6k-THY)$_4$ | 55.06 | 55 | 0.400 | 30.3 | 61 |
| 2 | Star(PCL6K-PIB8K)$_4$ | 55 | 22 | 0.360 | No $T_c$ observed | Not observed |
| 3 | Linear PCL5K-Thy | 57 | 83 | 0.613 | 34 | 83 |
| 4 | Linear-PCL5K-PIB7K | 56 | 37 | 0.677 | 25 | 34 |
| 5 | Star(PCL1.7k-THY) | 47.19 | 51 | 0.369 | 9.9 | 39.2 |
| 6 | Star(PCL1.7k-PIB8k)$_4$ | --- | --- | 0.0 | --- | --- |

$f_{PCL}$: Degree of crystallinity of the PCL components calculated from $f_c=(\Delta H_m M_n)/(\Delta H_m^{100\%} M_{PCL})$, where $\Delta H_m$ is the measured melting enthalpy, $\Delta H_m^{100\%}$=146 J/g is the melting enthalpy for 100% crystalline PCL.

To understand effect of architecture on crystallinity of supramolecular BCP, star shaped supramolecular BCP were compared with linear supramolecular BCP (Table 4.6). star(PCL6k-THY)$_4$ shows crystallization peak at 30.3$^o$C with enthalpy change 61J/g which does not show crystallinity after block copolymer formation, whereas Linear-PCL5K-PIB7K which is having almost similar molecular weight like star(PCL6K-PIB8K)$_4$, shows crystallization temperature 25$^o$C with enthalpy change 38J/g. Hence architecture reduced the crystallinity of BCP.

### 4.3.2 SAXS analysis of star shaped supramolecular BCP:

SAXS is an important tool to understand the microstructure of a polymer. The temperature dependent SAXS measurements were carried out in range of 20$^o$C to 140$^o$C. There are various morphologies are possible in BCP's e.g. BCC (body centered cubic structure), HCP (hexagonal close packing) or lamellar morphology. These morphologies are generally depending on the block ratio of a block copolymer. SAXS analysis of star shaped

supramolecular BCP's are summarized in the table given below. Three different molecular weights of star shaped thymine functionalized poly(Ɛ-caprolactone) were connected with two different molecular weights of PIB, to form six different block copolymers. SPCL homopolymer shows a crystallization peak at q=0.04/A$^o$. PIB-3K-Triazine and PIB-8K-Triazine homo-polymers show d-spacing of 7.05 nm and 9.96 nm respectively.

**TABLE 4.7: SAXS analysis of supramolecular star shaped SPCL-PIB block copolymers**

| Sr. No. | Polymer | Morphology | q (1/A$^o$) | d (nm) | $d_{cryst}$ (nm) |
|---|---|---|---|---|---|
| 1 | PIB3K | BCC | 0.090 | 7.05 | --- |
| 2 | Star(PCL**13**K-PIB**3**K)$_4$ | BCC | 0.090 | 7.05 | 13.6 |
| 3 | Star(PCL**6**K-PIB**3**K)$_4$ | BCC | 0.090 | 7.05 | 13.6 |
| 4 | Star(PCL**1.7**K-PIB**3**K)$_4$ | HCP | 0.035 | 17.9 | ---- |
| 5 | Star(PCL**13**K-PIB**8**K)$_4$ | BCC | 0.063 | 9.96 | 15.3 |
| 6 | Star(PCL**6**K-PIB**8**K)$_4$ | ---- | 0.063 | 9.96 | ---- |
| 7 | Star(PCL**1.7**K-PIB**8**K)$_4$ | Lamella | 0.025 | 25.1 | ---- |

Star(PCL13K-PIB3k)$_4$ and star(PCL6K-PIB3k)$_4$ show similar d-spacing like their homopolymer block- PIB-3k-Tri i.e. 7 nm. Similarly star(PCL13K-PIB8K)$_4$ and star(PCL6K-PIB8K)$_4$ show same d-spacing like their homopolymer block PIB-8K i.e. 9.96 nm, which indicates that PIB chains form clusters due to the formation of unspecific hydrogen bonds between triazine groups of PIB which results into ***macrophase*** separation of PCL and PIB chains.(Fig 4.12 & Fig 4.13)

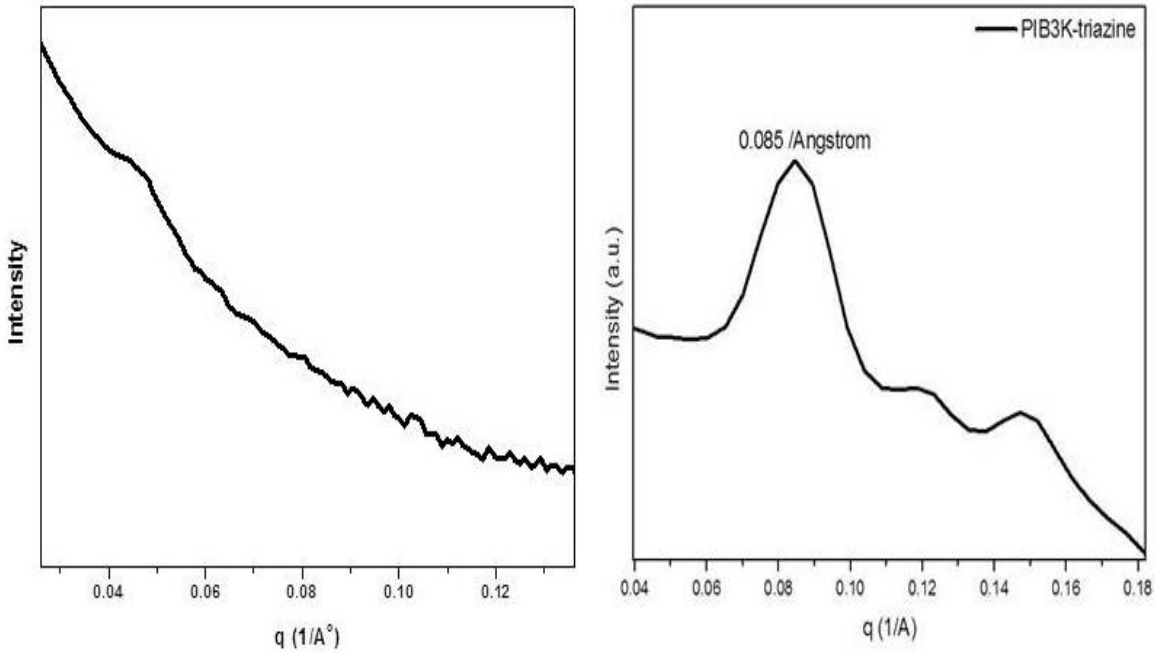


**Fig. 4.12 SAXS analysis of homopolymers (a) star shaped thymine functionalized PCL (b) PIB-3K-triazine**

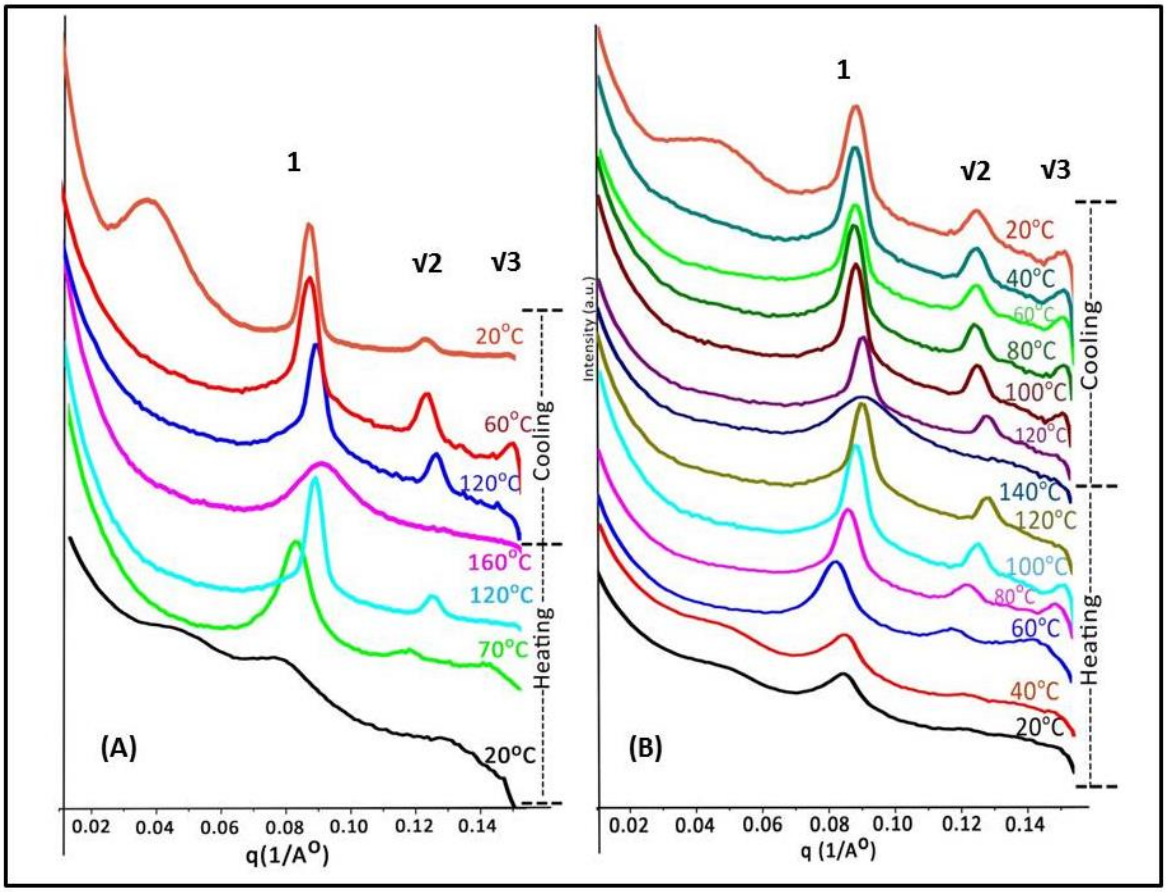


**Fig. 4.13 SAXS analysis: Macrophase separation of Supramolecular BCP's (A) Star(PCL13K-PIB3k)$_4$ and (B) Star(PCL6K-PIB3k)$_4$.**

But the d-spacing values increases in case of Star(PCL1.7K-PIB3k)$_4$ and Star(PCL1.7K-PIB8k)$_4$ block copolymers to 17nm and 15 nm respectively, which indicates that microphase separation takes place in BCPs of low molecular weight SPCL. In comparison with homopolymers, the fluctuation of SAXS peaks in Star(PCL1.7K-PIB3K)$_4$ and Star(PCL1.7K-PIB8k)$_4$ block copolymers shows that the hydrogen bonds between thymine and 2,4-diaminotriazine are in closed state. (Fig. 4.14)

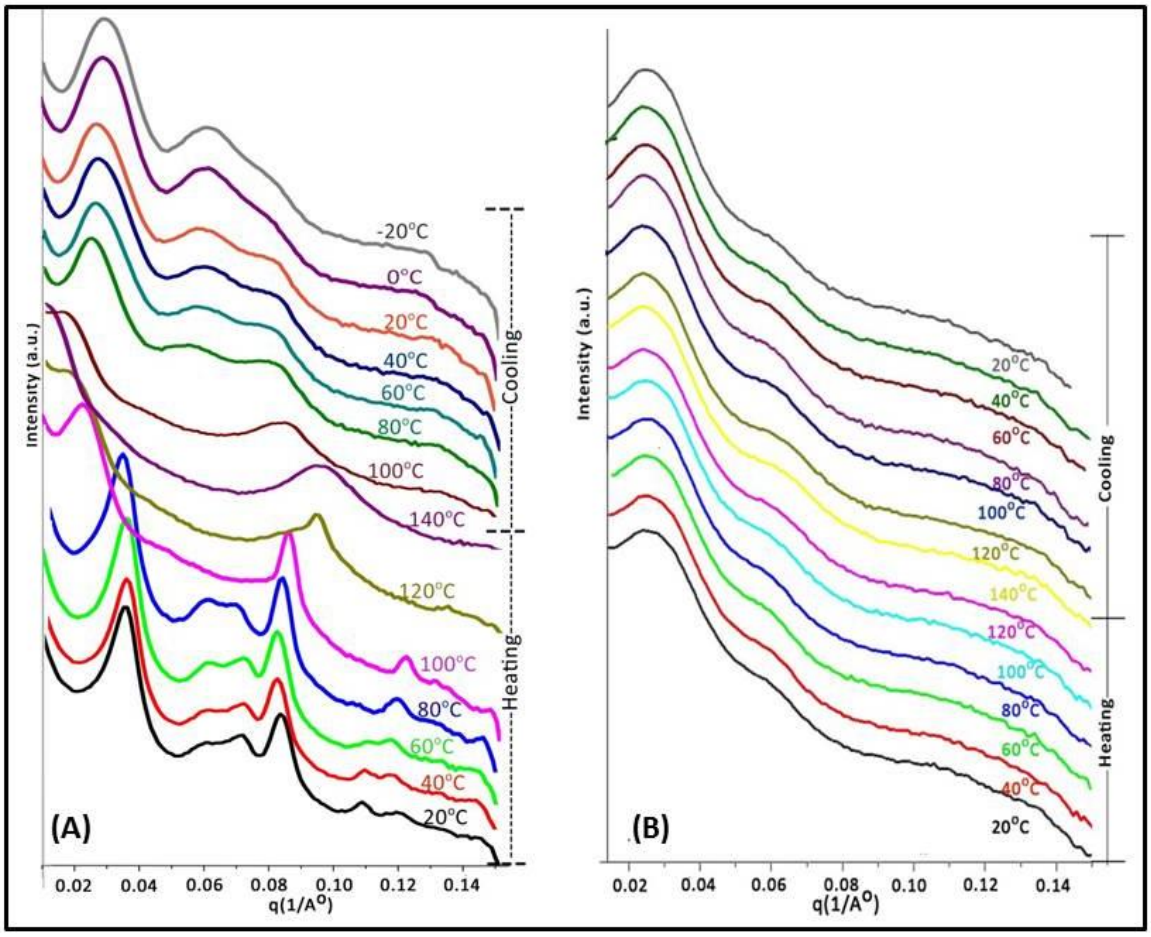


**Fig. 4.14 SAXS analysis: Microphase separation of Supramolecular BCP's (A) Star(PCL1.7K-PIB3k)$_4$ and (B) Star(PCL1.7K-PIB8k)$_4$.**

### 4.3.3 AFM analysis of star shaped supramolecular SPCL-PIB block copolymers:

To confirm the phase separation results obtained by SAXS analysis, additional AFM analysis was carried out (Fig 4.15). Two selected star supramolecular BCP's Star(PCL1.7K-PIB3K)$_4$ and Star(PCL13K-PIB3K)$_4$ were used for AFM analysis. AFM image of Star(PCL13K-PIB3K)$_4$ clearly shows macrophase separation whereas that of Star(PCL1.7K-PIB3K)$_4$ shows that there is no existence of macrophase separation. Hence SAXS and AFM data indicate that the BCP's containing high molecular weight SPCL i.e. Star(PCL13K-PIB3K)$_4$, Star(PCL13K-PIB8K)$_4$, Star(PCL6K-PIB3K)$_4$ and Star(PCL6K-PIB8K)$_4$ forms the macrophase separated structures, whereas the BCP's Star(PCL1.7K-PIB3K)$_4$ and

Star(PCL1.7K-PIB8K)$_4$ containing low molecular weight SPCL form microphase separated structures.

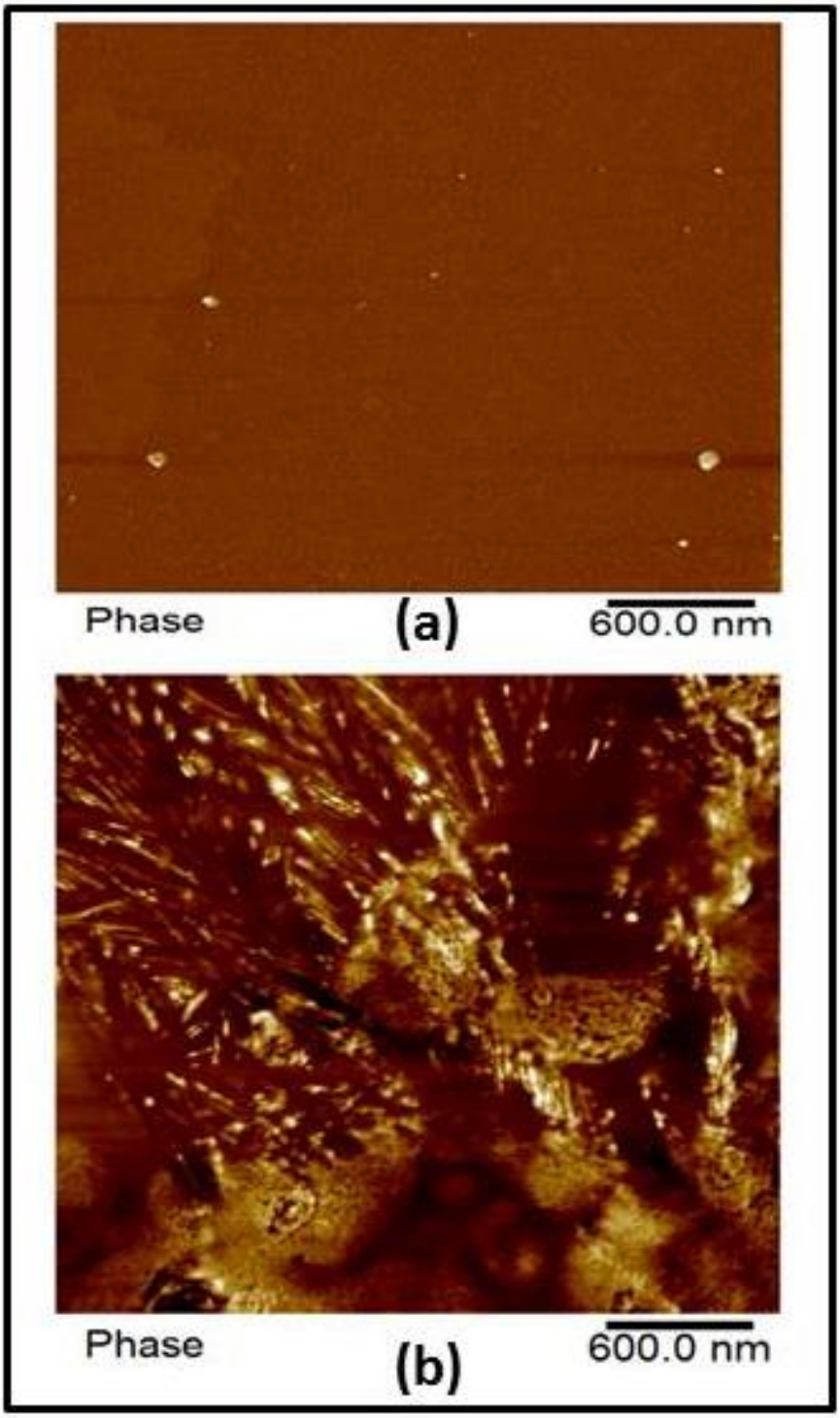


**Fig. 4.15: AFM analysis of star shaped supramolecular SPCL-PIB block copolymers (a) Star(PCL1.7K-PIB3K)$_4$ and (b) Star(PCL13K-PIB3K)$_4$.**

The above discussion about microphase and macrophase separation is summarized in a table below (Table 4.8)**.**

**TABLE 4.8: Macrophase and microphase separation in star shaped sPCL-PIB block copolymers**

| Sr. No. | Polymer | Phase separation |
|---|---|---|
| 1 | Star(PCL**13**K-PIB**3**K)$_4$ | Macrophase |
| 2 | Star(PCL**13**K-PIB**8**K)$_4$ | Macrophase |
| 3 | Star(PCL**6**K-PIB**3**K)$_4$ | Macrophase |
| 4 | Star(PCL**6**K-PIB**8**K)$_4$ | Macrophase |
| 5 | Star(PCL**1.7**K-PIB**3**K)$_4$ | **Microphase** |
| 6 | Star(PCL**1.7**K-PIB**8**K)$_4$ | **Microphase** |

## 4.4 Synthesis of supramolecular star poly(Ɛ-caprolactone) network:

Supramolecular polymer networks are the network of macromolecules consisting of characteristics of chemical and physical networks, connected by non-covalent interactions such as H-bonding, ionic interaction, π-π interactions, transition metal complexation, etc. Assembly of these materials are strong materials whereas they can easily be easily disassembled. In most of the cases chemical modification of polymeric chains allows them to be tailored as per specific need. These polymers are useful in self-healing materials, drug delivery, tissue engineering, etc.[113]

Few numbers of supramolecular networks of PCL chains are reported for various purposes. The rheology of various supramolecular PCL polymers with two or more ureido-pyrimidinone was studied by Sijbesma et. al. The branched polymers formed the supramolecular networks by dimerization of ureido-pyrimidinone. After crosslinking the supramolecular networks did not show platue whereas the optical microscopy, WAXS, and

DSC experiments indicated that the formation of crystallites is prevented by network.[114] The same strategy was used to prepare supramolecular network of polyethylene oxide and ethylene oxide block copolymers, the incorporation of ureido-pyrimidinone or urea units in trifunctional telechelic polyether polyols by the selective reaction sequence of IMCI results in the formation of H-bonded supramolecular network.[115] Pyridyl terminated four arm star shaped polymer also formed supramolecular network with disulfonic acids as well as adipic acid, shown a thermoreversible organogel-solution behaviour in DMF, ethanol, and methanol. The crystallization temperature and enthalpy change of that were lower in case of supramolecular network than that of its precursors.[116]

**Synthesis of supramolecular star poly(Ɛ-caprolactone) network:**

The synthesis of supramolecular network of thymine functionalized star PCL was prepared by using a di-triazine connector i.e. 4,4-Bis-[3-(2,4-Diamino-[1,3,5]-triazin-6-yl)-phenoxy]benzophenone. Two separate solutions of both components in THF were mixed together, filtered and dried and annealed at 60$^{o}$C for three days to promote hydrogen bond formation and achieve equilibrated conditions. The synthetic reaction scheme is shown in the scheme 4.6. The networks of three different molecular weights were prepared and their thermal properties were studied.

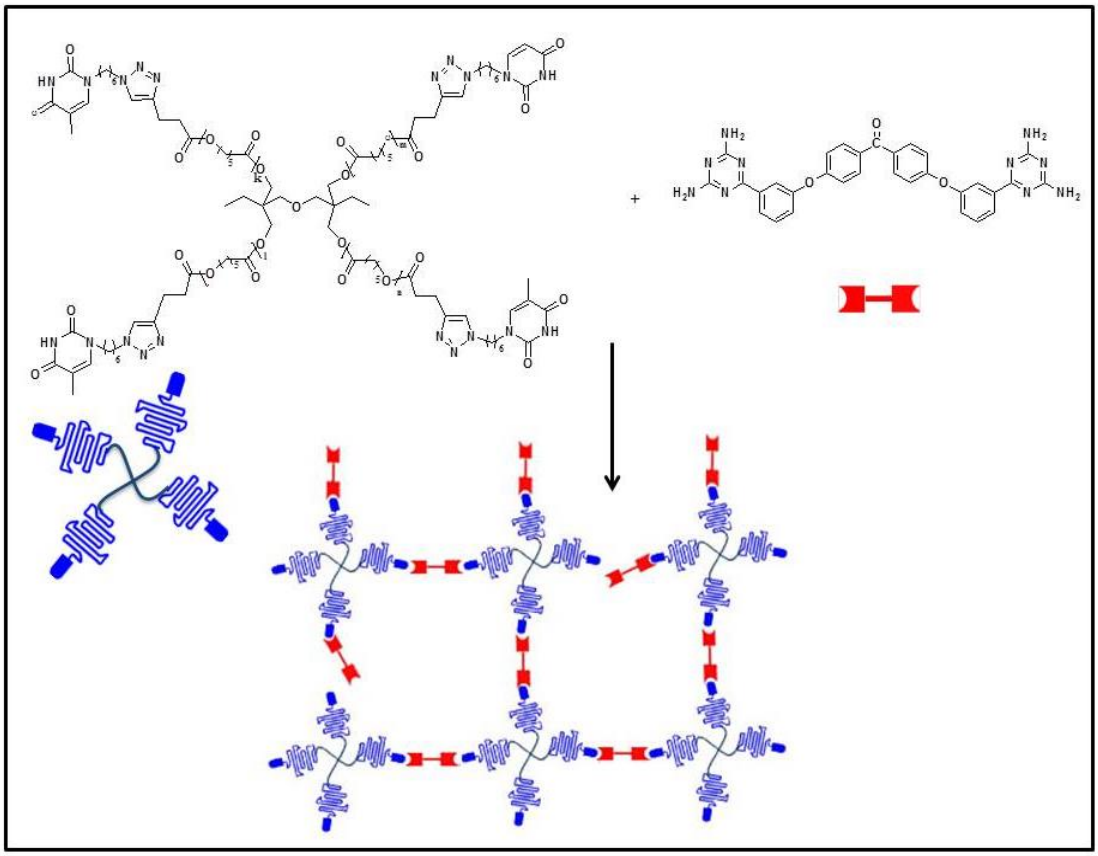

**Scheme 4.6: Synthesis of supramolecular star poly(Ɛ-caprolactone) network**

**Thermal analysis of supramolecular star poly(Ɛ-caprolactone) network:**

The thermal properties of synthesized polymer networks were studied using differential scanning calorimetry i.e. DSC. Table 4.9 shows the comparison of thermal characteristics of the three different molecular weights of the homopolymers with their supramolecular networks. The thermal behaviour of synthesized supramolecular networks differs distinctly from homopolymers as the crystallization temperatures of the networks are much lower compared to homopolymers. Entry no. 1 & 2 show the difference between thermal properties of high molecular weight homopolymer and its network, indicate slight decrease in the crystallization temperature after network formation. The large shift of crystallization temperature was observed in case of medium size molecular weights, entry no. 3 & 4 show a shift of $T_c$ from 30.3$^o$C to -17$^o$C i.e. shift of 47$^o$C. Entry 5 & 6 show the comparison of lowest molecular weight homopolymer with its network, indicate no crystallization as well as melting temperature in its supramolecular network due to shorter chain length. The melting temperatures were not much affected after network formation whereas crystallinity was lower in case of networks which completely disappeared in lowest molecular weight networks.

**TABLE 4.9 Thermal properties comparison of star shaped PCL with their networks.**

| Sr. No. | Polymer | $T_m$ ($^o$C) | $\Delta H_m$[a] J/g | $T_c$ ($^o$C) | $\Delta H_c$ (J/g) |
|---|---|---|---|---|---|
| 1 | star-(PCL13K-Thy)$_4$ homopolymer | 57 | 68 | 31.6 | 67.5 |
| 2 | star-(PCL13K-Thy)$_4$- network | 56 | 54 | 20.8 | 56 |
| 3 | star-(PCL6K-Thy)$_4$ homopolymer | 55.06 | 55 | 30.3 | 66.0 |
| 4 | star-(PCL6K-Thy)$_4$ - network | 53 | 37 | -17 | 40 |
| 5 | star-(PCL1.7K-Thy)$_4$ homopolymer | 47.19 | 51 | 9.9 | 49.5 |
| 6 | star-(PCL1.7K-Thy)$_4$- network | No $T_m$ | ---- | No $T_c$ | ---- |

**SAXS analysis of supramolecular networks:**

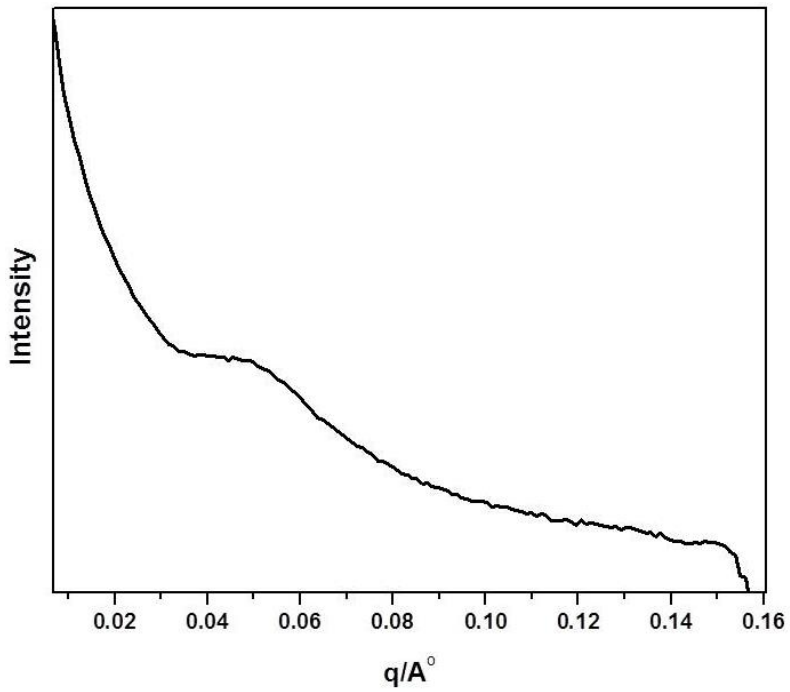


**Fig. 4.16 SAXS analysis of supramolecular network star-(PCL6K-Thy)$_4$-NET**

The SAXS data of star-(PCL6K-Thy)$_4$ – NET has shown quite similar nature like its homopolymer. The spectrum shown only one crystalline peak like homopolymer at q=0.046 and it indicates that there is no ordered structure.

# Chapter 5: Multivalent Photo-cleavable Initiators for polymerization of lactones

The combination of photochemistry and polymer chemistry has opened a wide range of new synthetic materials and applications thereof. One of them, photo-cleavable polymers are the polymers containing photo-cleavable unit which get cleaved after exposure to UV-light, and hence light acts as a stimuli to change properties of the materials. Photo-cleavable polymers have received more attention since they can be degraded or cleaved into smaller molecular fragments or polymer chains by light irradiation, which holds great promise for many applications in broad fields including drug release, gene delivery, nanocontainers, biomaterials, and photodynamic therapeutics, etc.[117] Such polymers are basically containing a photosensitive chemical moiety, called as photo-cleavable junctions. Numbers of such junctions are reported till now e.g. *o*-nitrobenzyl alcohol derivatives, α-ketoester derivatives, benzoin esters, phenacyl esters, acyling agents, etc. Amongst them *o*-nitrobenzyl esters are mostly used as photo-cleavable junction in polymers, which on photo-isomerization yields *o*-nitrobenzyl aldehyde. Mechanism of photo-chemically induced photo-isomerization is as shown below. [117,118]

Photochemistry is the study of chemical reactions and isomerisation's which occur under the influence of visible (wavelength from 400 to 750 nm) and/or ultraviolet (wavelength from 100 to 400 nm) light. A photochemical reaction is the reaction between atoms, molecules and light which is initiated by electronically excited molecule by the absorption of a photon. Electronic transitions involves a shift of one electrons from a lower to a higher energy molecular orbital and these molecular orbitals are associated with a specific part or functional group of the molecule called as chromophore e.g. –NO2, carbonyl, N=N, C-S, C-Br etc. The energy in a mole of photons at 365 nm is 130 times more than the thermal energy available to activate a reaction at 25$^{o}$C, whereas at 254 nm the photons have 190 times more energy than kT at 25$^{o}$C. Thus, photochemical reactions are readily initiated upon irradiation and subsequent absorption. Photon contains higher energy, due to which light enables chemical processes to occur at ambient conditions. The application of photochemistry in polymer field has been increased widely in recent years, which includes photo-polymerization, polymer degradation, polymer functionalization, etc. In field of polymers photo-initiated polymerization and photo-polymerization are used in photography, litho-printing and circuits in electronic industry.[119,120]

## 5.1 Photochemical reactions:

The photo-induced transformations in chromophores such as azobenzene are the **photo-induced isomerization** reactions. On irradiation with specific wavelength of light, azobenzene undergoes *trans* → *cis* isomerization, and the reverse *cis* →*trans* isomerization of these azobenzenes can be conducted by light or by thermal energy in the dark.[120,121]

For example, vinyl copolymers carrying crowned azobenzene and biphenyl moieties at the side chain, UV-light-induced isomerization of the azobenzene moiety results in some disorder in the crown ether moiety, thus decreasing ionic conductivity. In another example, the trans-cis isomerization of chiral azobenzene has enhanced the change in the transmitted light intensity**,** which is attributable to a cooperative alignment of mesogens in ferroelectric polymer liquid crystal, owing presumably to induced dipoles by the photoisomerization. The composite asymmetrical membranes based on poly(vinyl alcohol)-co-ethylene as the host material and new polyethers that contain azobenzene moieties in the side chain, when irradiated with UV light, the morphology of the top surfaces changes drastically. The contact angle with water decreased about 30$^{o}$ on the top membrane surfaces due to the enhanced concentration of azo polymer on the top surface as well as due to conformational change in copolymer caused by photo-irradiation. [122-124]

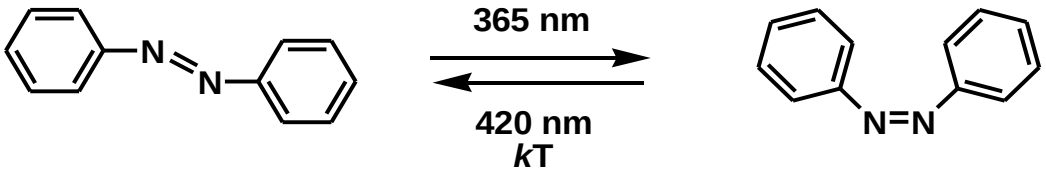


**FIGURE 5.1: Photo-induced cis-trans transformations in azobenzene**

Another type of photochemical reaction is bond forming reaction. Thiol-ene reaction has very broad applications in both polymer as well as synthetic chemistry, which includes synthesis of cross-linked polymer composites, development of initiator-free reaction conditions,[125] selective functionalization and modification of molecular structures,[126] functionalization of polymer side chains using thiol-ene coupling conditions[127]

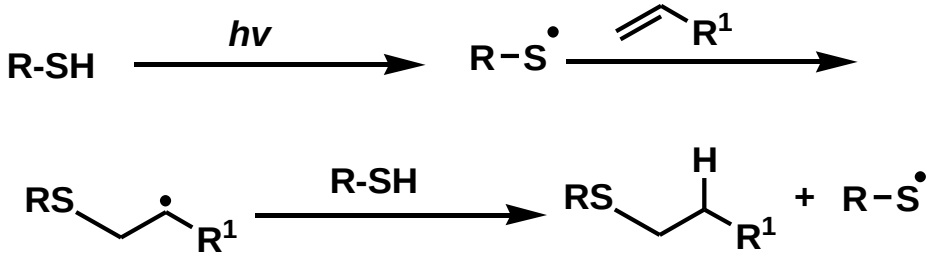


**FIGURE 5.2: Thiol-ene reaction between thiol and alkene**

In this process, two thiol groups react with one ethynyl group via a two-step reaction to yield fully additive product with branched structure. The application of thiol-yne click polymerization to synthesize polymers with topological structures especially for synthesis of

photo-initiated sulphur containing hyperbranched polymers is well known.[128] Reactions of octanethiol, pentaerythritol tetra(3-mercaptopropionate) (PETMP), and butyl 3-mercaptopropionate with various alkynes such as 1-octyne, propargyl acetate, methyl propargyl ether, ethyl propiolate, methyl propargylamine, 2-octyne, and cyclooctyne have been reported in order to study the reaction rates, mechanism and step growth formation. [129,130]

**Photo-initiated CuAAC** click reactions are well controllable by choosing appropriate light intensities, which control the copper concentration of the system and consequently, coupling efficiency. Photoinduced copper(I)-catalyzed Huisgen 1,3- dipolar cycloaddition (CuAAC) has been has been reported by Yagsi et. al. to synthesize various macromolecular architectures including telechelic polymers and block copolymers. e.g. reaction of azide functionalized polystyrene with various alkyne moieties like propargyl alcohol, 4-pentynoic acid, propargyl pyrene to synthesize telechelic polymers, and with alkyne functionalized PCL to synthesize (PSt-b-PCL) block copolymer. [131]

**Photo-cleavable reactions**:

The interesting feature of photolabile protecting groups or linkers is that they break bonds smoothly by using light only, they don't need harsh conditions like strong acids or nucleophiles which are frequently required, hence photochemical cleavage solve the problems associated with sensitive compounds.[118]

There are several photo-cleavable linkers are reported till date. The photo-oxidation of **α-keto esters** on irradiation with Xe/UV lamps in the presence of $O_2$ results in controlled release of the desired aldehydes and ketones, having bodycare or household applications, such as shampoos, cleaners, fabric softeners and detergents.[132,133] Another linker **2-benzoylbenzoate esters** of primary and secondary alcohols, on photolysis in the presence of a hydrogen donor such as 2-isopropanol or an electron donor such as primary amines gives the corresponding alcohol.[134] Benzyl esters dissociate on irradiation with ultraviolet light, hence a it is a well-known photo-cleavable linker, the photolytic fission involves a heterolysis of the benzyl-oxygen bond.[135-137]

An *o*-nitrobenzyl (ONB) linker is the favourite photo-responsive molecule due to its chemical stability and rapid cleavage by near-UV irradiation (wavelength>320 nm). The o-nitrobenzyl group is get used frequently in field of polymer and materials science, variety of research papers for various purposes have been reported on photo-cleavable materials containing o-nitrobenzyl linkage. *o*-nitrobenzyl derivatives are the wellknown photoprotecting groups used for alcohols, amines, thiols etc. Photocleavage of *o*-nitrobenzyl ether gives alcohol and nitroso biproduct, whereas photocleavage of *o*-nitrobenzyl thioether results in thiol and nitrosobenzaldehyde formation. The *o*-nitro benzyl esters are widely used photocleavable compounds. The irradiation of UV light on *o*-nitrobenzyl esters results in synthesis of

carboxylic acid and *o*-nitrosobenzaldehyde. When amines get protected with [(*o*-nitrobenzyl)oxy]carbonyl groups, it acts as a photogenerator of organic base, the resulting protected amines on photocleavage liberate free amine in solid and solution state. The photocleavage of *o*-nitrobenzyl derivatives from the carboxylic function can be shown below. [118,138-140]

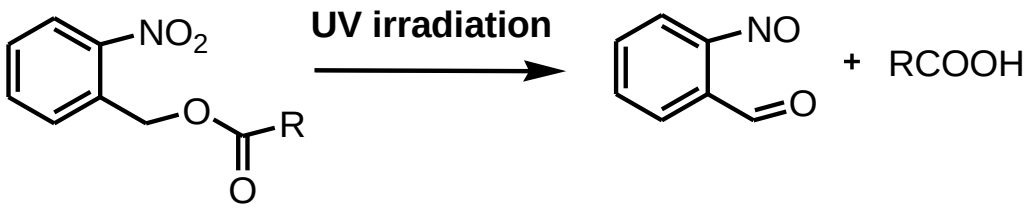


**FIGURE 5.3: Photo-cleavage of *o*-nitrobenzyl ester into aldehyde and carboxylic acid.**

**Table 5.1: Photocleavable linkers**

| Sr. No | Photocleavable linker | Wavelength | Reference |
|---|---|---|---|
| 1 | α-keto esters | 350 nm | 133 |
| 2 | 2-benzoylbenzoate esters | 366nm | 134 |
| 3 | *o*-nitrobenzyl (ONB) | >320 nm | 118,138-140 |

## Photocleavable polymers:

The synthesis of single-/two-photon sensitive monomer, (E)-5-(4-ethoxystyryl)22-nitrobenzyl methacrylate and its copolymer with methyl methacrylate gives a series of photosensitive copolymers having micro-patterning application.[141] Micelles of PEO-b-poly(disulfide-alt-nitrobenzene)-b-PEO whose hydrophobic block contains one disulfide and two o-nitrobenzyl methyl ester groups in the repeating unit, disintegrate under the effect UV light that cuts the o-nitrobenzyl methyl ester groups, the study shows that photo-induced degradation of the BCP micelles is much faster than the reduction-induced degradation.[142] Mc Grath et. al. synthesized photolabile dendrimers containing o-nitrobenzyl ether as a photolabile core with several sites for attachment of dendrons, afterwards studied their photo-cleavage.[143] The block copolymer synthesized by using o-nitrobenzyl-substituted poly(g-methyl-e-caprolactone) (PmCL-ONB) as the hydrophobic block, and poly(acrylic acid) (PAA) as the

hydrophilic block containing a photo-cleavable linker at its junction, they can self-assemble into different structures, including micelles and vesicles which are photo-responsive, having application in the release of large hydrophilic molecules such as b-cyclodextrin.[139]
Photocontrolled release of a model hydrophobic guest from light-dissociable polymer micelles of photoactive amphiphilic diblock copolymer composed of PEO and poly(2-nitrobenzyl methacrylate) (PNBM), upon UV light irradiation, the photosolvolysis of pyrenyl methyl esters cleaves the pyrene moiety from the polymer which converts the hydrophobic block into hydrophilic poly(methacrylic acid) (PMA), which leads to straightforward dissociation of BCP micelles.[144]

Photocleavage of polystyrene-*block*-poly(methyl methacrylate) copolymers containing [4*ð* + 4*ð*] anthracene photodimer at the junction point between the blocks (PS-AA-PMMA) gives the parent homopolymer blocks, which produces various domain sizes and morphologies.[145]
The photocleavable star polymers were prepared by the combination of Atom transfer radical polymerization (ATRP) and the copper-catalyzed azide-alkyne cycloaddition (CuAAC). In detail, first a tetravalent azide was connected with four chains of photo-cleavable moiety having bromo group and alkyne group on either sides by CUAAC, which furthermore acts as a ATRP initiator to prepare star shaped photo-cleavable polymer, this star polymer acts as a precursor for photodegradable model network.[146] Synthesis of photo-cleavable Poly(styrene-*block*-ethylene oxide) having *o*-nitrobenzyl (ONB) group at the junction of two blocks by atom transfer radical polymerization (ATRP) using a ONB-functional PEO macroinitiator. This BCP can be utilised in the fabrication of nanoporous thin films.[147] Triblock copolymer of which the end poly(ethylene oxide) block is water-soluble (PEO) and the middle hydrophobic block polyurethane containing nitrobenzyl groups (PEO-b-PUNB-b-PEO) forms micelles with photodegradable core, which can be disintegrated very quickly on photo-irradiation.[148] Another method i.e. combination of RAFT and click was used for synthesis of photocleavable Poly(styrene-b-ethylene oxide) block copolymer with an o-nitrobenzyl ester photo-cleavable junction, the synthesized BCP formed highly ordered nanoporous thin films.[149] In order to study the effects of space confinement and chain confinement on the crystallization of long chains confined in microphase separated nanocylinders, the photo-cleavable PCL-block-polystyrene (PCL-b-PS) block copolymer containing ONB group at its junction was prepared.[150] Synthesis of rod like core-crystalline micelles of *polyferrocenyldimethylsilane-block-poly(2-vinylpyridine)* block copolymer with a photo-cleavable o-nitrobenzyl ester (ONB) group at the junction and their photo-cleavage have been studied, the rod like micelles maintained their colloidal stability even after 70% of the corona chains had been cleaved.[151]

The above mentioned all polymers are summarized in a table below with their citation.

**Table 5.2: Photo-cleavable polymers**

| Sr. No. | Polymer | Linker | Study | Reference |
|---|---|---|---|---|
| 1 | (E)-5-(4-ethoxystyryl)22-nitrobenzyl methacrylate and its copolymer | *o*-nitrobenzyl ester (ONB) | Micropatterning application | 141 |
| 2 | PEO-b-poly(disulfide-alt-nitrobenzene)-b-PEO | *o*-nitrobenzyl methyl ester groups | Photo-induced degradation vs. reduction-induced degradation | 142 |
| 3 | photolabile dendrimers | *o*-nitrobenzyl ether | a photolabile core with several sites for attachment of dendrons | 143 |
| 4 | poly(g-methyl-e-caprolactone) (PmCL-ONB) | *o*-nitrobenzyl ester (ONB) | release of large hydrophilic molecules such as b-cyclodextrin | 139 |
| 5 | diblock copolymer composed of PEO and poly(2-nitrobenzyl methacrylate) (PNBM) | pyrenyl methyl esters | dissociation of BCP micelles | 144 |
| 6 | Polystyrene-*block*-poly(methyl methacrylate) | anthracene photodimer | Various polymer morphologies | 145 |
| 7 | (PEO-b-PUNB-b-PEO) | nitrobenzyl groups | micelles with photodegradable core | 148 |
| 9 | (PCL-b-PS) | *o*-nitrobenzyl ester (ONB) | crystallization of long chains confined in microphase separated nanocylinders | 150 |
| 10 | polyferrocenyldimethylsilane-block-poly(2-vinylpyridine) | *o*-nitrobenzyl ester (ONB) | colloidal stability | 151 |

## 5.2 Three arm photo-cleavable initiator

### 5.2.1 Synthesis of the three arm photo-cleavable initiator (8)

Triazine derivatives have many important applications bio-medical research fields, e.g. cancer chemotherapeutic agents, multidrug resistance modulators and tri-functional scaffolds in bundle protein preparation,[152] as well as in pharmaceutical, textile, plastic, and rubber industries.[153] Cyanuric chloride is a less expensive and widely used reagent for the synthesis of 1,3,5-triazine derivatives and also has selective reactivity of three chlorine atoms towards various nucleophiles. Therefore it is also used in hyperbranched polymers and dendrimers synthesis.[154-156] There are various photo-cleavable initiators for ring opening polymerization of lactones are reported till now, but in order to synthesize star architecture of poly-lactones, we planned the synthesis of trivalent- and hexavalent alcohols.

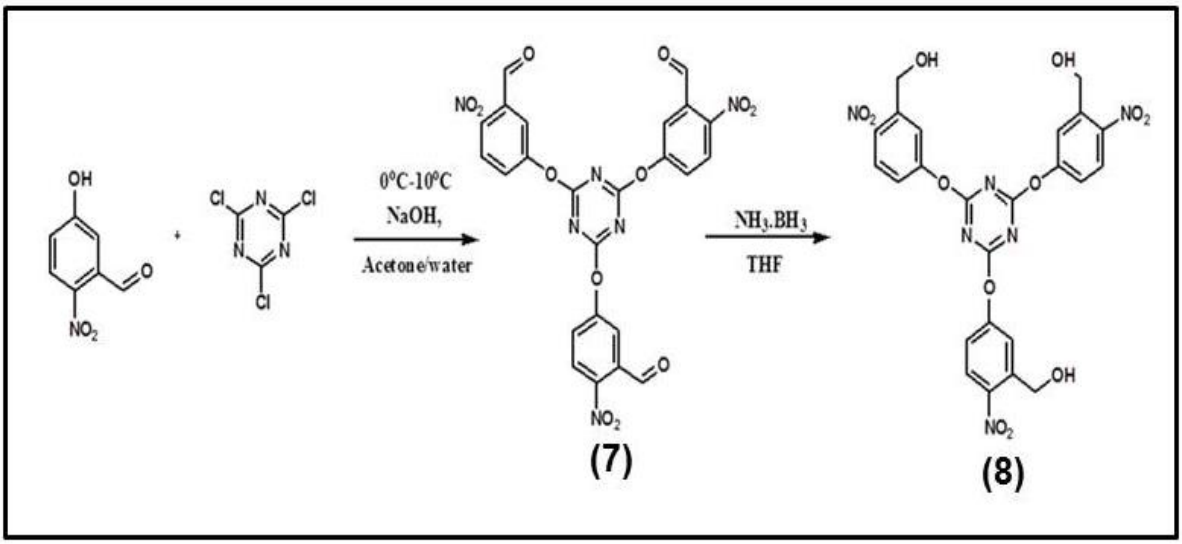


**SCHEME 5.1: Synthesis of the three arm photo-cleavable initiator 2,4,6-tris(3-hydroxymethyl,4-nitrophenoxy)-1,3,5-triazine (8)**

The three arm photo-cleavable initiator 2,4,6-tris(3-hydroxymethyl,4-nitrophenoxy)-1,3,5-triazine (**8**) was prepared in order to synthesize star-shaped photo-cleavable poly(Ɛ-caprolactone)s. Cyanuric chloride was chosen as the pivotal molecule for our synthetic scheme. Cyanuric chloride containing three chlorine substituents and a stable aromatic triazine ring has the possibility to form branching in three directions. The first aryloxy-1,3,5-triazine was reported by Hofmann in 1886 who synthesised triphenoxy-l.3,5-triazine by the reaction between sodium phenoxide and cyanuric chloride at elevated temperature.[157] Later on Allan & Allan[158] reported the reaction of cynuric chloride and salicylaldehyde in presence of sodium hydroxide in an ice bath. We used the similar procedure for etherification reaction between cyanuric chloride and 2-nitro-5-hydroxy benzaldehyde in the presence of sodium

hydroxide to give 2,4,6-tris(3-formyl,4-nitrophenoxy)-1,3,5-triazine (**7**), the detailed synthetic route is shown in the Scheme 2. The synthesized trialdehyde was recrystallized from ethyl acetate. The second step of the reaction i.e. reduction of aldehyde group becomes critical due to presence of $–NO_2$ group. Although the $NaBH_4$ is selective reagent for reduction of aldehyde group, its use was unsuccessful to reduce the trialdehyde compound **(7)**. Akamanchi et. al.[159] used aluminium isopropoxide/ trifluoroacetic acid to reduce aldehyde group of nitrobenzaldehyde, this reagent also not useful for reduction of trialdehyde compound **(7)**. Therefore, amminetrihydroboron, an excellent selective reducing agent of aldehydes and ketones[160], was used for the reduction of the aldehyde moieties of compound **(7)** to give the compound 2,4,6-tris(3-hydroxymethyl,4-nitrophenoxy)-1,3,5-triazine (**8**). The final product was purified by using column chromatography by using the mobile phase ethyl acetate and hexane (Scheme 5.1).

The structure of the synthesized compounds 2,4,6-tris(3-formyl,4-nitrophenoxy)-1,3,5-triazine (**7**) and 2,4,6-tris(3-hydroxymethyl,4-nitrophenoxy)-1,3,5-triazine (**8**) were confirmed by $^1$H NMR, $^{13}$C NMR and ESI-TOF as discussed in the next paragraph.

### 5.2.2 Characterization of 2,4,6-tris(3-formyl,4-nitrophenoxy)-1,3,5-triazine [$C_3N_3(OC_6H_3NO_2$-CHO$)_3$](7) and 2,4,6-tris(3-hydroxymethyl,4-nitrophenoxy)-1,3,5-triazine [$C_3N_3(OC_6H_3NO_2$-$CH_2OH)_3$](8)

#### 1. $^1$H NMR and $^{13}$C NMR of trivalent aldehyde [$C_3N_3(OC_6H_3NO_2$-CHO$)_3$](7)

Both $^1$H-NMR and $^{13}$C-NMR measurements of 2,4,6-tris(3-formyl,4-nitrophenoxy)-1,3,5-triazine **[$C_3N_3(OC_6H_3NO_2$-CHO$)_3$]**(**7**) were carried out in DMSO-$d_6$. In the $^1$H-NMR spectrum of 2,4,6-tris(3-formyl,4-nitrophenoxy)-1,3,5-triazine (**7**), the protons of the three aldehyde groups show a singlet at 10.19 ppm and the aromatic protons show the peaks in the region of 7.73-8.2 ppm. The presence of the central triazine ring and the aldehyde carbons in 2,4,6-tris(3-formyl,4-nitrophenoxy)-1,3,5-triazine (**7**) was confirmed by $^{13}$C NMR, showing peaks at 172.8 and 189.2 ppm respectively. Peaks at 122.6, 127.2, 133.2, 147.0, 154.9 represent aromatic carbons(Fig 5.4). The $^1$H-NMR and $^{13}$C-NMR data gives the confirmation about the complete structure of the trivalent aldehyde i.e. [$C_3N_3(OC_6H_3NO_2$-CHO$)_3$]**(7).**

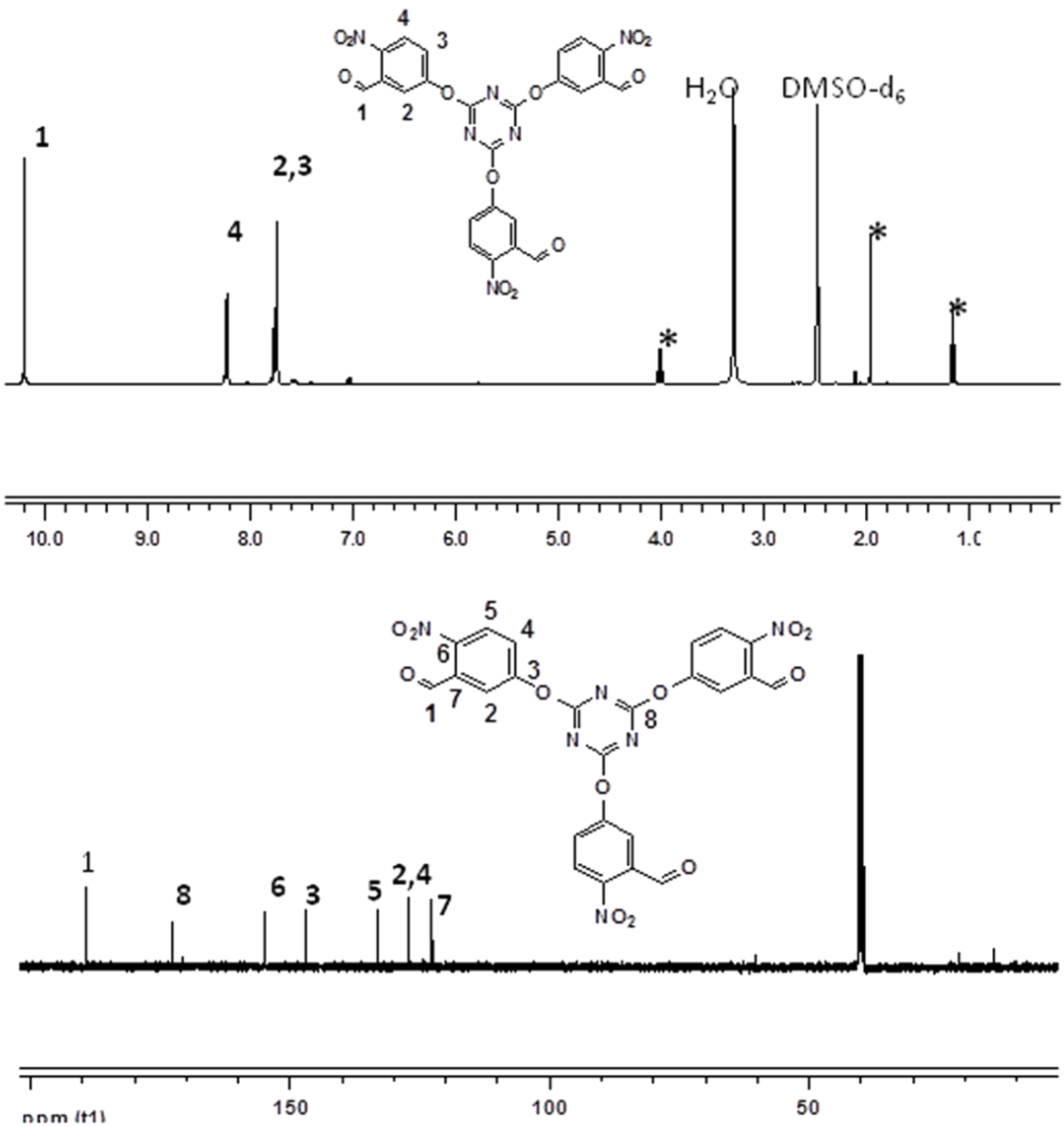


**FIGURE 5.4: $^{1}$H NMR (upper) and $^{13}$C NMR (lower) of 2,4,6-tris(3-formyl-4-nitrophenoxy)-1,3,5-triazine(7).**

## 2. $^{1}$H NMR and $^{13}$C NMR of 2,4,6-tris(3-hydroxymethyl,4-nitrophenoxy)-1,3,5-triazine [$C_3N_3(OC_6H_3NO_2\text{-}CH_2OH)_3$](8)

Furthermore the synthesis of photo-cleavable initiator i.e. 2,4,6-tris(3-hydroxymethyl,4-nitrophenoxy)-1,3,5-triazine [$C_3N_3(OC_6H_3NO_2\text{-}CH_2OH)_3$](**8**) was confirmed by $^{1}$H NMR as well as $^{13}$C NMR (Fig 5.5). The measurement was carried out in DMSO-$d_6$. In fig.5.5, $^{1}$H NMR spectrum of (**8**) shows a triplet at 5.6ppm and a doublet at 4.8ppm for –*C<u>H</u>$_2$-OH* and –*O<u>H</u>* protons. In case of aromatic protons, the proton no. 3 at 7.4 ppm shows doublet of doublet due to presence protons at *meta* and *ortho* positions, whereas two doublets at 7.6ppm and 8.1ppm are for proton no. 2 & 4 respectively. The $^{13}$C-NMR of (**8**) peaks at 60.1ppm and 173.0 ppm represent –*<u>C</u>H$_2$-OH* and carbon of central triazine

ring respectively. The aromatic carbons show signals at 121.2, 121.3, 127.0, 141.8, 144.4 and 155.2 are for aromatic carbons.

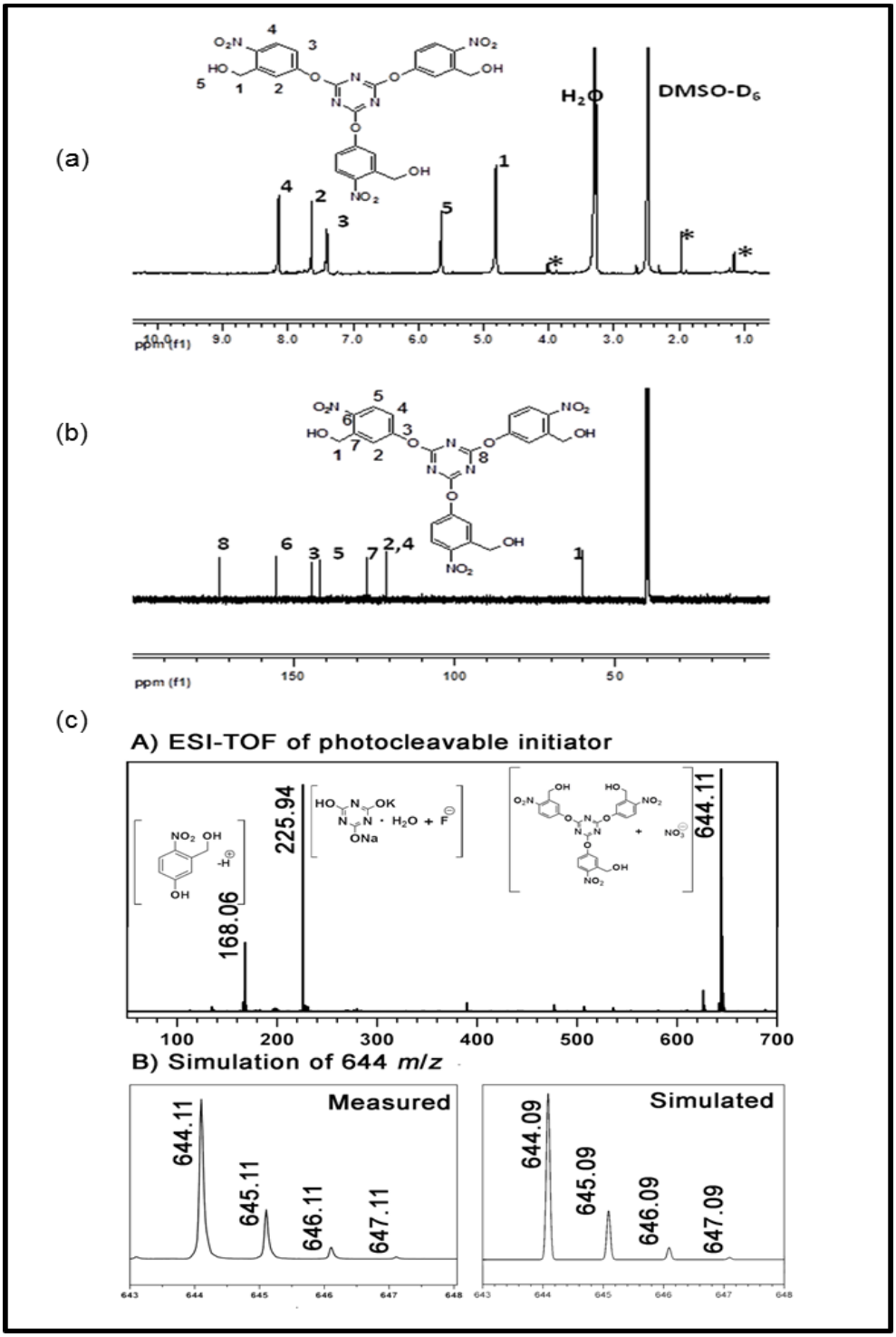


**FIGURE 5.5: (a) $^{1}$H NMR and (b) $^{13}$C NMR spectra of 2,4,6-tris(3-hydroxymethyl,4-nitrophenoxy)-1,3,5-triazine (8). The peaks designated by (*) are residual solvent peaks of ethyl acetate. (c) ESI-TOF MS analysis of 2,4,6-tris(3-hydroxymethyl,4-nitrophenoxy)-1,3,5-triazine (8) initiator.**

In the $^{1}$H-NMR spectrum of 2,4,6-tris(3-formyl,4-nitrophenoxy)-1,3,5-triazine (**7**), the protons of the three aldehyde groups show a distinct peak at 10.19 ppm, which is disappearing after reduction together with a new triplet peak at 5.6 ppm for the hydroxyl group and a doublet at 4.8 ppm for the $–CH_2$ group in the spectrum of the final initiator (**8**), confirming that all of the aldehyde groups are completely reduced into the alcohol groups. In $^{13}$C-NMR, after reduction of the aldehyde groups of **(7)** into the alcohol groups of **(8)**, the peak at 189.2 ppm disappears and the appearance of a peak at 60.1 ppm in the $^{13}$C NMR of **(8)** indicates the formation of the hydroxymethyl-moieties. This confirms the successful synthesis photo-cleavable initiator.

Furthermore, ESI-TOF-MS analysis conducted to confirm the structure of the compound **(8)**. In fig. 5.5(c), the full spectrum of ESI-TOF-MS analysis as well as the measured and simulated peak pattern is shown. The measurement was carried out in the negative modus with solvent THF, provides confirmation of the structure of compound **(8)** via the isotopic pattern of the peak at *m*/*z* = 644.11 g/mol calculated for $[M+NO_3]^-$. This is an important analysis to confirm the presence of all three *o*-nitrobenzyl alcohol groups in the initiator. The isotopic peaks at 168.06 g/mol and 225.94 g/mol are in full agreement with the simulated patterns of $[(C_6H_3)(CH_2OH)(NO_2)(OH)-H^+]$ and $[C_3N_3O_3HKNa(H_2O)+F^-]$ respectively, demonstrating the full substitution of all three arms of the triazine-core with the 3-hydroxymethyl-4-nitrophenyl-moiety.

## 5.3 Synthesis of a six arm photo-cleavable initiator

Cyclophosphazenes are inorganic heterocyclic ring systems; consist of alternating phosphorus and nitrogen atoms. Nucleophilic substitution reactions with nucleophiles such as amines, alcohols, phenols and organometallic reagents have been studied widely. 2,2,4,4,6,6-Hexakis(4-formylphenoxy)-1,3,5,2,4,6-triazatriphosphine (HEPT) has been used in synthesis of some star polymers.[161,162] Various hexavalent alcohols such as di-pentaerythritol, hexachlorocyclotriphosphazene, etc. are reported as initiators for ring opening polymerization of lactones, in order to synthesize star shaped polymers. Moving ahead from this, we planned the synthesis of photo-cleavable hexavalent alcohols as a initiator for polymerization of lactones. Over the years, there are several cyclophosphazene derivatives are reported. Here, we are reporting the hexachlorocyclotriphosphazene derivative as a photo-cleavable initiator, which can be used for ROP of lactones.

### 5.3.1 Synthesis of photocleavable hexavalent alcohol as an initiator:

In the first step, reaction of 5- hydroxyl, 2-nitrobenzaldehyde with hexachlorocyclotriphosphazene was conducted via an etherification reaction using NaH as

a base. The sodium salt of 5- hydroxyl, 2-nitrobenzaldehyde reacts with $P_3N_3Cl_3$ to yield 30% of hexasubstituted phosphazene $N_3P_3(-O–C_6H_3NO_2–CHO)_6$ (**9**) in the reaction time of 72 hrs. At the same time, when $K_2CO_3$ was used as a base for generation of alkoxide, the reaction was much faster i.e. just six hours and high yielded (45%). The reaction conditions are summarized in table 5.1. In both cases THF was used as a solvent and reactions were carried out at reflux temperature. The final compound was purified by column chromatography.

**TABLE 5.1: Synthesis of Hexakis(3-formyl,4-nitrophenoxy)cyclotriphosphazene $N_3P_3(-O–C_6H_3NO_2–CHO)_6$ (9)**

| Sr. No. | $P_3N_3Cl_3$ | 2-nitro,5-hydroxy benzaldehyde | base | solvent | time | temp | Yield |
|---|---|---|---|---|---|---|---|
| 1 | 1mmol | 8mmol | NaH | THF | 72 hrs. | Reflux | 30% |
| 2 | 1mmol | 9mmol | $K_2CO_3$ | THF | 6 hrs. | Reflux | 45% |

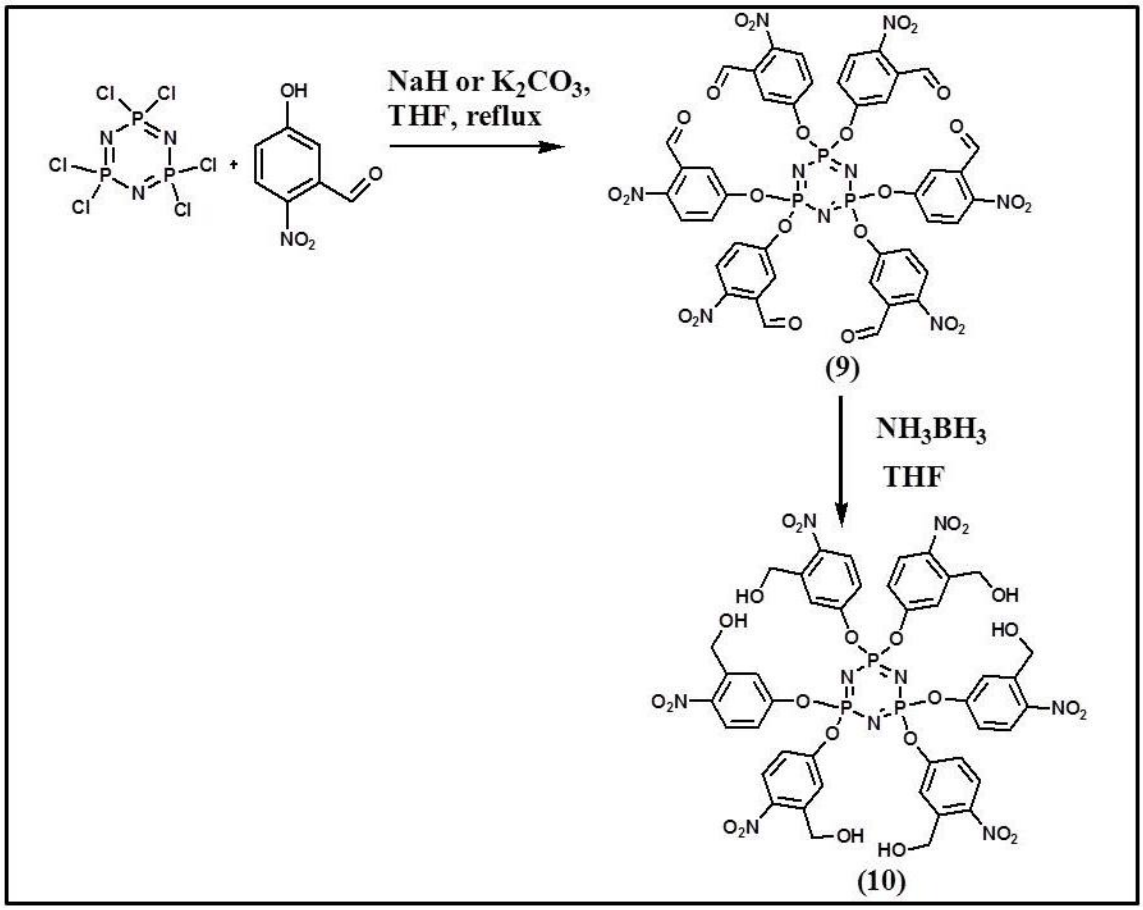


**SCHEME 5.2: Synthesis of six arm photo-cleavable initiator $N_3P_3(-O–C_6H_3NO_2–CH_2OH)_6$**

The compound Hexakis(3-formyl,4-nitrophenoxy)cyclotriphosphazene $N_3P_3(-O–C_6H_3NO_2–CHO)_6$ **(9)** was further reduced into hexavalent alcohol Hexakis(3-hydroxymethyl,4-nitrophenoxy)cyclotriphosphazene $[N_3P_3(-O–C_6H_3NO_2–CH_2OH)_6]$ **(10)** by using the ammonia-borane complex as a reducing agent in THF. The resulting product and the precursor were characterized by $^1$H-NMR, $^{13}$C-NMR and $^{31}$P-NMR spectroscopy.

We are reporting here the synthesis of two photo-cleavable initiators i.e. trivalent and hexavalent photo-cleavable initiators, but in this work our focus is on synthesis and photo-cleavage of three arm photo-cleavable star shaped poly(ε-caprolactone)s which is described in the next chapter.

### 5.3.2 Characterization of the precursor Hexakis(3-formyl,4-nitrophenoxy)-cyclotriphosphazene $[N_3P_3(-O–C_6H_3NO_2–CHO)_6]$ (9):

The six arm aldehyde precursor $\mathbf{N_3P_3(-O–C_6H_3NO_2–CHO)_6}$ was characterized by by $^1$H NMR and $^{31}$P-NMR spectroscopy. In $^1$H NMR spectrum (fig. 5.6), signal at 10.1 ppm represents protons of aldehyde groups. In case of aromatic protons, the proton no. 2 & 4 show an overlapped signal at 7.5 ppm, whereas a doublet at 8.1 ppm represents proton no. 3. It is important to know the complete substitution of all six chorine groups by phenoxy groups, in this case the nature of P atoms would be symmetric and it will show one singlet in $^{31}$P-NMR spectrum. The $^{31}$P-NMR spectrum (fig. 5.7) shows the expected singlet at 6.9 ppm, indicates the formation of a symmetric structure.

### 5.3.3 Characterization of Hexakis(3-hydroxymethyl,4-nitrophenoxy)cyclotriphosphazene $[P_3N_3(OC_6H_3NO_2\text{-}CH_2OH)_6]$ (10):

To confirm the synthesis of $\mathbf{N_3P_3(-O–C_6H_3NO_2–CH_2OH)_6}$, the synthesized product **(10)** was characterized by $^1$H NMR, $^{13}$ C NMR. The measurements were carried out in DMSO-$d_6$. In $^1$H NMR spectrum (Fig 5.7a), doublet of doublet at 7.1 ppm represents aromatic proton $\underline{H}^2$, other two aromatic protons $\underline{H}^3$ & $\underline{H}^1$ show singlet and doublet at 7.5 ppm and 8.0 ppm respectively. Protons $C\underline{H}_2$-O- and –O$\underline{H}$ resonated as singlets in the downfield region at 4.7 ppm and 5.6 ppm respectively. The –$\underline{C}H_2$-O carbon observed at 60.0 ppm in the $^{13}$C NMR spectrum (Fig 5.7b) of $\mathbf{N_3P_3(-O–C_6H_3NO_2–CH_2OH)_6}$. The other aromatic carbons show resonances at 119.5 ppm, 119.9 ppm, 127.3 ppm, 142.2 ppm, 143.8 ppm and 153.5 ppm. The $^{31}$P NMR spectrum (Fig 5.7c) of $\mathbf{N_3P_3(-O–C_6H_3NO_2–CH_2OH)_6}$ exhibited a unique sharp singlet at 7.1 ppm indicate the uniform substitution and formation of symmetric structure. In comparison with $\mathbf{N_3P_3(-O–C_6H_3NO_2–CH_2OH)_6}$, the peak shifts from 6.9 ppm to 7.1 ppm after reduction of aldehyde group.

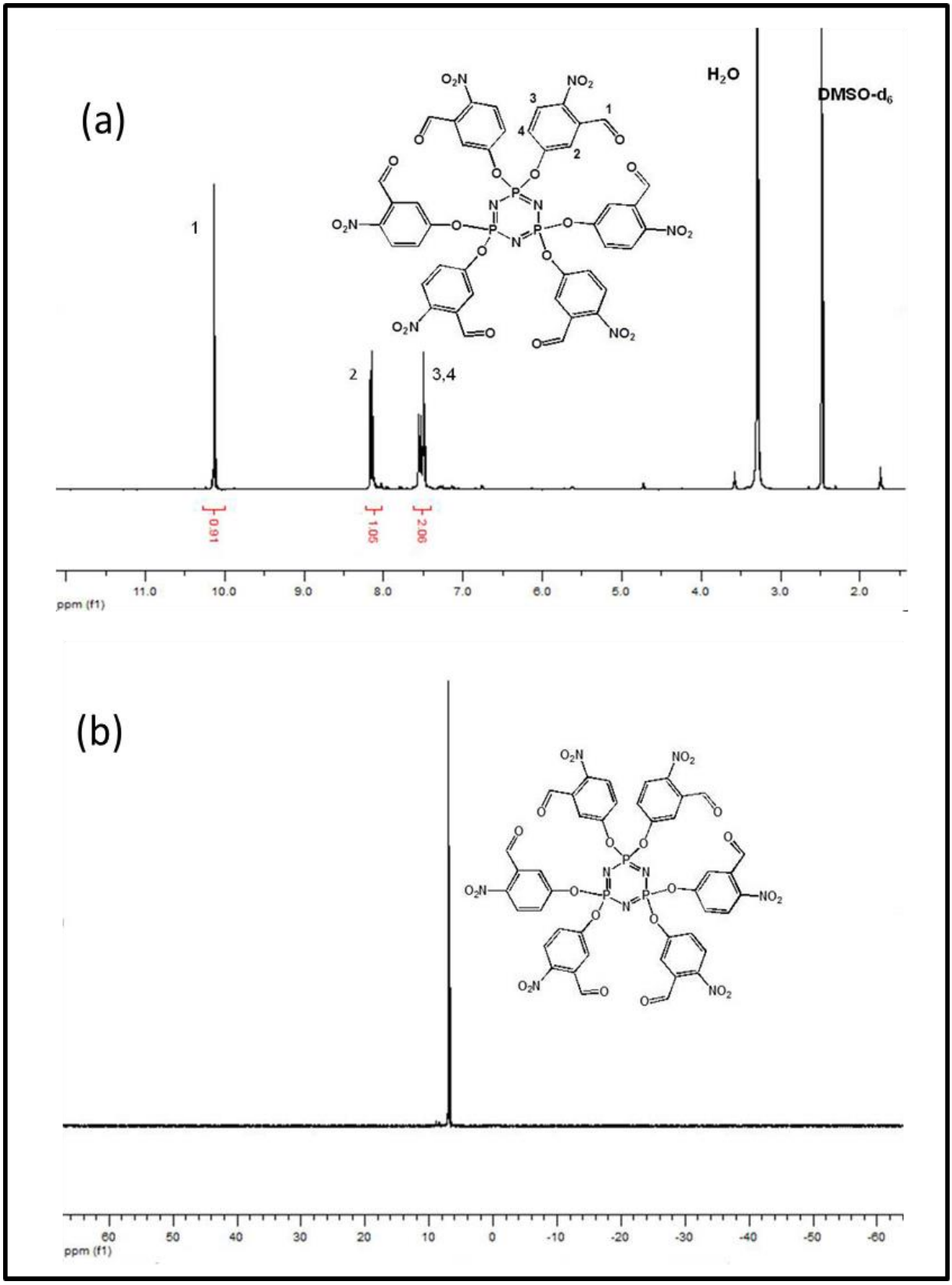


**FIGURE 5.6: (a) $^{1}$H NMR of Hexakis(3-formyl,4-nitrophenoxy)cyclotriphosphazene [$N_3P_3$(-O–$C_6H_3NO_2$–CHO)$_6$] (9) (b) $^{31}$P NMR of Hexakis(3-formyl,4-nitrophenoxy)cyclotriphosphazene [$N_3P_3$(-O–$C_6H_3NO_2$–CHO)$_6$](9)**

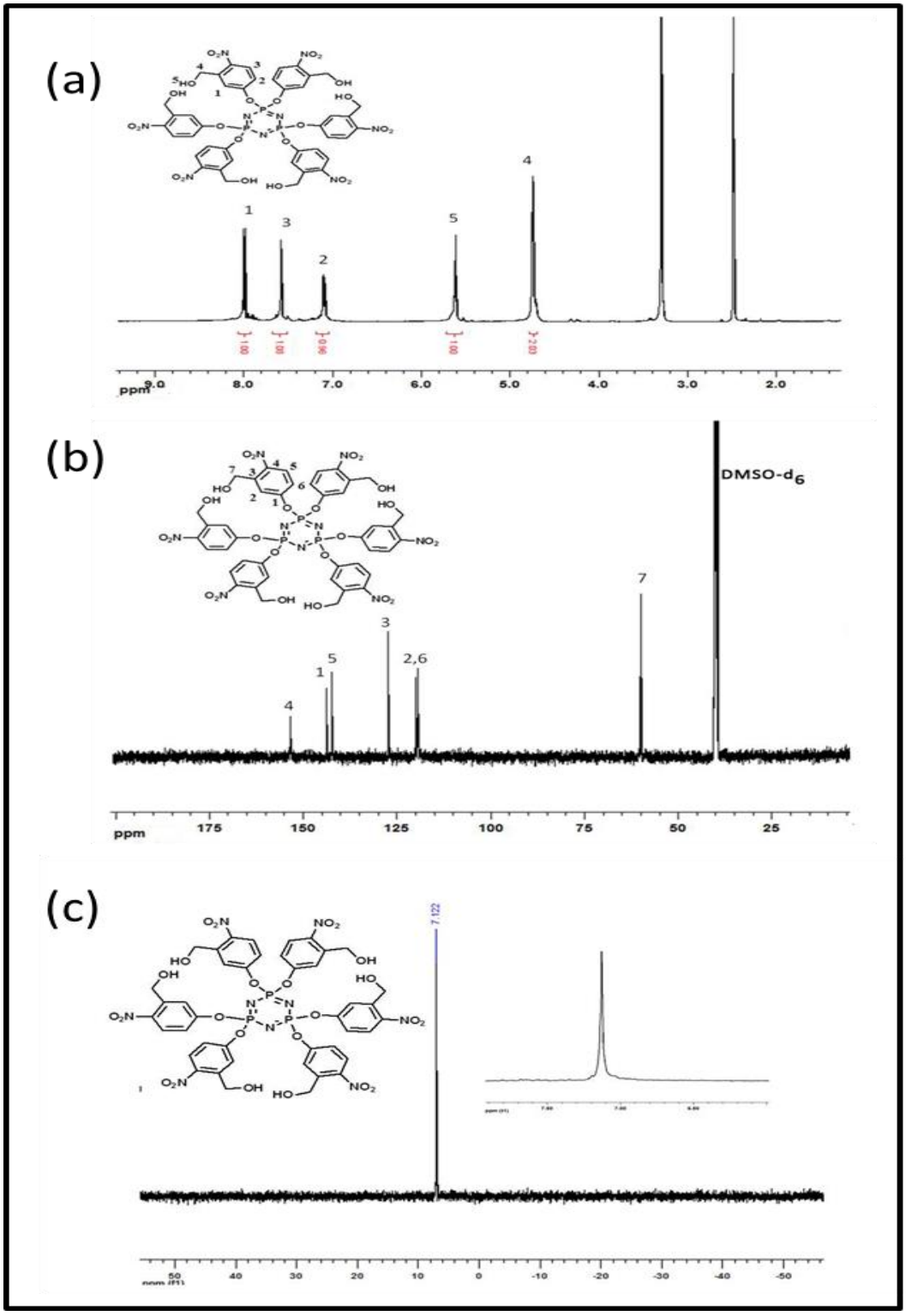


**FIGURE 5.7: (a) $^{1}H$ NMR spectrum of Hexakis(3-hydroxymethyl,4-nitrophenoxy)cyclotriphosphazene $[P_3N_3(OC_6H_3NO_2\text{-}CH_2OH)_6]$(4) (b) $^{13}C$ NMR of Hexakis(3-hydroxymethyl,4-nitrophenoxy)cyclotriphosphazene $[P_3N_3(OC_6H_3NO_2\text{-}CH_2OH)_6]$(4) (c) $^{31}P$ NMR of Hexakis(3-hydroxymethyl,4-nitrophenoxy)-cyclotriphosphazene $[P_3N_3(OC_6H_3NO_2\text{-}CH_2OH)_6]$(10)**

In $^{1}H$ NMR spectra, the peak at 10.1 ppm of $N_3P_3(-O–C_6H_3NO_2–CHO)_6$ disappears and appearance of peaks at 4.7 ppm ($CH_2$ group) and 5.6 ppm (OH group) indicates that all the aldehydes groups are reduced successfully in to alcohol groups. The $^{13}C$ NMR shows the peak at 60.06 ppm for carbon of $CH_2OH$ group confirms the complete reduction of all aldehyde groups. Also all other peaks in the $^{13}C$ NMR are well assigned. The singlet at 7.12 ppm in $^{31}$ P NMR, is the peak for phosphorous in central core, the comparison with $N_3P_3(-O–C_6H_3NO_2–CHO)_6$ indicates that the peak is shifted from 6.9 ppm to 7.12 ppm after formation of $CH_2OH$ groups.

**ESI-TOF-MS analysis of Hexakis(3-hydroxymethyl,4-nitrophenoxy)-cyclotriphosphazene $[P_3N_3(OC_6H_3NO_2\text{-}CH_2OH)_6]$(10):**

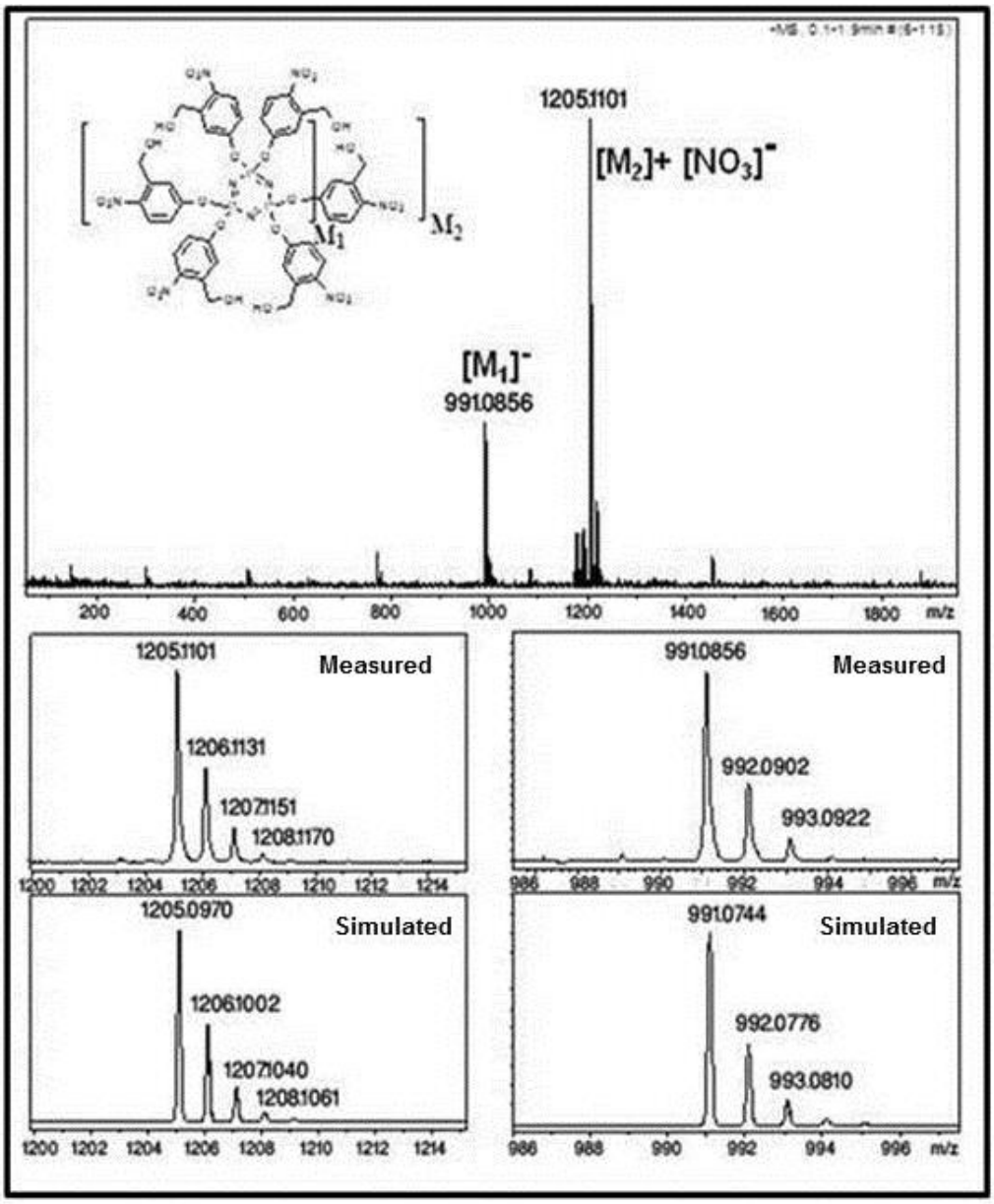


**FIGURE 5.8: ESI-TOF-MS analysis of six arm initiator**

The final structure of the synthesized hexavalent photo-cleavable initiator was confirmed by ESI-TOF-MS analysis (Fig 5.8). The spectrum shown two main peaks in negative modus, the first one is due to the synthesized hexavalent alcohol dissociate in to single charged negative ion $M_1$ at m/z= 991.08, another peak at m/z=1205.11 is due to $M_2$+NO3$^-$ where $M_2$ is complete structure of the synthesized hexavalent initiator. The figure shows the full spectrum of ESI-TOF-MS and the simulated and measured isotopic patterns at m/z= 991.08 and 1205.11.

The synthesis of two initiators i.e. trivalent and hexavalent photo-cleavable initiators are described here but in this work our focus is on synthesis and photo-cleavage of three arm photo-cleavable star shaped poly(ε-caprolactone)s.

# 6. Synthesis of photo-cleavable star-shaped poly(Ɛ-caprolactones)

The synthesis of photocleavable three-arm-star PCL's was planned via a cyanuric-acid based initiator (**8**), linked to an o–nitrobenzyl-alcohol as the photocleavable moiety (Scheme 1) via an ether-linkage. In the past, the synthesis of star-PCL's has been carried out via a coordination insertion mechanism,[163] relying on the use of multivalent alcohols as initiators resulting in a reasonable control of molecular weights by adjusting the molar ratio of monomer to initiator ([CL]/[–OH]). Often used initiators include trimethylol propane for three arm star-polymers[60,164], pentaerythritol and ditrimethylol propane for four arm star-polymers[60,164-166] and dipentaerythritol for the synthesis of six arm star-polymers.[60,61,166,167] As stannous octanoate is among the most used catalysts for the preparation of star-shaped PCL's with different arm numbers and soluble in molten monomers as well as in most of the organic solvents,[60,61,165-175] it was used in this work as catalyst together with the photocleavable multivalent initiator (**8**).

## 6.1 Ring opening polymerization of Ɛ-caprolactone by using the three arm photocleavable initiator (8) to synthesize star shaped poly(Ɛ-caprolactone) (11)

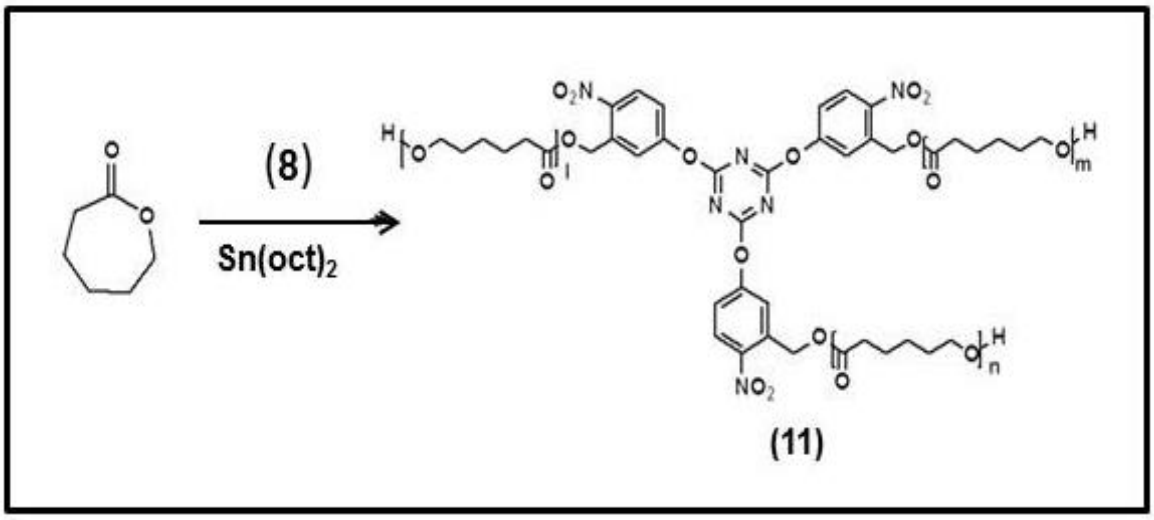


**SCHEME 6.1 Polymerization of caprolactone by using 2,4,6-tris(3-hydroxymethyl,4-nitrophenoxy)-1,3,5-triazine (8)**

In order to prepare a three arm photocleavable PCL's (PC-sPCL's), the above synthesized 2,4,6-tris(3-hydroxymethyl,4-nitrophenoxy)-1,3,5-triazine (**8**) was used as an initiator for polymerization of Ɛ-caprolactone, together with stannous octanoate as the catalyst (Scheme 5.1). The three –OH groups initiates the ring opening polymerization of Ɛ-

caprolactone in presence of $Sn(oct)_2$ via coordination insertion mechanism with formation of a ester linkage between the initiator and polymer chain, to form a star shaped three arm photo-cleavable star shaped poly(Ɛ-caprolactone). The polymerization was conducted via a bulk polymerization of Ɛ-caprolactone in a well dried schlenk flask under inert atmosphere. The polymerization data are summarized in the Table 6.1, it describes the conditions of polymerization of Ɛ-caprolactone as well as the molar mass characteristics of the synthesized polymer. The three different molecular weights of star PCL were prepared in range of 10000 g/mol to 28000 g/mol with good polydispersities i.e. less than 1.4.

**TABLE 6.1 Polymerization of Ɛ-caprolactone by using 2,4,6-tris(3-hydroxymethyl,4-nitrophenoxy)-1,3,5-triazine (8)**

| Entry | Sample | [M]/[I] | Temp. ($^oC$) | Catalyst | $M_n^a$ g/mol | $M_n^b$ g/mol | $M_n^c$ g/mol | PDI |
|---|---|---|---|---|---|---|---|---|
| 1 | PC-sPCL-1 | 90 | 105 | $Sn(oct)_2$ | 10000 | 14500 | 10500 | 1.3 |
| 2 | PC-sPCL-1 | 125 | 105 | $Sn(oct)_2$ | 15000 | 20500 | 14200 | 1.3 |
| 3 | PC-sPCL-1 | 250 | 105 | $Sn(oct)_2$ | 28000 | 38400 | 27000 | 1.4 |

[a] Projected molecular weights of the star-shaped PCL
[b] Number average molecular weight calculated by using GPC calibrated with polystyrene standard
[c] Number average molecular weight calculated by using proton NMR.

**$^1$H-NMR analysis of three-arm photo-cleavable poly(caprolactone):**

In Fig. 6.1, the $^1$H NMR spectrum of the PC-sPCL-1 sample shows the peaks of the central initiating core as well as the peaks for the PCL arms. The measurement was carried out in $CDCl_3$ at 400MHz. The peak at 5.51 ppm represents the $-CH_2$ group of the central initiator-core, the peak at 3.64 ppm is indicative for the terminal-$CH_2$ group of each PCL arm. To calculate the molecular weight of the polymer, the integration ratio of peak no. 8 and 8' were used, yielding molecular weights in good agreement with the expectations adjusted by the monomer/initiator ratio.

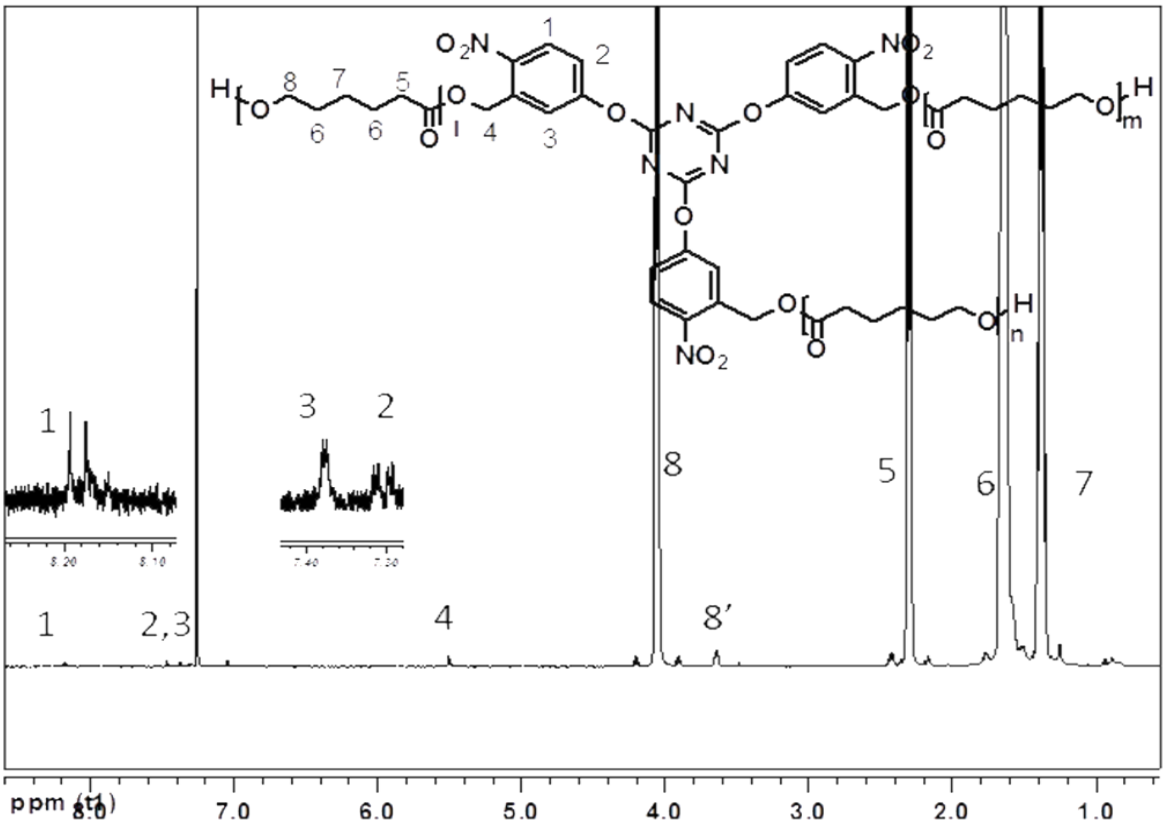


**FIGURE 6.1 $^{1}$H NMR spectrum of the three-arm photocleavable poly(Ɛ-caprolactone) (PC-sPCL-1).**

**ESI analysis of three-arm photo-cleavable poly(caprolactone) (11)**

The expected chemical composition of the polymer was confirmed by a straightforward ESI-TOF-MS analysis. The measurement was carried out in positive modus by using THF/Methanol/Acetonitrile solvent mixture in 1.0:0.3:0.1 ratios. Fig. 6.2 shows the full mass spectrum of PC-sPCL-1, expanded region between m/z=970 to m/z=1090, and the measured as well as simulated isotopic patterns. The spectrum represents the different series of star-shaped photo-cleavable poly(Ɛ-caprolactone)s with several charge state order. The isotopic peaks at *m*/*z*= 1001.55, 1012.54 and 1020.03 successfully simulated to match to the corresponding species $[M+CH_4OH+H_3O]^{+2}$, $[M+CH_3OH+H_3O+Na]^{+2}$ and $[M+CH_3OH+H_3O+K]^{+2}$, respectively. Whereas, the molecular ions peaks at *m*/*z*= 986.86 and 991.86 with a charge state of +3 agree with the simulated species $[M+CH_3OH+H_3O+2Na]^{+3}$ and $[(C_3N_3O_3)(C_7H_5N_1O_3)3)(C_6H_{10}O_2)_{19}K_3+CH_3OH+H_3O+K+Na]^{+3}$ ions respectively, the isotopic peak at *m*/*z*= 1052.35 g/mol is identified as a high charge state of +5, which corresponds to the species $[M+5Na]^{5+}$. Hence, the ESI analysis confirms the structure of the three arm star-shaped poly(Ɛ-caprolactone).

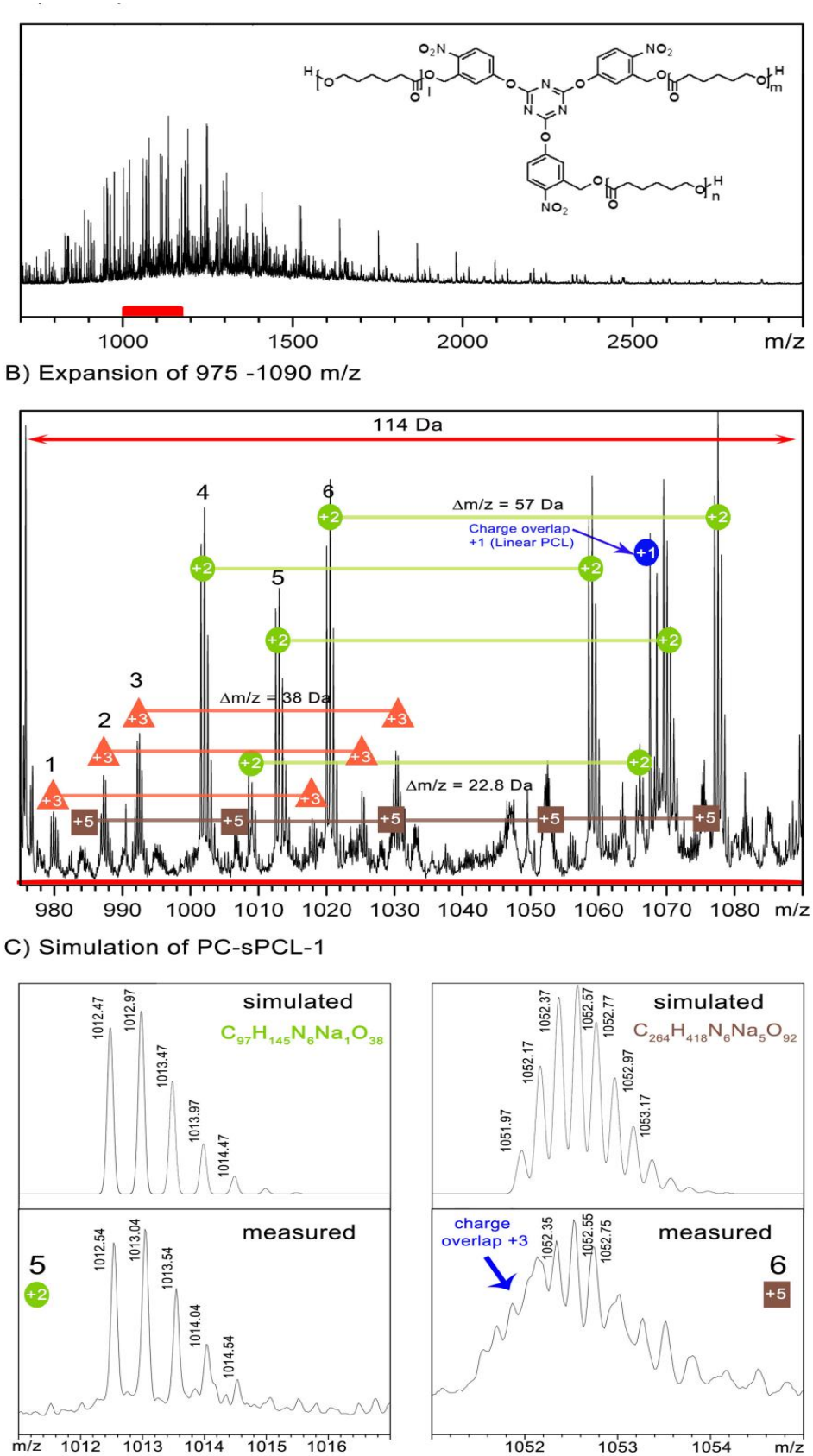


**FIGURE 6.2: ESI-TOF spectrum of the photocleavable polymer PC-sPCL-1.**

## 6.2 Photo degradation of star-shaped poly(Ɛ-caprolactone) to linear poly(Ɛ-caprolactone) (12)

Three different molecular weights of the three arm star-PCL's were used to study the UV controlled degradation based on the cleavage of the *o*-nitrobenzyl esters, which are well-known photocleavable linkers. The ONB esters are well-known photocleavable linkers and photo-cleavage of this group takes place as shown in the mechanism below (Fig. 6.2).

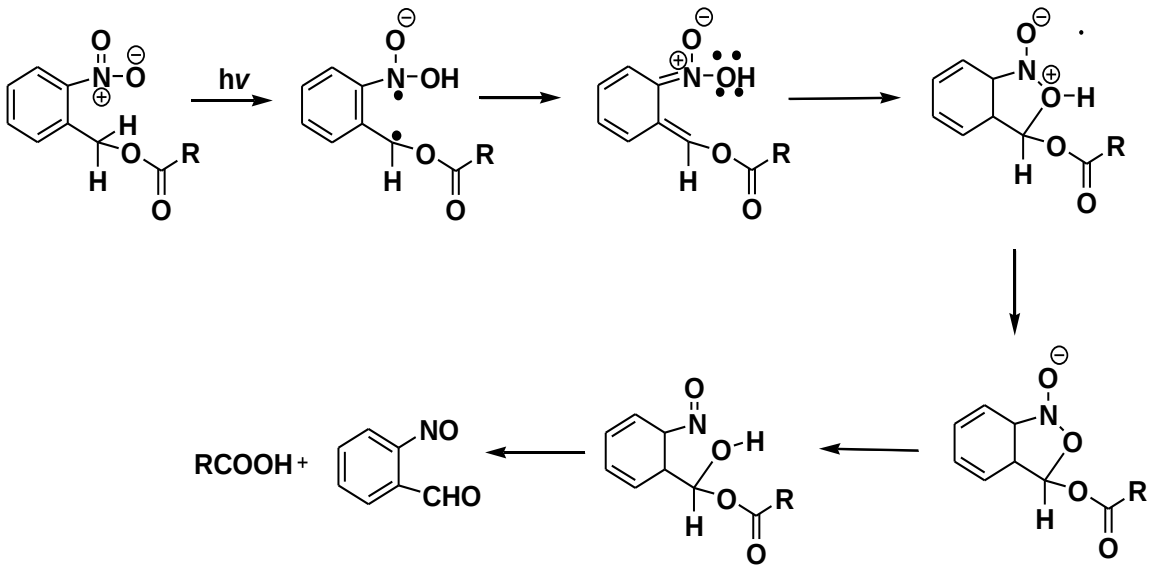


**FIGURE 6.3: Photo-cleavage of *o*-nitrobenzyl ester linkage (Mechanism)**

**TABLE 6.2 Photo-degradation study of three-arm star PCL's before and after photo-irradiation via SEC-analysis**

| Entry | Polymer | Before Photocleavage | | After photocleavage | |
|---|---|---|---|---|---|
| | | $M_n$[a] g/mol | PDI[a] | $M_n$[a] g/mol | PDI[a] |
| 1 | PC-sPCL-1 | 14500 | 1.3 | 5100 | 1.3 |
| 2 | PC-sPCL-2 | 20500 | 1.3 | 7000 | 1.4 |
| 3 | PC-sPCL-3 | 38400 | 1.4 | 13900 | 1.4 |

[a] Number average molar mass calculated by means GPC

To study the photodegradation of the three arm star polymers, the above synthesized polymers were exposed to UV light for various irradiation times. As after the photocleavage the three arm star-shaped polymer results in three linear homo-polymer chains, the degraded polymer thus should only display ~1/3 of the molecular weight in comparison to the three-arm-star PCL before photocleavage. Comparison of GPC data (see Table 6.2) of the polymeric samples before and after photo-cleavage shows that the molecular weights 5100 g/mol, 7000 g/mol and 13900 g/mol of the photo-degraded samples are equivalent to 1/3 molecular weight of the respective star-shaped polymeric samples.

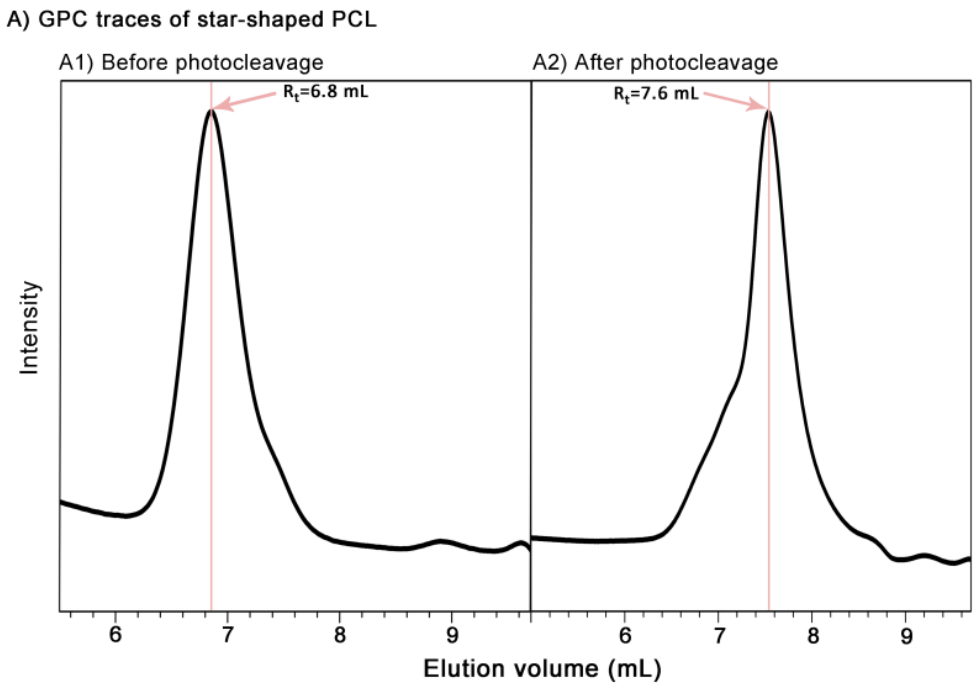


**FIGURE 6.4 Photo-degradation study of photo-cleavable three-arm star-shaped poly(Ɛ-caprolactone) (PC-sPCL-3) by using GPC analysis.**

One example of the difference in the elution volumes in GPC of the star-shaped polymer vs. the photo-cleaved linear polymers is shown in Fig. 6.4. The GPC peak of the native polymer PC-sPCL-3 at time t=0 min shows an elution volume 6.8 mL which shifts to 7.6 ml at t=60 min. At an intensity level of irradiation of 1.3 W/cm$^2$, a complete photo-degradation is accomplished after 60 min.

**Separation of linear and star shaped polymer in HPLC by using liquid chromatography critical condition:**

As GPC technique is not sufficient as a proof, HPLC was used to confirm the complete photocleavage of the star-shaped poly(Ɛ-caprolactone). Liquid chromatography of polymer samples can be devided in three types viz. size exclusion chromatography (SEC), liquid chromatography at critical condition (LCCC) and Liquid adsorption *chromatography* (*LAC*).

Depending on polarity and pore size of the stationary phase and the composition of the mobile phase, one of these modes will direct retention of the macromolecules. In SEC, the higher molar mass chains get eluted first followed by smaller mass, in case of LAC, it is reverse, the small molar mass get eluted first. LCCC is the method in which repeating units are chromatographically invisible and separation takes place based on chemical structure or end groups. Therefore now days LCCC becomes a technique to investigate functionality type distribution in polymers.[176]

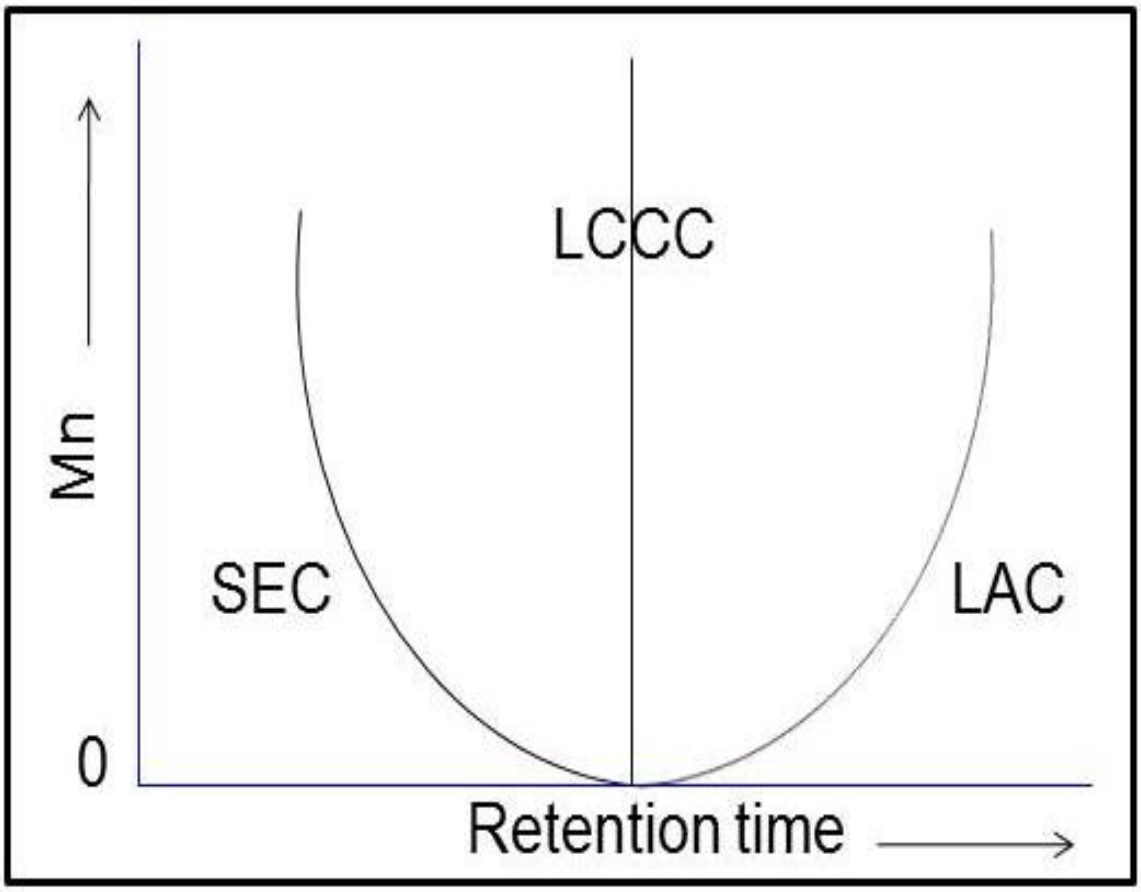


**FIGURE 6.5: SEC, LCCC and LAC behaviour of HPLC.**

In order to achieve LCC conditions of linear poly(ε-caprolactone)s the following experiments were carried out. When Atlantis reverse phase column was used, the linear polymers were eluted with SEC condition in all conditions mentioned in serial no. 1 to 6. The polar column Nucleosil-OH was also unable to give LCCC for linear PCL's (Sr. No. 7). Finally when Nucleosil $–NH_2$ column used, it gave LCCC for linear PCL's at 15$^{o}$C temperature with solvent composition of DCM/THF/Isopropanol (Sr. No. 8). It indicates that end groups are interacting with $NH_2$ groups of the column and polymer separation is not dependent on hydrodynamic volume but it depends on end group interaction.

**Table 6.3: Experiments to achieve LCCC for linear PCL's**

| Sr. No. | Column | *T* ($^oC$) | Solvents | Solvents ratio | Sample | F.G. | Mn | Elution Time (min) | Result |
|---|---|---|---|---|---|---|---|---|---|
| 1 | Atlantis (RP column) | 35 | THF-MeOH | 92:8 | PCL-4Q<br>PCL-11<br>PCL-25 | Alkyne<br>Alkyne<br>Alkyne | 15000<br>34000<br>41000 | 4.01<br>3.93<br>3.92 | SEC |
| 2 | | 30 | THF-MeOH | 92:8 | PCL-4Q<br>PCL-11<br>PCL-25 | Alkyne<br>Alkyne<br>Alkyne | 15000<br>34000<br>41000 | 4.03<br>3.96<br>3.95 | SEC |
| 3 | | 22 | THF-MeOH | 92:8 | PCL-4Q<br>PCL-11<br>PCL-25<br>PCL-OH<br>PCL-OH | Alkyne<br>Alkyne<br>Alkyne<br>COOH<br>COOH | 15000<br>34000<br>41000<br>45000<br>5600 | 4.06<br>3.99<br>3.98<br>4.08<br>3.94 | SEC |
| 4 | | 35 | THF-MeOH | 82.5:17.5 | PCL-10K<br>PCL-4Q<br>PCL-25<br>PCL-70K | COOH<br>Alkyne<br>Alkyne<br>COOH | 5600<br>15000<br>41000<br>45000 | 4.04<br>4.02<br>3.92<br>3.89 | SEC |
| 5 | | 22 | THF-Water | 82.5:17.5 | PCL-2<br>Pcl-4<br>PCL-25 | Alkyne<br>Alkyne<br>Alkyne | 3600<br>15000<br>41000 | 30.21<br>32.11<br>32.48 | LAC |
| 6 | | 35 | DCM-THF | 92:8 | PCL-2<br>PCL-25 | Alkyne<br>Alkyne | 3600<br>41000 | 4.47<br>3.95 | SEC |
| 7 | Nucleosil-OH | 35 | THF-MeOH | 82.5:17.5 | PCL-4<br>PCL-29<br>PCL-25 | Alkyne<br>Alkyne<br>Alkyne | 15000<br>24000<br>41000 | 6.50<br>5.82<br>5.78 | SEC |
| 8 | *Nucleosil-$NH_2$* | 15 | DCM/ THF/ Isopropanol | 95:3:2 | PCL-4<br>PCL-29<br>PCL-25 | Alkyne<br>Alkyne<br>Alkyne | 15000<br>24000<br>41000 | 9.6<br>9.6<br>9.8 | LCCC |

In Fig. 6.6, the HPLC chromatogram shows the separation of photo-cleavable star-PCL from their photocleaved linear counterpart, achieved under liquid critical conditions (LCCC) of linear poly(Ɛ-caprolactone) and hence separating according to the chemical nature of

their endgroup, eluting all polymers irrespective of their chain length.[177] Samples PC-sPCL-2, PC-sPCL-3 show elution peaks at 6.4 and 5.4 minutes respectively, whereas, the photo-cleaved linear counterparts of these polymers (PC-sPCL-2-PC, PC-sPCL-3-PC) show elution peaks at 9.8 and 9.6 min, respectively. This proves the successful quantitative degradation of the star-polymers to their linear counterparts; displaying now OH- and COOH endgroups on either side (see ESI-TOF for details, Fig. 6.7).

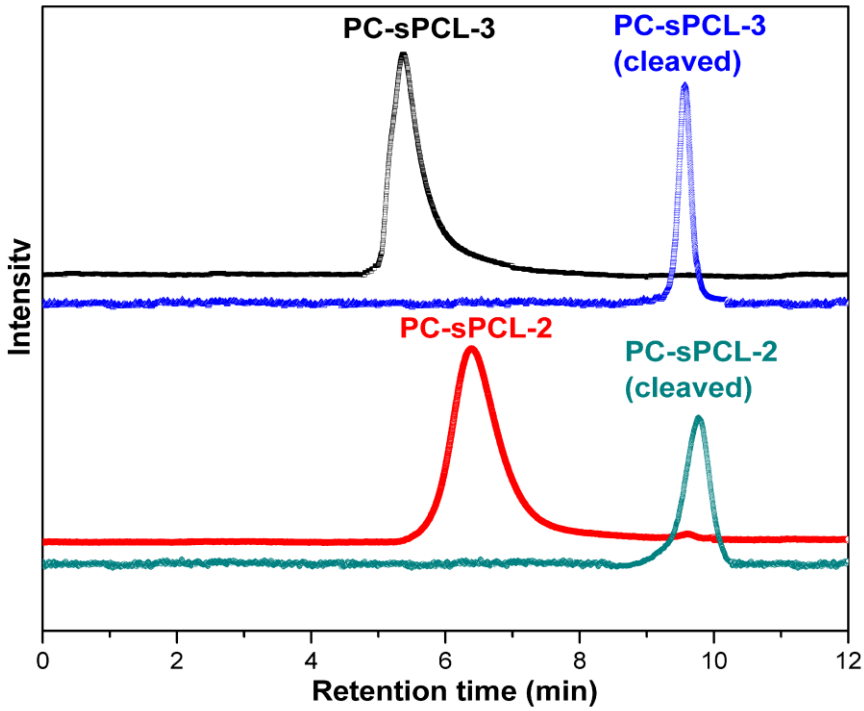


**FIGURE 6.6 HPLC analysis of photocleavable star polymers PC-sPCL-2 and PC-sPCL-3.**

**ESI-TOF-MS of the photocleaved polymer (12)**

The structure of the photo-cleaved sample is again confirmed by using ESI-TOF-MS analysis as shown in Fig. 6.7. When photo-cleavable star polymers are irradiated with UV light, the ester bond between initiator and PCL arms get photo-cleaved to form a carboxy-telechelic linear PCL. Hence, photo-degraded PCL chains are consisting of COOH and OH end groups. This structure is confirmed by analysing various peaks in the range of m/z = 1285 – 1400 g/mol, where multiply charged peaks (charged from +1 to +10) are overlapped. The respective simulated and measured peaks are shown in Fig. 6.7, thus confirming via ESI the complete photo-cleavage of the star-shaped PCL's.

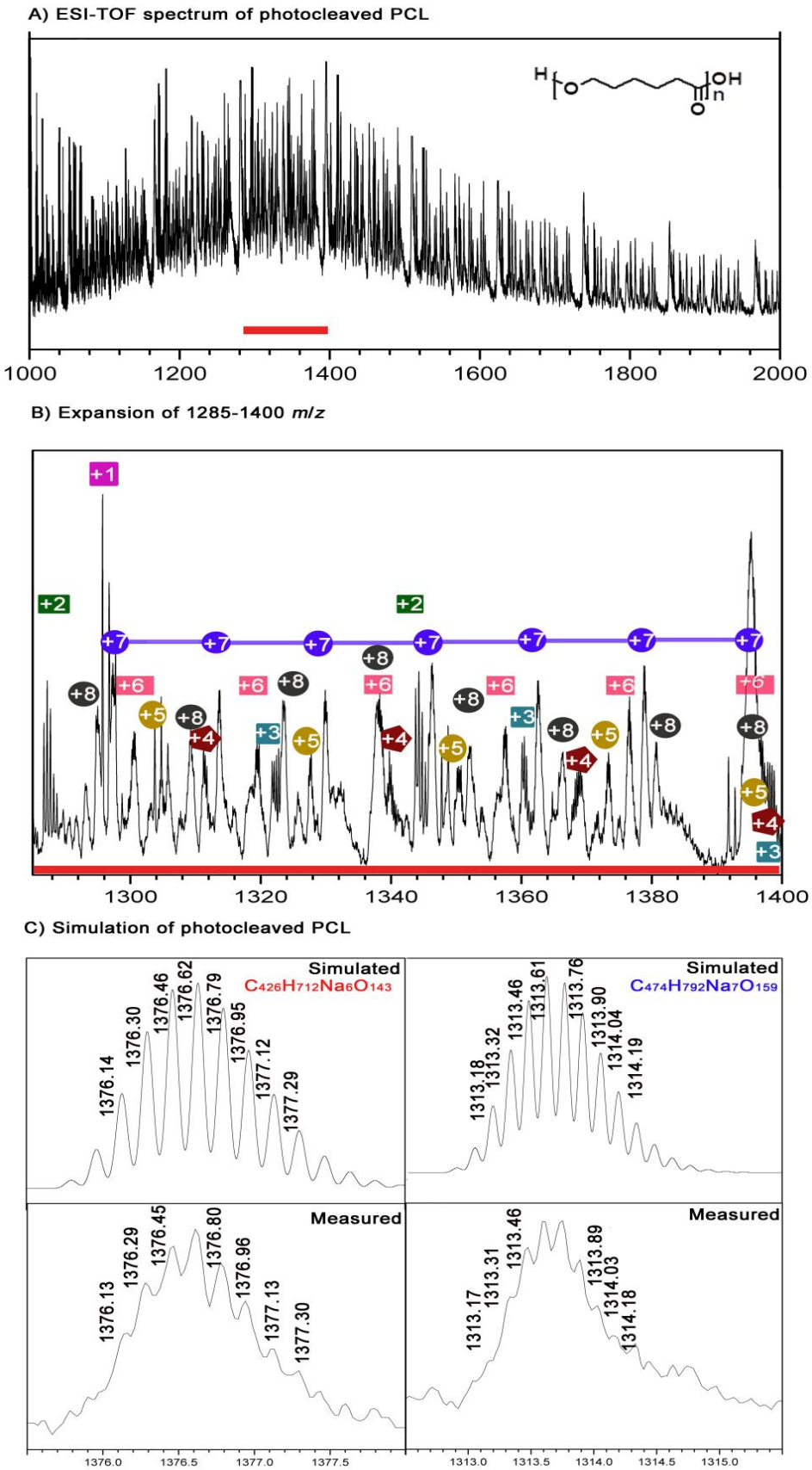


**FIGURE 6.7: ESI-TOF spectrum of the photo-cleaved PC-sPCL-1.**

### 6.3 DSC study of star-shaped photo-cleavable polymers before and after photocleavage

The star-shaped polymers show a lower melting and lower crystallization temperature in comparison to the respective linear (photo-cleaved) PCL-polymers. Comparison of the crystallization temperature and the melting enthalpies of star-shaped polymers before photo-cleavage and after photocleavage (see Table 6.3 and Fig. 6.8) show a significant increase after photocleavage due to the change in architecture *i.e.* changing from a star to a linear architecture. This change is in good agreement with the DSC results of a conventional star-shaped poly(Ɛ-caprolactone) reported by Dong et. al.[61], which shows that crystallization temperature and melting enthalpies are lower in star-shaped polymers in comparison to linear polymers.

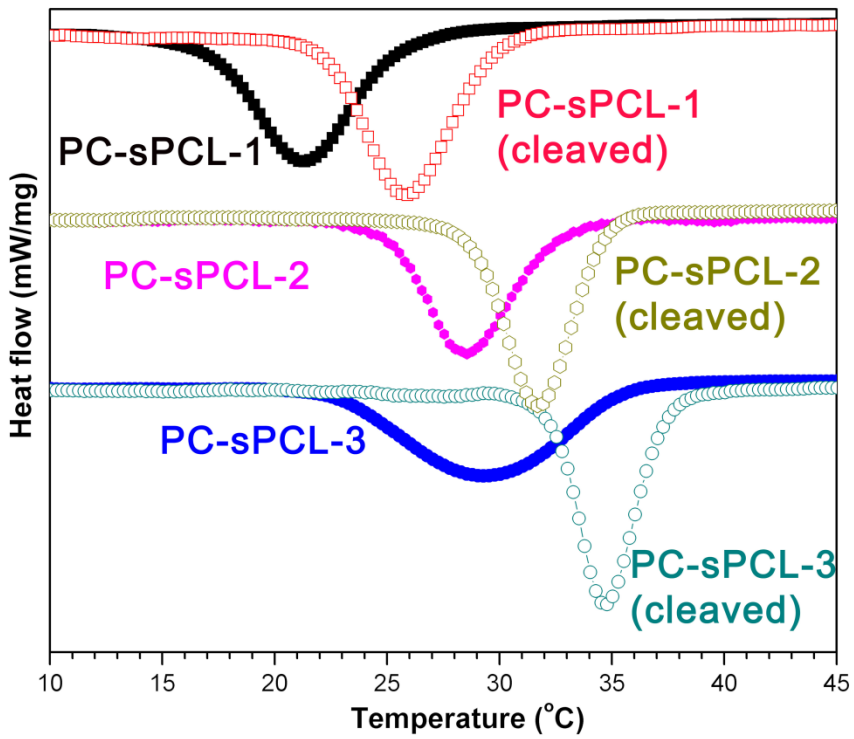


**FIGURE 6.8 DSC plot comparison of three-arm photo-cleavable polymers before and after photo-cleavage.**

Fig. 6.8 shows the comparison of crystallization temperatures before and after photocleavage, obtained from DSC analysis. The crystallinity $X_c$ (%) was calculated by using the formula,

$$X_c\ (\%) = (\Delta H_m / \Delta H_m^o)*100$$

**TABLE 6.3: DSC results of three-arm photocleavable polymers before and after photocleavage**

| Entry | Polymer | Before photocleavage | | | | | After photocleavage | | | | |
|---|---|---|---|---|---|---|---|---|---|---|---|
| | | $T_m$ (°C) | $\Delta H_m$ (J/g) | $T_c$ (°C) | $\Delta H_c$ (J/g) | $X_c$ (%) | $T_m$ (°C) | $\Delta H_m$ (J/g) | $T_c$ (°C) | $\Delta H_c$ (J/g) | $X_c$ (%) |
| 1 | PC-sPCL-1 | 46 | 58.2 | 21.2 | 61.2 | 41.7 | 48.8 | 69 | 25.8 | 66.2 | 49.4 |
| 2 | PC-sPCL-2 | 53 | 61.8 | 28.6 | 65.3 | 44.3 | 56.5 | 72 | 31.7 | 73.4 | 51.6 |
| 3 | PC-sPCL-3 | 56.3 | 71.1 | 29.3 | 68.1 | 51.0 | 56.4 | 74.9 | 34.7 | 73.0 | 53.7 |

where, $\Delta H_m^o$=139.6 J/g , the enthalpy of fusion for 100% crystalline poly(Ɛ-caprolactone)[178].

# Chapter 7: Experimental

## Materials and characterization techniques

Ɛ-Caprolactone (Alfa Aesar) was dried and distilled over calcium hydride under vacuum. 5-Hydroxy-2-nitro benzaldehyde (Alfa Aesar), amminetrihydroboron (Sigma Aldrich) and cyanuric chloride (Sigma Aldrich), Hexachlorophosphazene (VWR) , 2,4-di-t-butyl phenol (Sigma Aldrich), 1-aminopropane (Sigma Aldrich), formaldehyde (Sigma Aldrich), *N,N'*-Dicyclohexylcarbodiimide (Sigma Aldrich), 4-Dimethylaminopyridine (*DMAP*), 4-pentynoic acid (Sigma Aldrich), Copper (II) sulphate(Sigma Aldrich),Titanium tetrachloride (Sigma Aldrich), bromophenoxy benzene (BPB) (Sigma Aldrich), **diisopropylethyl amine** (Sigma Aldrich), sodium ascorbate (Sigma Aldrich), were used as received. Stannous octanoate (Sigma Aldrich), was distilled twice under vacuum (140 ° C, 0.01 mbar). Pure tin(II)-2-ethylhexanoate was stored in a glove box. Tetrahydrofuran was dried and distilled over sodium and benzophenone. DCM & DMF were freshly distilled on $CaH_2$ before use. All solvents were purchased from VWR with chromatographic purity. All reaction products were dried on a high vacuum pump of ILMVAC (final pressure <0.002 mbar).

NMR spectroscopy was carried out on a Varian Gemini 2000 FT-NMR spectrometer (400 MHz). Chloroform (99.8 atom % D) and dimethyl sulfoxide-$d_6$ (99.9 atom % D) were used as solvents. The evaluation of the FID was performed by using Software MestReC 4.9.9.6. Chemical shifts (δ) are in parts per million (ppm) in reference with the residual non-deuterated protons of the solvent ($CDCl_3$: 7:26 ppm (1H), 77.0 ppm (13C); $(CD_3)_2SO$ 2:54 ppm (1H) ; 39.5 ppm (13C)) Indicated. The coupling constants (J) are given in hertz (Hz), using conventional abbreviations (s = singlet, d = doublet, t = triplet, m = multiplet) specified.

GPC measurements were done on a Viscotek GPCmax VE 2001 with a column set CLM3008 (guard column) + $GMH_{HR}$ (analytical column). THF was used as a eluent with 1 mL/min at 22 °C (column temperature) with a sample concentration of approximately 2 mg/mL and injection volume of 100 µL. For PCL-samples polystyrene standards (in the range of 1050–115000 g/mol) were used for conventional external calibration, using a VE 3580RI refractive index detector (detector temperature 35 °C), and for the PIB measurements PIB was used as a standards (from 340 to 87,600 g / mol).

DSC measurements were carried out on NETZSCH DSC 204F1 Phoenix calibrated with indium, tin, bismuth and zinc. Samples with a mass of about 4–6 mg were encapsulated in standard aluminium pans. Nitrogen with 20 mL/min flow was used as a protective or inert gas. Liquid nitrogen was used to cool the samples. Evaluation of the data was conducted by using Proteus Software (version 5.2.1). Samples were heated from room temperature with a

heating rate of 10 °C/min up to 75 °C, held for 10 min, cooled down to −80 °C with a cooling rate of 10 °C/min, held at −80 °C for 10 min, heated to 75 °C with a heating rate of 10 °C/min. The melting temperature was evaluated from the peak maximum of the second heating run and the crystallization temperature was evaluated from the peak maximum of the first cooling run. Isothermal measurements were performed with the following temperature program: heating up to 75 ° C (1st Heat), hold at 75 ° C for 10 minutes, then cool with approximately 50°C/min up to the selected temperature, depending on the sample finally this temperature was holded between 20 to 120 minutes until the DSC signal has again reached the level of the baseline.

Photo-cleavage of polymers was carried out by using an omnicure-2000 UV lamp (Filter : 320-500 nm). A solution of 100mg of the star-shaped photo-cleavable polymer in 2 mL of THF was exposed to UV light of 1.3 W in inert atmosphere.

HPLC measurements were performed on a *Elite LaChrom* HPLC, *Hitachi VWR*, equipped with an autosampler, a quaternary gradient pump, a degasser, a diode array detector (UV-DAD; 190-900 nm) and a column oven with temperature control (temperature = 15 °C). The LCCC separation was carried out on a *Nucleosil-$NH_2$* column, 100 Å, 5 µm, dimension 25×0.46 cm whereas DCM/THF/isopropanol (95/3/2) was used as a mobile phase with the flow rate 0.3 mL/min. The samples prepared were approximately 1.5 mg/ml and injected the volume of 20 µL. The analysis of HPLC data was carried on EZ Chrome Elite 3.3.2 software.

ESI-TOF-MS measurements were carried out on a Bruker Daltonics microTOF time-of-flight LC-MS system. Spectra were recorded in the positive/ negative mode with an accelerating voltage of 4.5 kV, a transfer line with 190 °C, and a scan range of 50–1000 m/z. The spectra were processed with Bruker Daltonics ESI compass 1.3 for micrOTOF (Data Analysis 4.0). Samples were prepared by dissolving 1 mg to 5 mg of the respective compound into 1 mL mixture of THF/ACN/Methanol (72/21/7).

SAXS measurements were carried out using a Rigaku rotating anode. A confocal optics company Osmic afforded the monochromatic $CuK_\alpha$ radiation was collimated by a system of three pinholes. The sample chamber and the flight tube were completely evacuated. The scattered radiation was detected by a Hi-Star area detector 91 from Bruker. The scattering measurements were calibrated with measurements of silver. As a sample holder a round 2mm thick aluminum plate with a hole in the middle was used, in which the sample was placed. For the temperature-dependent measurements, the sample holder was mounted on a hot stage of the company Linkam. During the measurements, the samples were heated

first to 70 ° C or 100 ° C and then cooled to the lower temperature (70 ° C, 50 ° C, 30 ° C and 10 ° C). Before each measurement, the tempering time was 15 minutes. The typical measuring time varied depending on the beam intensity between 30 min and 1 h.

Reactions under microwave irradiation were performed using a CEM Discover LabMate with a PLC control system (switching on and off of the microwave radiation at defined values of pressure and temperature). For 10 mL tubes were used with a snap-on cap IntelliVentTM system.

**Synthesis:**

**Synthesis of star shaped poly(ε-caprolactone) (1):**

Two Schlenk tubes were dried by three consecutive cycles of heating under vacuum and argon purging and argon purging. Caprolactone (2 ml;18 mmol) of and ditrimethylol propane (DiTMP) (22.5 mg; 0.09mmol) were added to a schlenk tube, at the same time catalytic amount of stannous octanoate and caprolactone (1ml; 9mmol) were added to another Schlenk tube. Both Schlenk tubes were heated at 90$^{o}$C, as the DiTMP initiator got dissolved in caprolactone, both solutions were mixed together. The reaction mixture was heated for one hour at 90$^{o}$C. The synthesized polymer was dissolved in dichloromethane and precipitated by addition of cold methanol. Precipitation procedure repeated for two times. The filtered polymer dried under high vacuum for 24 h.

$^{1}$H NMR (400MHz, CDCl3): 4.04 (t, $C\underline{H}_2$), 3.64 (t, $C\underline{H}_2OH$), 2.28 (t, $C\underline{H}_2$), 1.65(m, -$C\underline{H}_2$-$C\underline{H}_2$-) ,1.38 (m, $C\underline{H}_2$), 3.96 (s, $C\underline{H}_2$ ).

| Sr. No. | Polymer code | [M]/[I] | $M_n$(GPC)$^a$ g/mol | PDI$^a$ | $M_n$(NMR)$^b$ g/mol | $M_n$(each arm) |
|---|---|---|---|---|---|---|
| 1 | Star[PCL-1.7k-OH]$_4$ | 75:1 | 9650 | 1.18 | 7050 | 1750 |
| 2 | Star[PCL-6k-OH]$_4$ | 200:1 | 28400 | 1.16 | 22800 | 5700 |
| 3 | Star[PCL-13k-OH]$_4$ | 500:1 | 61000 | 1.2 | 52000 | 13000 |

**Synthesis of alkyne functionalized star shaped polycaprolactone (2):**

In a dried and nitrogen purged round bottom flask, 5-pentynoic acid (60 mg; 0.61mmol) and dicyclohexyl carbodiimide (0.3 mmol) dissolved in 3ml of dichloromethane and stirred for 6 h

at 0°C. The star shaped PCL (0.5 g; 0.03 mmol) and DMAP (20 mg; 0.2 mmol) were dissolved in dichloromethane (3ml). Both solutions were mixed together and stirred for 48 h at room temperature. Then the filtered solution was precipitated in cold methanol, after filtration the synthesized polymer was dried under high vacuum for 24 h.

1H NMR (CDCl3): 4.04 (t, $C\underline{H_2}$), 2.28 (t, $C\underline{H_2}$), 1.97 (t, 1H), 1.65(m, -$C\underline{H_2}$-$C\underline{H_2}$-), 1.38 (m, $C\underline{H_2}$), 3.96 (s, $C\underline{H_2}$ ).

**The thymine functionalized star shaped PCL (3):**

The synthesis of thymine functionalized star shaped PCL was carried out by azide alkyne click reaction. The star shaped alkyne functionalized polycaprolactone (0.005 mmol; 150 mg) and azide functionalized thymine (0.2 mmol; 50 mg) were added to a well dried round bottom flask. Then 5 ml of DMF was added to the reaction mixture, followed by the addition of $CuSO_4.5H_2O$ (0.02mmol; 5mg) and Na-ascorbate (0.06 mmol;12mg). The reaction mixture was stirred for 18 h. The solution was passed through a column of neutral alumina, and then precipitated by using cold methanol. The synthesized polymer was dried under vacuum for 24 hrs.

$^1$H-NMR (400 MHz, CDCl3): (ppm): 8.13 (s, 1H), 6.96 (s, 1H), 4.31 (t, 2H), 4.06 (t, 113H), 3.96 (s, 2H), 3.64 (t, 2H), 2.74 (t, 2H), 2.30 (t, 112H), 2.03 (s, 1H), 1.92 (s, 3H), 1.65 (m, 225H), 1.38 (m, 230H).

**Synthesis of bromo functionalized PIB (4)**

Synthesis of bromo functionalized PIB was carried out by using procedure reported in literature.[89]

$^1$H-NMR (400 MHz, $CDCl_3$) δ ppm: 7.27 (d, J = 8.8 Hz, 2H), 6.82 (d, J = 8.8 Hz, 2H), 4.08 (t, J = 5.8 Hz, 2H), 3.60 (t, J = 6.5 Hz, 2H), 2.31 (m, 2H), 0.99 (s, 15H)

$^{13}$C NMR (101 MHz, $CDCl_3$) δ ppm: 156.3, 142.8, 127.1, 113.7, 65.3, 59.5, 58.2.

| Sr. No. | Polymer code | $M_n$(Calc.) g/mol | $M_n$(NMR) g/mol | $M_n$(GPC) g/mol | PDI |
|---|---|---|---|---|---|
| 1 | PIB-3k | 2500 | 2700 | 2600 | 1.2 |
| 2 | PIB-8k | 8000 | 7800 | 7600 | 1.2 |
| 3 | PIB-11k | 12000 | 11500 | 11000 | 1.4 |

**Synthesis of azide functionalized PIB (5):**

Synthesis of azide functionalized PIB was carried out by using procedure reported in literature.[89]

$^1$H-NMR (400 MHz, $CDCl_3$) δ ppm: 7.27 (d, J = 8.8 Hz, 2H), 6.82 (d, J = 8.8 Hz, 2H), 4.08 (t, J = 5.8 Hz, 2H), 3.54 (t, J = 6.5 Hz, 2H), 2.07 (m, 2H), 0.99 (s, 15H).

**Synthesis of triazine functionalized PIB (6):**

Synthesis of triazine functionalized PIB was carried out by using procedure reported in literature.[89]
$^1$H-NMR (500 MHz, CDCl3): (ppm): 7.60 (s, 1H), 7.26 (d), 6.91 (d, J = 8.6 Hz, 2H), 6.79 (d, J = 8.8 Hz, 2H), 5.18 (s, 2H), 5.04 (b, 4H), 4.58 (t, 2H), 3.96 (t, 2H), 3.75 (s, 2H), 2.39 (q, 2H), 1.80 (s, 2H), 1.42 (m, 113H), 1.11 (m, 420H), 0.99 (m, 15H).

**Synthesis of hydrogen bonded star shaped SPCL-PIB block copolymer:**

Thymine functionalized star shaped SPCL and 2,6 diaminotriazine functionalized PIB were dissolved in dry $CHCl_3$ in separate flasks. Both solutions were mixed together, filtered over filter paper and the solvent was removed on rotavapour. The mixture was dried on high vacuum pump for two days and finally heated at 50$^o$C for two days to promote the formation of hydrogen bonds.

**Synthesis of 2,4,6-tris(3-formyl-4-nitrophenoxy)-1,3,5-triazine [$C_3N_3(OC_6H_3NO_2$-CHO$)_3$] (7)**

The synthesis of compound (**7**) was accomplished by using an analogous procedure as reported by Allan et al.[26] To a solution of sodium hydroxide (0.32g; 8mmol) in water (3 ml), 5-hydroxy-2-nitro benzaldehyde (1.336 g ;8 mmol) were added. To this solution, over a time period of 15 minutes, a solution of cyanuric chloride (0.372 g; 2mmol) in 3 ml of acetone was added, cooled in an ice bath. The solution was kept stirring for 3hrs, after which a yellowish white solid precipitated, which was filtered and washed three times with water and three times with methanol. Finally, the product was recrystallized from ethyl acetate, filtered and dried under high vacuum. (Yield: 30%)

$^1$H NMR (DMSO-$d_6$): 10.2 (s, 1H, *C<u>H</u>O*); 8.2 (*J*=9Hz, d, 1H, Ar-H); 7.73-7.77 (m, 2H, Ar-H).

$^{13}$C NMR (DMSO-$d_6$): 189.2, 172.8, 154.9, 147.0, 133.2, 127.1, 127.0, 122.6.

**Synthesis of 2,4,6-tris(3-hydroxymethyl,4-nitrophenoxy)-1,3,5-triazine [$C_3N_3(OC_6H_3NO_2$-$CH_2OH)_3$](8)**

To a round bottom flask 288 mg (0.5 mmol) of (**7**) were added, followed by the addition of 3 ml of dry THF. Subsequently 46.0 mg (1.5 mmol) of amminetrihydroboron were added to the flask and stirred for 10 min at room temperature. Then the solvent was filtered and the solution was evaporated under reduced pressure. 10 ml of water were then added to the flask and stirred for 1 hr. The crude product was filtered and dried under vacuum. The pure product obtained by column chromatography using the mobile phase ethyl acetate: hexane (50:50). (Yield: 55%)

$^1$H NMR (DMSO-$d_6$): 8.1(*J*=8.4, d, 3H, Ar-H); 7.6(*J*=2.4, d, 3H, Ar-H); 7.4(*J*=8.8, dd, 3H, Ar-H); 5.6(*J*=5Hz, t, 3H, OH); 4.8 (*J*=5.3, d, 6H, $CH_2$).

$^{13}$C NMR (DMSO-$d_6$): 173.0, 155.2, 144.4, 144.8, 127.0, 121.3, 121.2, 60.1.

M.S. : 644.11 *m/z*

**Synthesis of Hexakis(3-formyl,4-nitrophenoxy)cyclotriphosphazene [$P_3N_3(OC_6H_3NO_2$-$CHO)_6$] ( by using NaH) (9)**

8mmol of 2-nitro,5-hydroxy benzaldehyde, 8 mmol of NaH and THF (5 mL) were added to a well dried two necked round bottom flask fitted with condenser to prepare sodium salt of 2-nitro,5-hydroxy benzaldehyde; to the same flask a solution of hexachlorophosphazene (1mmol) in THF (5 ml) was added drop-wise. The reaction mixture was refluxed for 72 h. The reaction mixture was filtered and product was separated by precipitation of filtrate in n-hexane. The final product was purified by column chromatography by using 10:90 ethyl acetate: hexane solvent system. (Yield : 30% )

$^1$H NMR (DMSO-$d_6$): 10.2 (s, 6H, -*C<u>H</u>O*); 8.13 (*J*=9Hz, d, 6H, Ar-H); 7.49-7.60 (m, 12H, Ar-H).

$^{31}$P NMR (DMSO-$d_6$): 6.9 ppm

**Synthesis of Hexakis(3-formyl,4-nitrophenoxy)cyclotriphosphazene [$P_3N_3(OC_6H_3NO_2$-$CHO)_6$] ( by using $K_2CO_3$) (9)**

1 mmol of hexachlorophosphazene, 8mmol of 2-nitro,5-hydroxy benzaldehyde, 8 mmol of $K_2CO_3$ and THF (5 ml) were added to a well dried two necked round bottom flask fitted with condenser, and refluxed for six hours in an inert atmosphere. After evaporating solvent the residue was extracted with ethyl acetate and washed with 5% NaOH and finally dried over

$Na_2SO_4$. The solvent was evaporated and the final product was purified by column chromatography by using 10:90 ethyl acetate: hexane solvent system. (Yield: 45%)

$^1$H NMR (DMSO-$d_6$): 10.2 (s, 6H, -*C<u>H</u>O*); 8.13 (*J*=9Hz, d, 6H, Ar-H); 7.49-7.60 (m, 12H, Ar-H).

$^{31}$P NMR (DMSO-$d_6$): 6.9 ppm

**Synthesis of Hexakis(3-hydroxymethyl,4-nitrophenoxy)cyclotriphosphazene [$P_3N_3(OC_6H_3NO_2$-$CH_2OH)_6$](10)**

300 mg of [$P_3N_3(OC_6H_3NO_2$-CHO$)_6$] **(9)** was added to dry THF (6 ml), followed by addition of ammonia borane (25 mg) and stirred for 18h. The solution was filtered and the THF was evaporated. Finally water (3ml) added to the flask and stirred for 2 h. The crude product was filtered and dried under high vacuum. The pure product was obtained by column chromatography by using solvent system hexane:ethyl acetate 50:50.

$^1$H NMR (DMSO-$d_6$): 8.0(*J*=8.4, d, 6H, Ar-H); 7.6(*J*=2.4, d, 6H, Ar-H); 7.1(*J*=8.8, dd, 6H, Ar-H); 5.6(*J*=5Hz, t, 6H, OH); 4.7 (*J*=5.3, d, 12H, $CH_2$).

$^{13}$C NMR (DMSO-$d_6$): 153.5, 144.8, 142.4, 127.3, 119.9, 119.5, 60.06.

$^{31}$P NMR (DMSO-$d_6$): 7.1 ppm

M.S. : 1208.11 *m/z*

**Preparation of star-shaped photocleavable poly(ε-caprolactone) (11)**

A Schlenk flask was dried by three consecutive cycles of heating under vacuum and argon purging, into which caprolactone (0.55ml, 5 mmol) was added, followed by the addition of the three arm initiator (**8**) (33.2 mg; 0.057 mmol) and a catalytic amount of stannous octanoate (0.0017 mmol) as a catalyst. The Schlenk tube was heated at 105$^o$C under stirring for 2.5 h in the dark. The synthesized polymer was dissolved in dichloromethane and precipitated into methanol, filtered and dried under high vacuum.

$^1$H NMR ($CDCl_3$): 8.19(*J*=8.2, d, *Ar-<u>H</u>*); 7.38 (*J*=2Hz, d, *Ar-<u>H</u>*); 7.3(*J*=9Hz, dd, 1H); 5.51(s, *C<u>H</u>$_2$*); 4.04 (*J*=6.7, t, $CH_2$); 3.64 (t, *C<u>H</u>$_2$OH*); 2.28 (*J*=7.4, t, *C<u>H</u>$_2$*); 1.65(m, -*C<u>H</u>$_2$-C<u>H</u>$_2$*-); 1.38 (m, *C<u>H</u>$_2$*).

**Photocleavage of star-shaped photocleavable poly(ε-caprolactone) (11) to obtain linear poly(ε-caprolactone):**

A solution of 100mg of the star-shaped photo-cleavable polymer in 2 ml of THF was exposed to UV light of 1.3 W in inert atmosphere to obtain photocleaved linear poly(ε-caprolactone).

# Chapter 8: Summary

## Supramolecular polymers

In this thesis, to prepare star shaped Supramolecular block copolymers of SPCL and PIB, the thymine functionalized star shaped poly(Ɛ-caprolactone) was designed. The synthesis of thymine functionalized star shaped poly(Ɛ-caprolactone) was carried out in three steps.

In the first step star shaped hydroxyl functionalized star shaped poly(Ɛ-caprolactone) was prepared by ROP of Ɛ-caprolactone in presence of Ditrimethylol propane initiator and $Sn(oct)_2$ catalyst. The polymerization takes place via coordination insertion polymerization. The incorporation of initiator in polymer chain was confirmed by the $^1$H-NMR and ESI-TOF-MS. In the second step the alkyne functionalization of star shaped PCL was achieved by the steglisch esterification reaction between hydroxyl functionalized star shaped poly(Ɛ-caprolactone) and pentynoic acid in presence of DCC and DMAP. At this stage structure of the polymer was again confirmed by using $^1$H-NMR and ESI-TOF-MS. Finally the thymine functionalized star shaped poly(Ɛ-caprolactone) was synthesized by CuAAC between azide and alkyne groups of thymine azide and the alkyne functionalization of star shaped PCL by using CuSO4 and sodium ascorbate. The synthesized compound was characterized by $^1$H-NMR and ESI-TOF-MS. Hence the novel thymine functionalized star shaped poly(Ɛ-caprolactone) having ability to form hydrogen bonding was synthesized successfully.

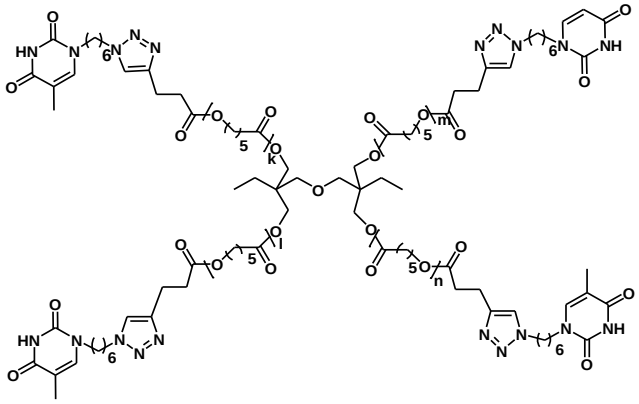

When the thermal properties of linear thymine functionalized PCL were compared with the equivalent total molecular weight of star shaped thymine functionalized PCL, the $T_c$ of star PCL was less than the linear PCL; the similar thing was observed when the linear thymine functionalized PCL was compared with thymine functionalized star PCL having equivalent arm length. The overall comparison of linear and star shaped PCL also indicates that the % crystallinity is much lower in case of thymine functionalized star shaped PCL.

The synthesis triazine functionalized PIB was carried out as reported in literature by living carbocationic polymerization of isobutylene and by using 2-chloro-2,4,4-trimethylpentane/$TiCl_4$ as an initiating system for the polymerization of isobutylene. Quenching with 1-bromo-3-phenoxy propane gives the bromo-functionalized PIB chain. Furthermore, the conversion of bromo functionalized PIB into azide functionalized PIB was carried out by by $SN^2$ reaction with $NaN_3$. Furthermore the triazine group was mounted on PIB chain by Copper-Catalyzed Azide-Alkyne Cycloaddition (CuAAC) between azide functionalized PIB and alkyne functionalized triazine moiety.

In order to study the crystallization behaviour of sPCL with less mobile barrier, PIB was used as a second block connected via the thymine and the 2,4-diaminotriazine supramolecular interaction. Each molecular weight of SPCL was connected with low as well as high molecular weight of PIB to study the effect of lower segregation strength (lower $\chi N$) as well as higher segregation strength (higher $\chi N$).

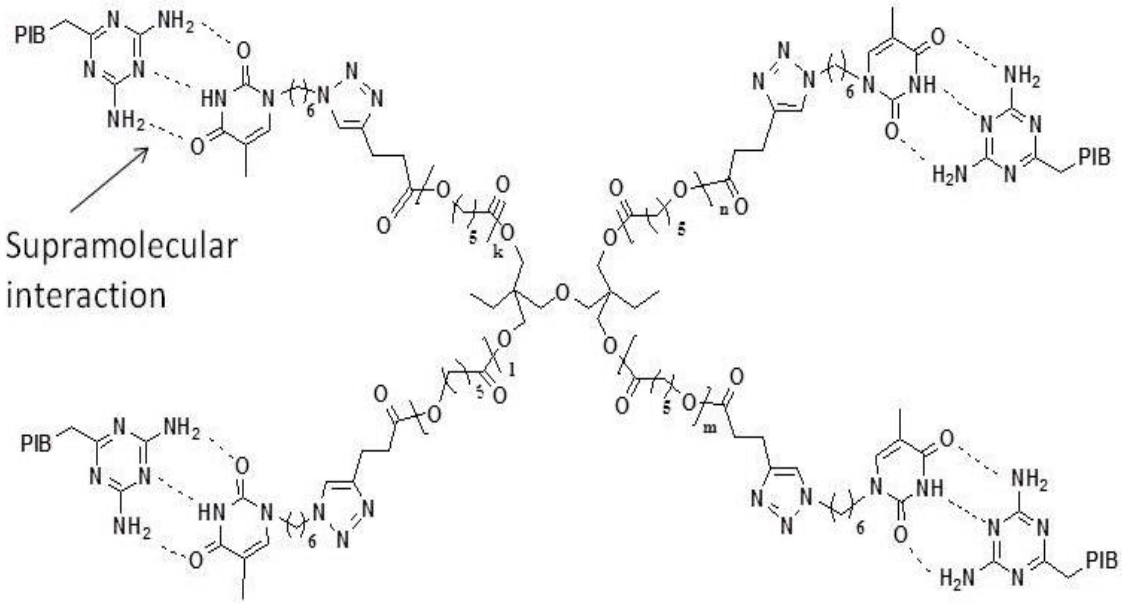


To understand the effect of architecture on the crystallinity of supramolecular BCP, star shaped supramolecular BCP were compared with linear supramolecular BCP. Star(PCL6k-THY)$_4$ shows crystallization peak at 30.3$^o$C with enthalpy change 67J/g which does not show crystallinity after block copolymer formation, whereas Linear-PCL5K-PIB7K having almost similar molecular weight like Star(PCL6K-PIB8K)$_4$, shows crystallization temperature 25$^o$C with enthalpy change 38J/g. Hence architecture reduced the crystallinity of BCP.

SAXS and AFM analysis shown that the Supramolecular interaction with high molecular weight star PCLs form the macrophase separated structures whereas the Supramolecular interaction with low molecular weight star PCLs form microphase separated structures.

Finally the synthesis of supramolecular network of thymine functionalized star PCL was carried out by using a di-triazine connector i.e. 4,4-Bis-[3-(2,4-Diamino-[1,3,5]-triazin-6-yl)-phenoxy]benzophenone. The DSC studies revealed that crystallization temperatures of thymine functionalized star PCL were reduced strongly after formation of their supramolecular networks.

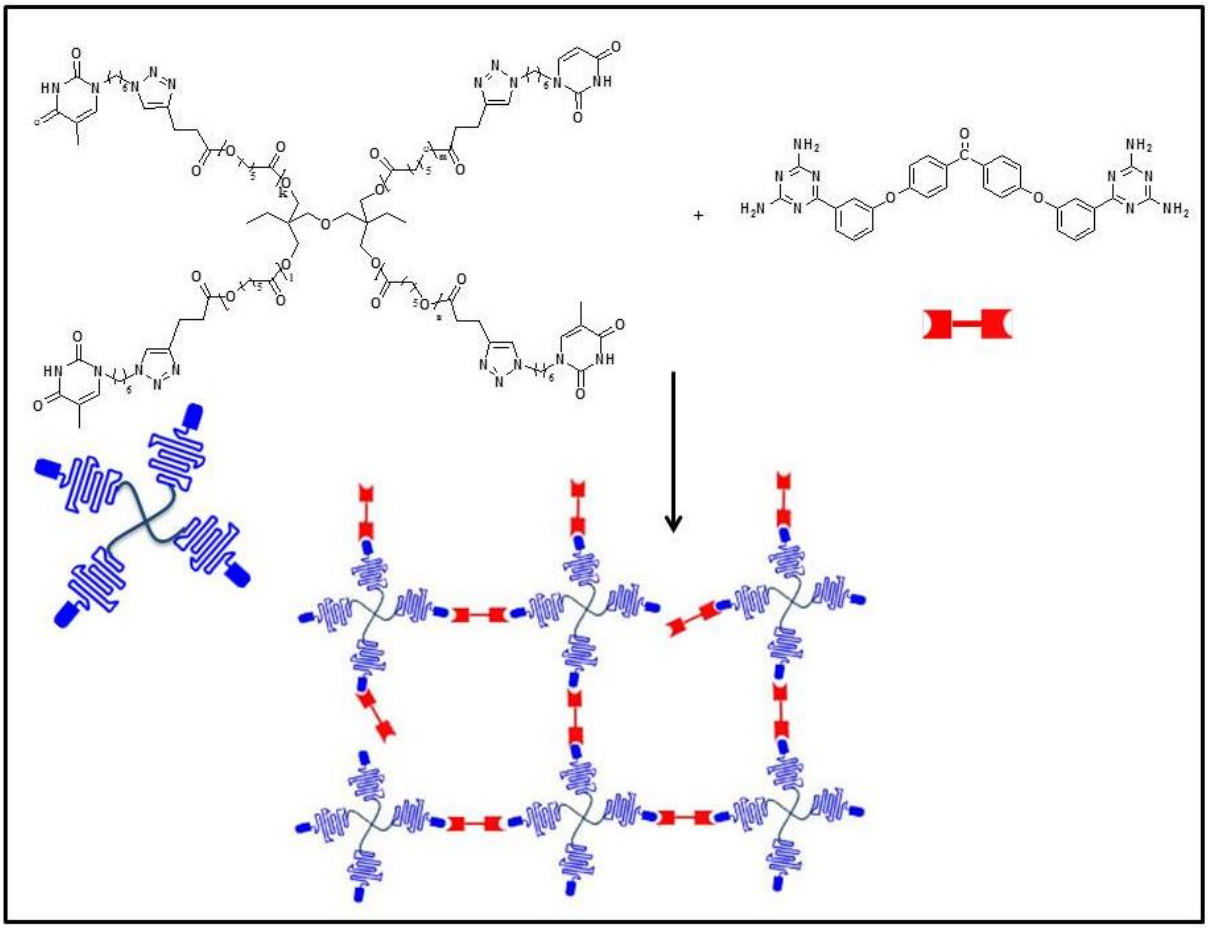

## Photocleavable polymers:

To achieve the synthesis of photo-cleavable star shaped polymers, synthesis of two novel photo-cleavable initiators were designed by using photo-cleavable linkers. The first three arm initiator i.e. **2,4,6-tris(3-hydroxymethyl,4-nitrophenoxy)-1,3,5-triazine [$C_3N_3(OC_6H_3NO_2\text{-}CH_2OH)_3$](8)** was successfully synthesized in two steps. At first, **2,4,6-tris(3-formyl,4-nitrophenoxy)-1,3,5-triazine [$C_3N_3(OC_6H_3NO_2\text{-}CHO)_3$](7)** was successfully synthesized by using the etherification reaction between 2-nitro,5-hydroxy benzaldehyde

and cynuric chloride in presence of NaOH. The structure of the synthesized compound (**7**) was confirmed by using characterization techniques like $^{1}$H-NMR, $^{13}$C-NMR. The reduction of the compound (**7**) was successfully achieved by the reduction of aldehyde groups into alcohols by using the reducing agent ammoniaborane to give the three arm photo-cleavable initiator **2,4,6-tris(3-hydroxymethyl,4-nitrophenoxy)-1,3,5-triazine [$C_3N_3(OC_6H_3NO_2$-$CH_2OH)_3$](8)** The final product was purified by column chromatography and structure of the compound (**8**) was confirmed by $^{1}$H-NMR, $^{13}$C-NMR and ESI-TOF-MS.

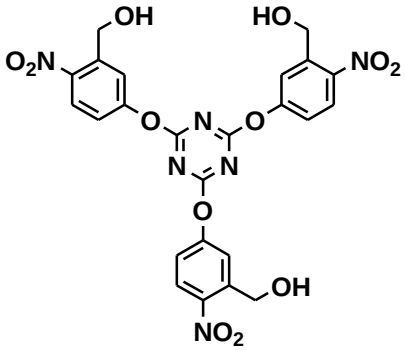

In quite similar way another initiator **Hexakis(3-hydroxymethyl,4-nitrophenoxy)cyclotriphosphazene [$P_3N_3(OC_6H_3NO_2$-$CH_2OH)_6$](10)** was also synthesized by a two-step synthetic pathway. The first step was the synthesis of **Hexakis(3-formyl,4-nitrophenoxy)cyclotriphosphazene [$P_3N_3(OC_6H_3NO_2$-$CHO)_6$] (9)** via an etherification reaction between hexachlorophosphazene and 2-nitro,5-hydroxy benzaldehyde by using NaH or $K_2CO_3$. The synthesized compound was characterized by using characterization techniques like $^{1}$H-NMR, $^{13}$C-NMR and $^{31}$P-NMR. The aldehyde groups of the purified compound (**9**) were successfully reduced into –CH2OH groups by using ammonia-borane as a reducing agent. The purification of the synthesized final product was carried out by column chromatography and the structure of the final product was confirmed by $^{1}$H-NMR, $^{13}$C-NMR, $^{31}$P-NMR and ESI-TOF-MS.

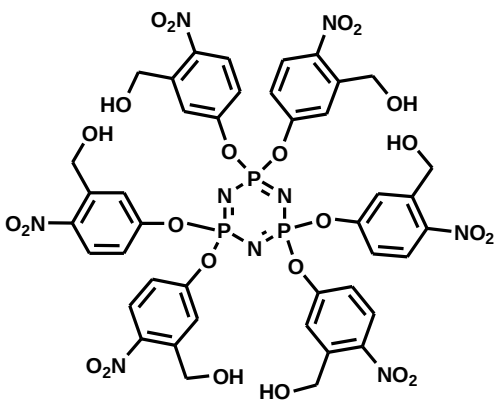

Both initiators having ability to polymerize caprolactone to give star shaped photo-cleavable PCLs are shown below.

The three arm photo-cleavable initiator was further used to synthesize star shaped photo-cleavable PCLs. The polymerization of Ɛ-caprolactone was successfully carried out by using the trivalent initiator (**8**) in presence of $Sn(oct)_2$ catalyst by ring opening polymerization. The polymerization mechanism type is coordination insertion polymerization. The three different molecular weights of photo-cleavable star shaped polymers were prepared in range of 1000 g/mol to 30000 g/mol. The molecular weights of the synthesized polymers were characterized by GPC as well as $^1$H-NMR analysis. The structure of the polymer was confirmed by ESI-TOF-MS analysis.

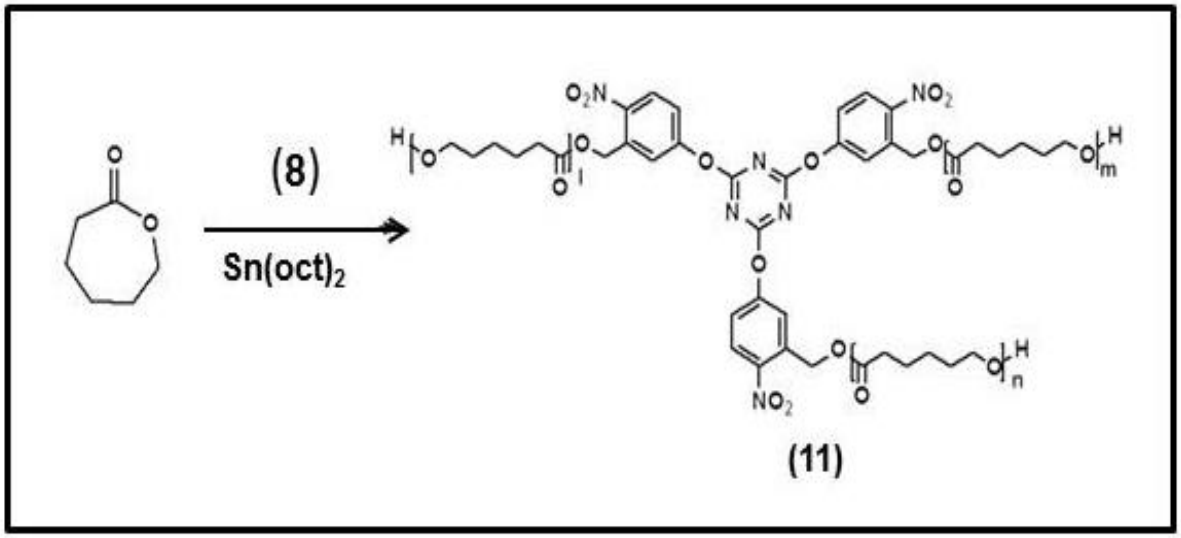


Furthermore the complete photo-cleavage of the synthesized star shaped photo-cleavable polymer was carried out by UV irradiation in inert atmosphere. ONB linker found to be best photo-cleavable linker, the ester linkage between initiator was successfully cleaved on UV irradiation. The comparison of molar masses of polymers before and after photo-cleavage shown that the molecular weights before photo-cleavage were three times higher than that of the photo-cleaved polymers that confirms the complete photo-cleavage. As GPC technique is not sufficient as a proof, HPLC was used to confirm the complete photo-cleavage of the star-shaped poly(Ɛ-caprolactone). The HPLC chromatogram shown the separation of photo-cleavable star-PCL from their photo-cleaved linear counterpart, achieved under liquid critical conditions (LCCC) of linear poly(Ɛ-caprolactone) and hence separated according to the chemical nature of their end-group, eluted all polymers irrespective of their chain length. Finally the structure of the photo-cleaved linear polymer was confirmed by the ESI-TOF-MS technique.

Finally the DSC analysis of polymers before and after photo-cleavage showed the significant increase in the crystallization temperature, % crystallinities and melting enthalpies after photo-cleavage due to photo-switching of star architecture to the linear architecture.

# References

1. G. Reiter; J. U. Sommer. Polymer Crystallization: Obervations, Concepts and Interpretations; Springer Berlin Heidelberg, 2008.
2. S. Z. D. Cheng. Phase Transitions in Polymers: The Role of Metastable States: The Role of Metastable States; Elsevier Science, 2008.
3. E. Piorkowska; G. C. Rutledge. Handbook of Polymer Crystallization; Wiley, 2013.
4. S. J. Spells. Characterization of Solid Polymers: New Techniques and Developments; Springer Netherlands, 1994.
5. L. Mandelkern. Crystallization of Polymers: Volume 1, Equilibrium Concepts; Cambridge University Press, 2002.
6. G. Allegra. Interphases and Mesophases in Polymer Crystallization III; Springer Berlin Heidelberg, 2005.
7. L. Mandelkern. Crystallization of Polymers: Volume 2, Kinetics and Mechanisms; Cambridge University Press, 2004.
8. R. O. Ebewele. Polymer Science and Technology; CRC Press, 2000.
9. L. C. B. Hal F. Brinson. **2007**.
10. R. J. Young; P. A. Lovell. Introduction to Polymers, Third Edition; CRC Press, 2011.
11. K. Herman, Gerngross, O., Abitz, W. Z. *Phys Chem* **1930**, *B10*, 371.
12. D. I. Bower. An Introduction to Polymer Physics; Cambridge University Press, 2002.
13. F. A. Bovey. In Macromolecules; Bovey, F. A.; Winslow, F. H., Eds.; Academic Press, 1979, p 317-337.
14. A. Peterlin. *Journal of Polymer Science Part C: Polymer Symposia* **1965**, *9*, 61-89.
15. Y. Teramoto; Y. Nishio. *Biomacromolecules* **2004**, *5*, 397-406.
16. A. S. Argon. The Physics of Deformation and Fracture of Polymers; Cambridge University Press, 2013.
17. G. Reiter; J. U. Sommer. Polymer Crystallization: Obervations, Concepts and Interpretations; Springer Berlin Heidelberg, 2003.
18. W. Hu. Polymer Physics: A Molecular Approach; Springer Vienna, 2012.
19. K. H. Storks. *Journal of the American Chemical Society* **1938**, *60*, 1753-1761.
20. A. Keller. *Faraday Discussions of the Chemical Society* **1979**, *68*, 145-166.
21. G. Reiter; G. R. Strobl. Progress in Understanding of Polymer Crystallization; Springer Berlin Heidelberg, 2007.
22. G. Strobl. *RevModPhys* **2009**, *81*, 1287-1300.
23. J. M. G. Cowie; V. Arrighi. Polymers: Chemistry and Physics of Modern Materials, Third Edition; CRC Press, 2007.
24. B. S. Mitchell. An Introduction to Materials Engineering and Science for Chemical and Materials Engineers; Wiley, 2004.
25. U. Gedde. In Polymer Physics; Springer Netherlands, 1999, p 169-198.
26. P. C. Painter; M. M. Coleman. Essentials of Polymer Science and Engineering; DEStech Publications, Incorporated, 2008.

27. V. P. M; M. J. M. Morlanes. Polyethylene-Based Blends, Composites and Nanocomposities; Wiley, 2015.
28. J. E. Mark. Physical Properties of Polymers Handbook; Springer New York, 2007.
29. J. I. L. John D. Hoffman. *Journal of Research of NBS, Section A: Physics and Chemistry* **1961**, *65A*, 297-336.
30. J. D. H. John I. Lauritzen. *Journal of Research of the National Bureau of Standards-A Physics and Chemistry* **1960**, *64 A*, 73-102.
31. D. M. Sadler; G. H. Gilmer. *Polymer* **1984**, *25*, 1446-1452.
32. R. A. Pethrick. Polymer Structure Characterization: From Nano to Macro Organization in Small Molecules and Polymers; Royal Society of Chemistry, 2013.
33. J. D. Menczel; L. Judovits; R. B. Prime; H. E. Bair; M. Reading; S. Swier. In Thermal Analysis of Polymers; John Wiley & Sons, Inc., 2008, p 7-239.
34. A. Budkowski; I. W. Hamley; T. Koike. ADVANCES IN POLYMER SCIENCE V148.: Interfaces crystallization viscoelasticity; Springer, 1999.
35. I. W. Hamley. Introduction to Soft Matter: Synthetic and Biological Self-Assembling Materials; Wiley, 2013.
36. A. G. Marangoni; S. S. Narine. Physical Properties of Lipids; CRC Press, 2002.
37. B. Nandan; J. Y. Hsu; H. L. Chen. *Journal of Macromolecular Science, Part C* **2006**, *46*, 143-172.
38. Y. Gogotsi; V. Presser. Carbon Nanomaterials, Second Edition; CRC Press, 2013.
39. A. Müller; V. Balsamo; M. Arnal. In Block Copolymers II; Abetz, V., Ed.; Springer Berlin Heidelberg, 2005, p 1-63.
40. S. Nojima; H. Nakano; T. Ashida. *Polymer* **1993**, *34*, 4168-4170.
41. Y.-L. Loo; R. A. Register; A. J. Ryan. *Macromolecules* **2002**, *35*, 2365-2374.
42. Y.-L. Loo; R. A. Register; A. J. Ryan. *Phys Rev Lett* **2000**, *84*, 4120-4123.
43. S. Li; R. A. Register; B. G. Landes; P. D. Hustad; J. D. Weinhold. *Macromolecules* **2010**, *43*, 4761-4770.
44. T. P. Lodge. *Macromolecular Chemistry and Physics* **2003**, *204*, 265-273.
45. H. F. Mark. Encyclopedia of Polymer Science and Technology, Concise; Wiley, 2013.
46. R. Borsali; R. Pecora. Soft-Matter Characterization; Springer Netherlands, 2008.
47. A. J. Müller; M. L. Arnal; M. Trujillo; A. T. Lorenzo. *European Polymer Journal* **2011**, *47*, 614-629.
48. C. L. T. Xiaofei Xu, Isamu Kusaka, Zhen-Gang Wang. *Annu Rev Phys Chem* **2014**, *65*, 449-475.
49. L. Leibler. *Macromolecules* **1980**, *13*, 1602-1617.
50. M. W. Matsen; M. Schick. *Phys Rev Lett* **1994**, *72*, 2660-2663.
51. M. W. Matsen. *J Phys: Condens Matter* **2002**, *14*, R21.
52. A. Budkowski; I. W. Hamley; T. Koike. Interfaces Crystallization Viscoelasticity; Springer Berlin Heidelberg, 2003.
53. B. Sitharaman. Nanobiomaterials Handbook; CRC Press, 2011.
54. E. Núñez; C. Ferrando; E. Malmström; H. Claesson; U. W. Gedde. *J Macromol Sci Part B Phys* **2004**, *43*, 1143-1160.

55. T. Ogawa; P. P. Federation. Selected Topics in Polymer Science in the Pacific Rim; Wiley, 2003.
56. E. Núñez; G. J. Vancso; U. W. Gedde. *Journal of Macromolecular Science, Part B* **2008**, *47*, 589-607.
57. B. G. Risch; G. L. Wilkes; J. M. Warakomski. *Polymer* **1993**, *34*, 2330-2343.
58. H. Takeshita; T. Shiomi; K. Takenaka; F. Arai. *Polymer* **2013**, *54*, 4776-4789.
59. E. Núñez. **2004**.
60. J. Choi; I.-K. Kim; S.-Y. Kwak. *Polymer* **2005**, *46*, 9725-9735.
61. J.-L. Wang; L. Wang; C.-M. Dong. *Journal of Polymer Science Part A: Polymer Chemistry* **2005**, *43*, 5449-5457.
62. H. Takeshita; M. Poovarodom; T. Kiya; F. Arai; K. Takenaka; M. Miya; T. Shiomi. *Polymer* **2012**, *53*, 5375-5384.
63. Y. Tezuka. Topological Polymer Chemistry: Progress of Cyclic Polymers in Syntheses, Properties, and Functions; World Scientific, 2013.
64. J. Xu; W. Shi. *Polymer* **2006**, *47*, 5161-5173.
65. J. Choi; S.-W. Chun; S.-Y. Kwak. *Macromolecular Chemistry and Physics* **2006**, *207*, 1166-1173.
66. G.-Y. Shi; L.-P. Yang; C.-Y. Pan. *Journal of Polymer Science Part A: Polymer Chemistry* **2008**, *46*, 6496-6508.
67. H. F. M. Ursu, I. Neuner, R. Thomann, M. Rusu. *Reports Romanian in Physics* **2004**, *56*, 445-452.
68. Q. Hao; F. Li; Q. Li; Y. Li; L. Jia; J. Yang; Q. Fang; A. Cao. *Biomacromolecules* **2005**, *6*, 2236-2247.
69. L. Wang; C.-M. Dong. *Journal of Polymer Science Part A: Polymer Chemistry* **2006**, *44*, 2226-2236.
70. E. S. Kim; B. C. Kim; S. H. Kim. *J Polym Sci, Part B: Polym Phys* **2004**, *42*, 939-946.
71. J.-L. Wang; C.-M. Dong. *Polymer* **2006**, *47*, 3218-3228.
72. A. T. Lorenzo; A. J. Müller; D. Priftis; M. Pitsikalis; N. Hadjichristidis. *Journal of Polymer Science Part A: Polymer Chemistry* **2007**, *45*, 5387-5397.
73. A. T. Lorenzo; A. J. Müller; M.-C. Lin; H.-L. Chen; U. S. Jeng; D. Priftis; M. Pitsikalis; N. Hadjichristidis. *Macromolecules* **2009**, *42*, 8353-8364.
74. N. Hadjichristidis; H. Iatrou; M. Pitsikalis; S. Pispas; A. Avgeropoulos. *Prog Polym Sci* **2005**, *30*, 725-782.
75. W. Lee; H.-L. Chen; T.-L. Lin. *J Polym Sci, Part B: Polym Phys* **2002**, *40*, 519-529.
76. E. Koutsopoulou; C. Tsitsilianis. *Macromolecular Chemistry and Physics* **2004**, *205*, 2116-2123.
77. G. Floudas; G. Reiter; O. Lambert; P. Dumas. *Macromolecules* **1998**, *31*, 7279-7290.
78. S. Uchida; A. Ichimura; K. Ishizu. *J Colloid Interf Sci* **1998**, *203*, 153-156.
79. M. Olvera de la Cruz; I. C. Sanchez. *Macromolecules* **1986**, *19*, 2501-2508.
80. J. Ren; Z. Zhang; Y. Feng; J. Li; W. Yuan. *Journal of Applied Polymer Science* **2010**, *118*, 2650-2658.
81. K. Ishizu; S. Uchida. *Prog Polym Sci* **1999**, *24*, 1439-1480.

82. S. Uchida; A. Ichimura; K. Ishizu. *Polymer* **1999**, *40*, 1019-1023.
83. C. Prisacariu. Polyurethane Elastomers: From Morphology to Mechanical Aspects; Springer Vienna, 2011.
84. T. F. A. de Greef; E. W. Meijer. *Nature* **2008**, *453*, 171-173.
85. D. Wei. Electrochemical Nanofabrication: Principles and Applications; Pan Stanford Publishing, 2011.
86. K. S. Lee; S. Kobayashi. Polymer Materials: Block-Copolymers, Nanocomposites, Organic/Inorganic Hybrids, Polymethylenes; Springer Berlin Heidelberg, 2010.
87. P. Bai; M. I. Kim; T. Xu. *Macromolecules* **2013**, *46*, 5531-5537.
88. S. B. W. H. Binder, C. Kluger, L. Petraru, M. J. Kunz. *Adv Mater* **2005**, *17*, 2824-2828.
89. E. Ostas; K. Schröter; M. Beiner; T. Yan; T. Thurn-Albrecht; W. H. Binder. *Journal of Polymer Science Part A: Polymer Chemistry* **2011**, *49*, 3404-3416.
90. E. Ostas; T. Yan; T. Thurn-Albrecht; W. H. Binder. *Macromolecules* **2013**, *46*, 4481-4490.
91. J. A. Clement Appiah, Herwig Peterlik, Wolfgang H. Binder. *European Polymer Journal*, *64*, 138-146.
92. J. R. L. Koji Yamauchi, David M. Hercules, Matthew J. Vergne,; T. E. Long. *J AM CHEM SOC* **2002**, *124*, 8599-8604.
93. L. de Lucca Freitas; M. M. Jacobi; G. Gonçalves; R. Stadler. *Macromolecules* **1998**, *31*, 3379-3382.
94. D. J. M. van Beek; A. J. H. Spiering; G. W. M. Peters; K. te Nijenhuis; R. P. Sijbesma. *Macromolecules* **2007**, *40*, 8464-8475.
95. D. J. M. van Beek; M. A. J. Gillissen; B. A. C. van As; A. R. A. Palmans; R. P. Sijbesma. *Macromolecules* **2007**, *40*, 6340-6348.
96. F. Yuan; W. Wang; M. Yang; X. Zhang; J. Li; H. Li; B. He; B. Minch; G. Lieser; G. Wegner. *Macromolecules* **2006**, *39*, 3982-3985.
97. K. Knop; G. M. Pavlov; T. Rudolph; K. Martin; D. Pretzel; B. O. Jahn; D. H. Scharf; A. A. Brakhage; V. Makarov; U. Mollmann; F. H. Schacher; U. S. Schubert. *Soft Matter* **2013**, *9*, 715-726.
98. C. von der Ehe; K. Kempe; M. Bauer; A. Baumgaertel; M. D. Hager; D. Fischer; U. S. Schubert. *Macromolecular Chemistry and Physics* **2012**, *213*, 2146-2156.
99. M. A. R. Meier; J.-F. Gohy; C.-A. Fustin; U. S. Schubert. *Journal of the American Chemical Society* **2004**, *126*, 11517-11521.
100. X. Chang; L. Liu; Y. Guan; C.-M. Dong. *Journal of Polymer Science Part A: Polymer Chemistry* **2014**, *52*, 2000-2010.
101. J. Cheng; J.-X. Ding; Y.-C. Wang; J. Wang. *Polymer* **2008**, *49*, 4784-4790.
102. Y. Zhang; Q. Zhao; H. Shao; S. Zhang; X. Han. *Advances in Materials Science and Engineering* **2014**, *2014*, 6.
103. K. Nagahama; Y. Ohya; T. Ouchi. *Polym J* **2006**, *38*, 852-860.
104. D. Kul; L. M. Van Renterghem; M. A. R. Meier; S. Strandman; H. Tenhu; S. S. Yilmaz; U. S. Schubert; F. E. Du Prez. *Journal of Polymer Science Part A: Polymer Chemistry* **2008**, *46*, 650-660.

105. J. Lin; Q.-H. Zhou; L.-D. Li; Z.-N. Li. *Colloid Polym Sci* **2014**, *292*, 3177-3185.
106. M. Filali; M. A. R. Meier; U. S. Schubert; J.-F. Gohy. *Langmuir* **2005**, *21*, 7995-8000.
107. S. Petrova; R. Riva; C. Jérôme; P. Lecomte; R. Mateva. *European Polymer Journal* **2009**, *45*, 3442-3450.
108. K. Kunal; M. Paluch; C. M. Roland; J. E. Puskas; Y. Chen; A. P. Sokolov. *J Polym Sci, Part B: Polym Phys* **2008**, *46*, 1390-1399.
109. R. F. Storey; L. B. Brister; J. W. Sherman. *Journal of Macromolecular Science, Part A* **2001**, *38*, 107-122.
110. M. Chanda. Introduction to Polymer Science and Chemistry: A Problem-Solving Approach, Second Edition; Taylor & Francis, 2013.
111. S. Bräse; K. Banert. Organic Azides: Syntheses and Applications; Wiley, 2011.
112. N. Jung; S. Bräse. In Kirk-Othmer Encyclopedia of Chemical Technology; John Wiley & Sons, Inc., 2000.
113. S. Seiffert. Supramolecular Polymer Networks and Gels; Springer International Publishing, 2015.
114. J.-L. Wietor; D. J. M. van Beek; G. W. Peters; E. Mendes; R. P. Sijbesma. *Macromolecules* **2011**, *44*, 1211-1219.
115. R. F. M. Lange; M. Van Gurp; E. W. Meijer. *Journal of Polymer Science Part A: Polymer Chemistry* **1999**, *37*, 3657-3670.
116. T. Nakamura; T. Fuke; M. Shibata. *Colloid Polym Sci* **2014**, *292*, 1261-1268.
117. Q. Yan; D. Han; Y. Zhao. *Polymer Chemistry* **2013**, *4*, 5026-5037.
118. C. G. Bochet. *Journal of the Chemical Society, Perkin Transactions 1* **2002**, 125-142.
119. K. K. Rohatgi-Mukherjee. Fundamentals of Photochemistry; Wiley, 1978.
120. S. Chatani; C. J. Kloxin; C. N. Bowman. *Polymer Chemistry* **2014**, *5*, 2187-2201.
121. H. M. D. Bandara; S. C. Burdette. *Chem Soc Rev* **2012**, *41*, 1809-1825.
122. T. Ikeda; O. Zushi; T. Sasaki; K. Ichimura; H. Takezoe; A. Fukuda; K. A. W. Skarp. *Molecular Crystals and Liquid Crystals Science and Technology Section A Molecular Crystals and Liquid Crystals* **1993**, *225*, 67-79.
123. H. Tokuhisa; M. Yokoyama; K. Kimura. *J Mater Chem* **1998**, *8*, 889-891.
124. B. Tylkowski; S. Peris; M. Giamberini; R. Garcia-Valls; J. A. Reina; J. C. Ronda. *Langmuir* **2010**, *26*, 14821-14829.
125. C. E. Hoyle; T. Y. Lee; T. Roper. *Journal of Polymer Science Part A: Polymer Chemistry* **2004**, *42*, 5301-5338.
126. A. Dondoni. *Angew Chem Int Ed* **2008**, *47*, 8995-8997.
127. W. J. Yang; K.-G. Neoh; E.-T. Kang; S. Lay-Ming Teo; D. Rittschof. *Polymer Chemistry* **2013**, *4*, 3105-3115.
128. B. Yao; J. Sun; A. Qin; B. Tang. *Chin Sci Bull* **2013**, *58*, 2711-2718.
129. B. D. Fairbanks; E. A. Sims; K. S. Anseth; C. N. Bowman. *Macromolecules* **2010**, *43*, 4113-4119.
130. B. D. Fairbanks; T. F. Scott; C. J. Kloxin; K. S. Anseth; C. N. Bowman. *Macromolecules* **2009**, *42*, 211-217.
131. M. A. Tasdelen; G. Yilmaz; B. Iskin; Y. Yagci. *Macromolecules* **2012**, *45*, 56-61.

132. S. Rochat; C. Minardi; J.-Y. de Saint Laumer; A. Herrmann. *Helv Chim Acta* **2000**, *83*, 1645-1671.
133. S. Hu; D. C. Neckers. *The Journal of Organic Chemistry* **1996**, *61*, 6407-6415.
134. P. B. Jones; M. P. Pollastri; N. A. Porter. *The Journal of Organic Chemistry* **1996**, *61*, 9455-9461.
135. J. A. Barltrop; P. Schofield. *Tetrahedron Lett* **1962**, *3*, 697-699.
136. J. A. Barltrop; P. Schofield. *Journal of the Chemical Society (Resumed)* **1965**, 4758-4765.
137. J. W. Chamberlin. *The Journal of Organic Chemistry* **1966**, *31*, 1658-1660.
138. J. F. Cameron; J. M. J. Frechet. *Journal of the American Chemical Society* **1991**, *113*, 4303-4313.
139. E. Cabane; V. Malinova; W. Meier. *Macromolecular Chemistry and Physics* **2010**, *211*, 1847-1856.
140. A. Patchornik; B. Amit; R. B. Woodward. *Journal of the American Chemical Society* **1970**, *92*, 6333-6335.
141. M. Jin; H. Xu; H. Hong; C. Bao; H. Pu; D. Wan; L. Zhu. *Journal of Applied Polymer Science* **2013**, *130*, 4099-4106.
142. D. Han; X. Tong; Y. Zhao. *Langmuir* **2012**, *28*, 2327-2331.
143. R. M. Kevwitch; D. V. McGrath. *New J Chem* **2007**, *31*, 1332-1336.
144. J. Jiang; X. Tong; D. Morris; Y. Zhao. *Macromolecules* **2006**, *39*, 4633-4640.
145. J. T. Goldbach; K. A. Lavery; J. Penelle; T. P. Russell. *Macromolecules* **2004**, *37*, 9639-9645.
146. J. A. Johnson; M. G. Finn; J. T. Koberstein; N. J. Turro. *Macromolecules* **2007**, *40*, 3589-3598.
147. M. Kang; B. Moon. *Macromolecules* **2009**, *42*, 455-458.
148. D. Han; X. Tong; Y. Zhao. *Macromolecules* **2011**, *44*, 437-439.
149. H. Zhao; W. Gu; E. Sterner; T. P. Russell; E. B. Coughlin; P. Theato. *Macromolecules* **2011**, *44*, 6433-6440.
150. S. Nakagawa; K.-i. Kadena; T. Ishizone; S. Nojima; T. Shimizu; K. Yamaguchi; S. Nakahama. *Macromolecules* **2012**, *45*, 1892-1900.
151. H. Zhou; Y. Lu; H. Qiu; G. Guerin; I. Manners; M. A. Winnik. *Macromolecules* **2015**, *48*, 2254-2262.
152. M. Falorni; G. Giacomelli; L. Mameli; A. Porcheddu. *Tetrahedron Lett* **1998**, *39*, 7607-7610.
153. G. Blotny. *Tetrahedron* **2006**, *62*, 9507-9522.
154. C. Afonso; N. Lourenco; A. Rosatella. *Molecules* **2006**, *11*, 81.
155. C. Kim; Y. Chang; J. S. Kim. *Macromolecules* **1996**, *29*, 6353-6355.
156. S. Y. Cho; Y. Chang; J. S. Kim; S. C. Lee; C. Kim. *Macromolecular Chemistry and Physics* **2001**, *202*, 263-269.
157. A. W. Hofmann. *Ber* **1886**, *19*, 2061.
158. F. J. Allan; G. G. Allan. *Recueil des Travaux Chimiques des Pays-Bas* **1959**, *78*, 375-381.

159. K. G. Akamanchi; N. R. Varalakshmy. *Tetrahedron Lett* **1995**, *36*, 3571-3572.
160. X. Yang; T. Fox; H. Berke. *Tetrahedron* **2011**, *67*, 7121-7127.
161. J. Y. Chang; H. J. Ji; M. J. Han; S. B. Rhee; S. Cheong; M. Yoon. *Macromolecules* **1994**, *27*, 1376-1380.
162. Y. Cui; X. Ma; X. Tang; Y. Luo. *European Polymer Journal* **2004**, *40*, 299-305.
163. A. Arbaoui; C. Redshaw. *Polymer Chemistry* **2010**, *1*, 801-826.
164. F. Sanda; H. Sanada; Y. Shibasaki; T. Endo. *Macromolecules* **2002**, *35*, 680-683.
165. M. Lang; C.-C. Chu. *Journal of Applied Polymer Science* **2002**, *86*, 2296-2306.
166. A. R. Meier Michael; S. Schubert Ulrich. In e-Polymers, 2005, p 902.
167. Z. Zhang; J. Ren; Y. Feng; J. Li; W. Yuan. *Journal of Polymer Science Part A: Polymer Chemistry* **2010**, *48*, 5063-5071.
168. W. Yuan; J. Yuan; M. Zhou; C. Pan. *Journal of Polymer Science Part A: Polymer Chemistry* **2008**, *46*, 2788-2798.
169. M. Morell; D. Foix; A. Lederer; X. Ramis; B. Voit; À. Serra. *Journal of Polymer Science Part A: Polymer Chemistry* **2011**, *49*, 4639-4649.
170. P.-F. Cao; R.-X. Zhao; L. Li; W.-W. Yang; F. Cheng; Y. Chen; C.-H. Lu; S.-C. Jiang. *Journal of Polymer Science Part A: Polymer Chemistry* **2012**, *50*, 227-236.
171. R. Wu; T. F. Al-Azemi; K. S. Bisht. *Chemical Communications* **2009**, 1822-1824.
172. S. Hecht; H. Ihre; J. M. J. Fréchet. *Journal of the American Chemical Society* **1999**, *121*, 9239-9240.
173. C. Ni; G. Wu; C. Zhu; B. Yao. *The Journal of Physical Chemistry C* **2010**, *114*, 13471-13476.
174. M. Trollsås; J. L. Hedrick. *Macromolecules* **1998**, *31*, 4390-4395.
175. W. Kai; L. Hua; L. Zhao; Y. Inoue. *Macromolecular Rapid Communications* **2006**, *27*, 1702-1706.
176. S. Fanali; P. R. Haddad; C. Poole; P. Schoenmakers; D. K. Lloyd. Liquid Chromatography: Applications; Elsevier Science, 2013.
177. H. Barqawi; E. Ostas; B. Liu; J.-F. Carpentier; W. H. Binder. *Macromolecules* **2012**, *45*, 9779-9790.
178. M. A. B. B. B. Youan, B. Rollmann, G. Riveau, J. Gillard. *J Microencapsul* **1999**, *16*, 601-612.

**Appendix:**

## Synthesis of azide functionalized PIB

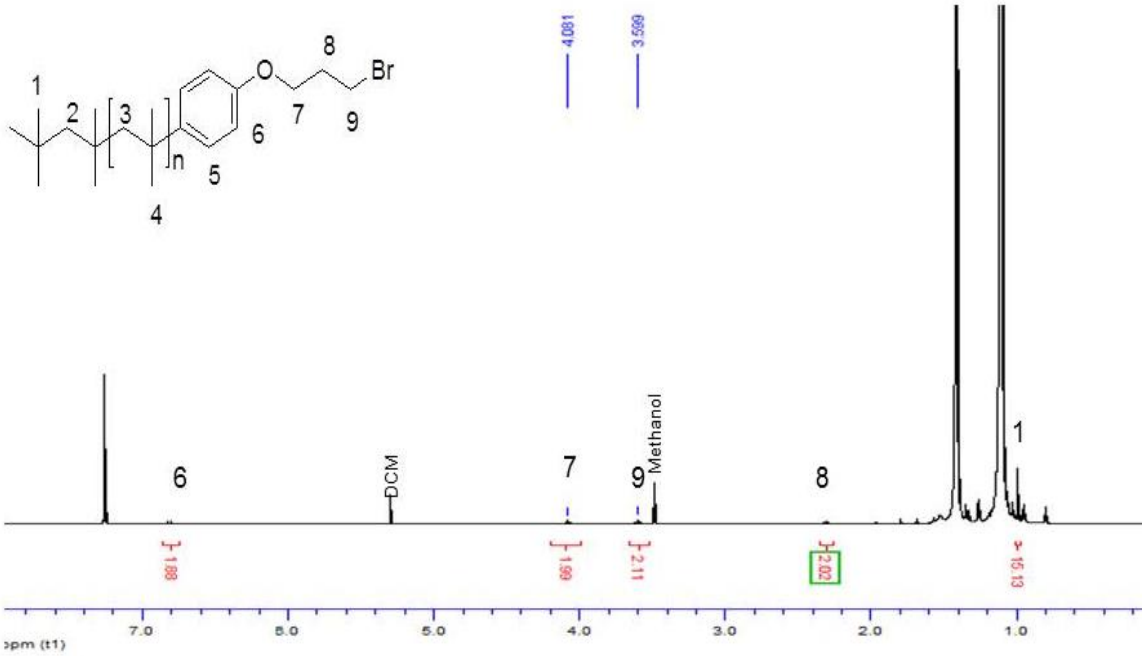


**Figure 1: $^{1}$H NMR of bromo-functionalized PIB**

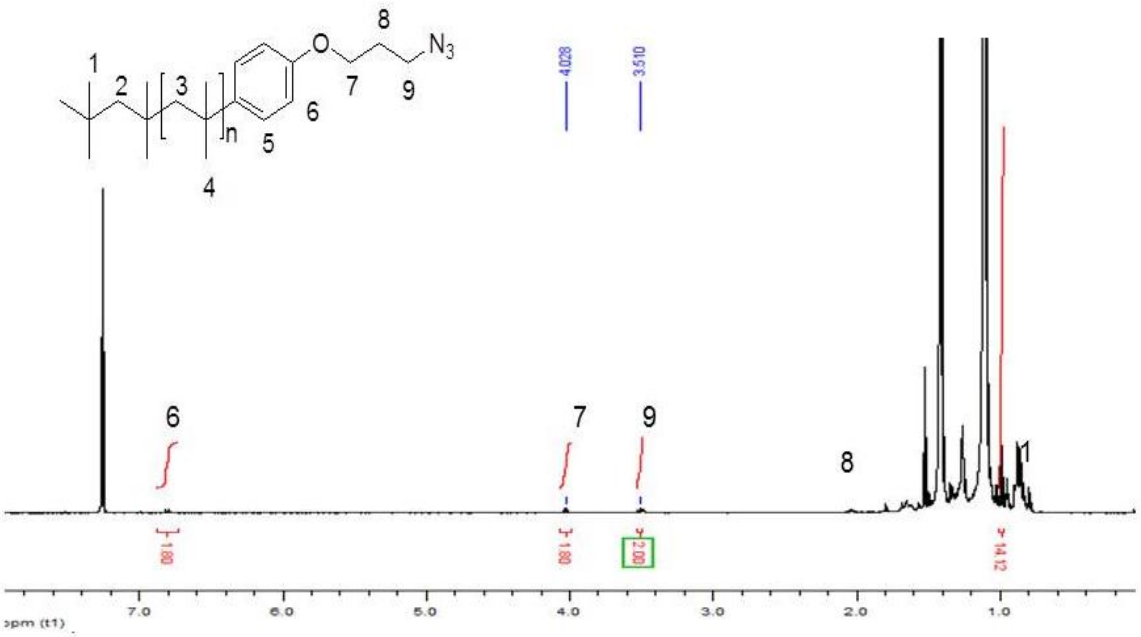


**Figure 2: $^{1}$H NMR of azide-functionalized PIB**

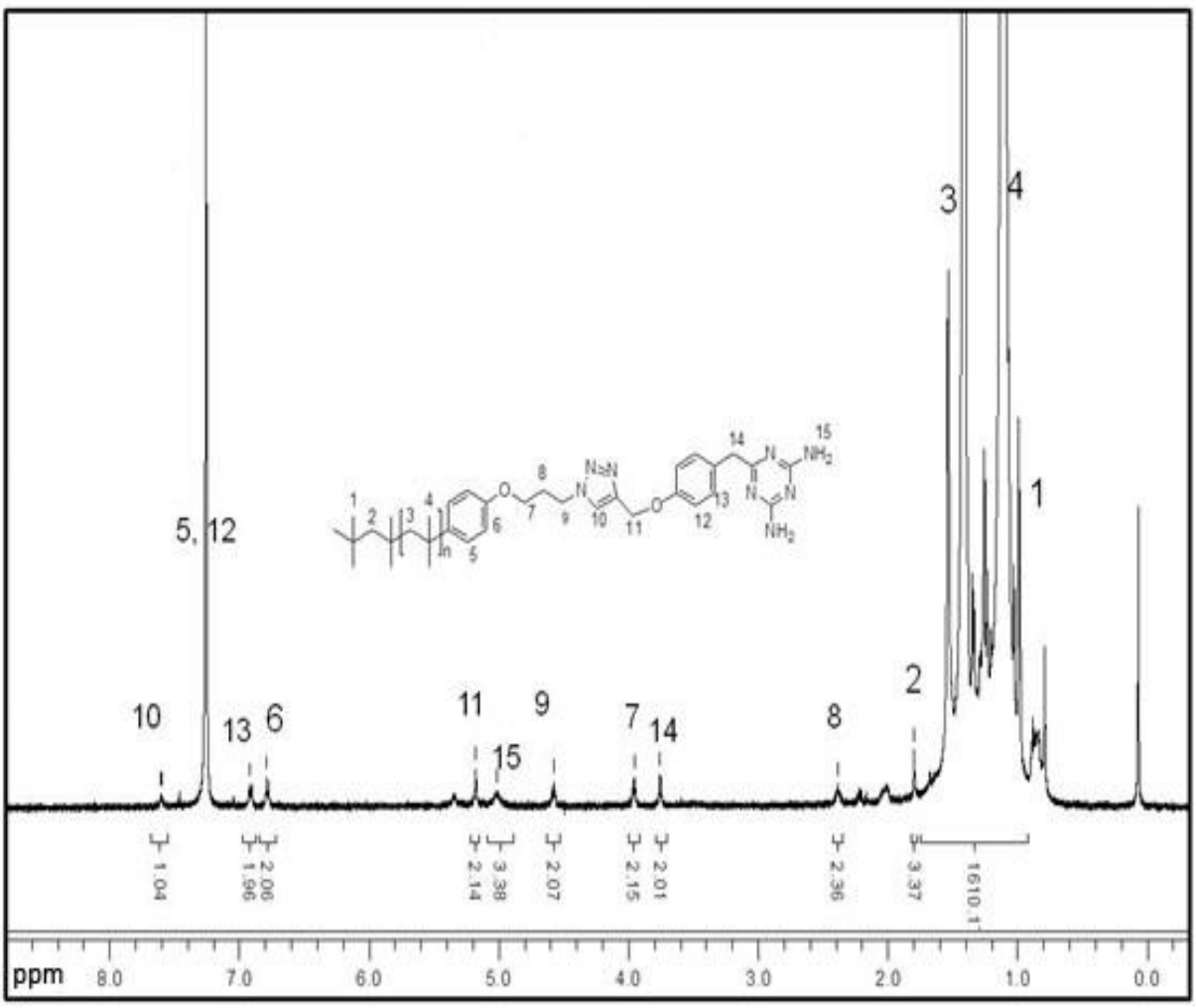


**FIGURE 3: $^{1}$H NMR of alkyne triazine functionalized poly(isobutylene) in $CDCl_3$.**

**Avrami exponents of star PCL-homopolymer and star shaped PCL-PIB block copolymer**

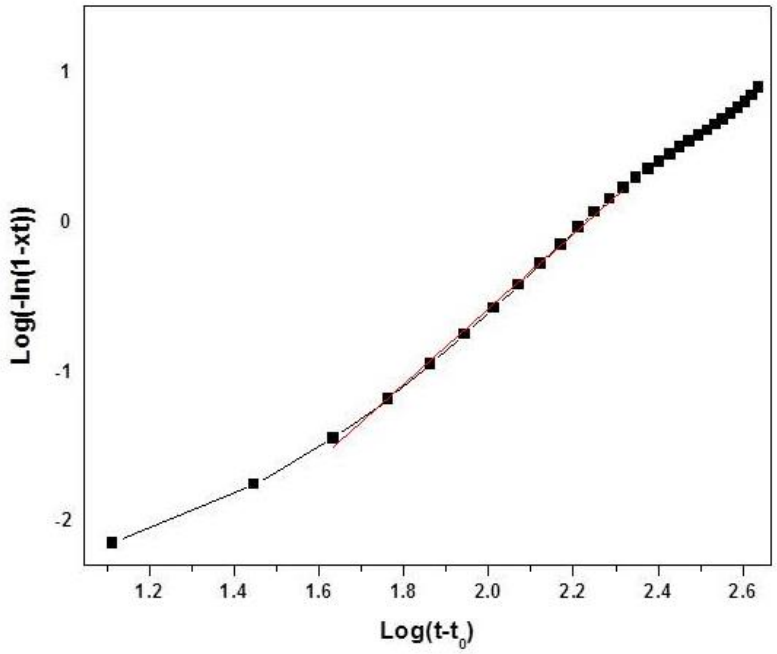


**Star shaped PCL homopolymer (n=2.55)**

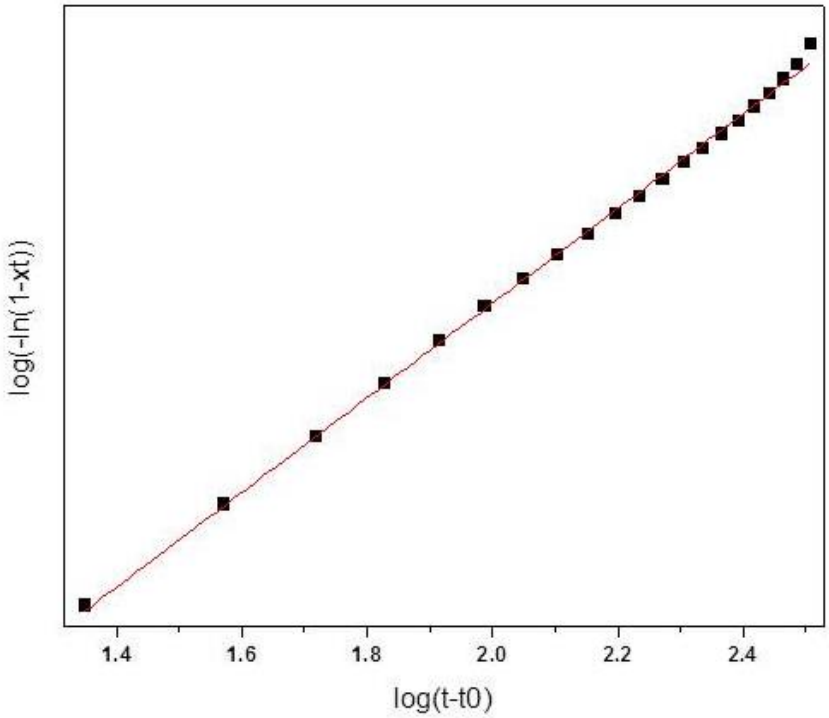


**Star shaped supramolecular block copolymer SPCL13K-PIB3K**

**(n=2.2)**

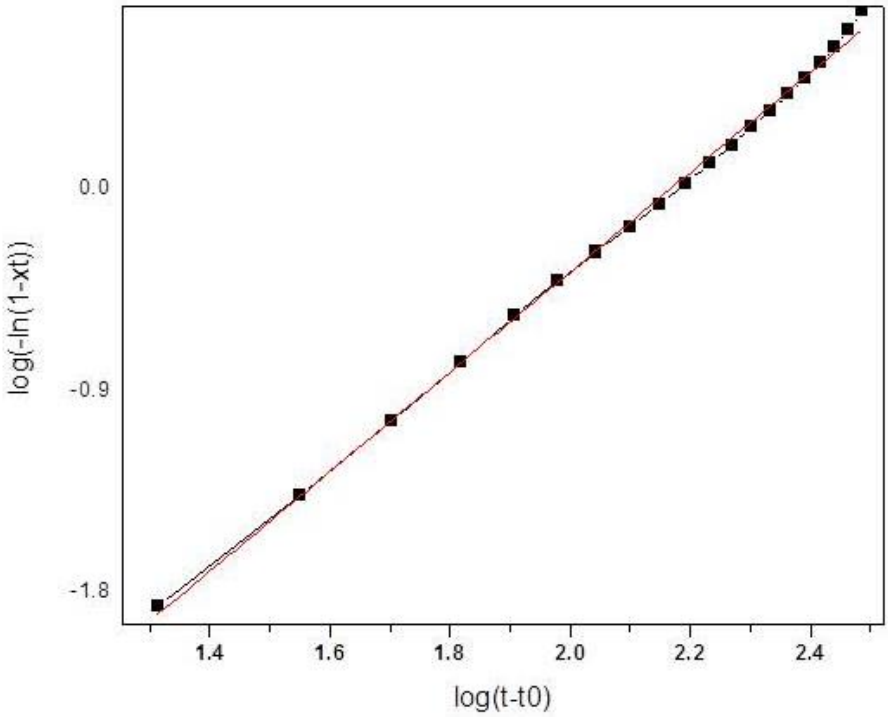


**Star shaped supramolecular block copolymer SPCL13K-PIB8K**

**(n=2.2)**

**SAXS images**

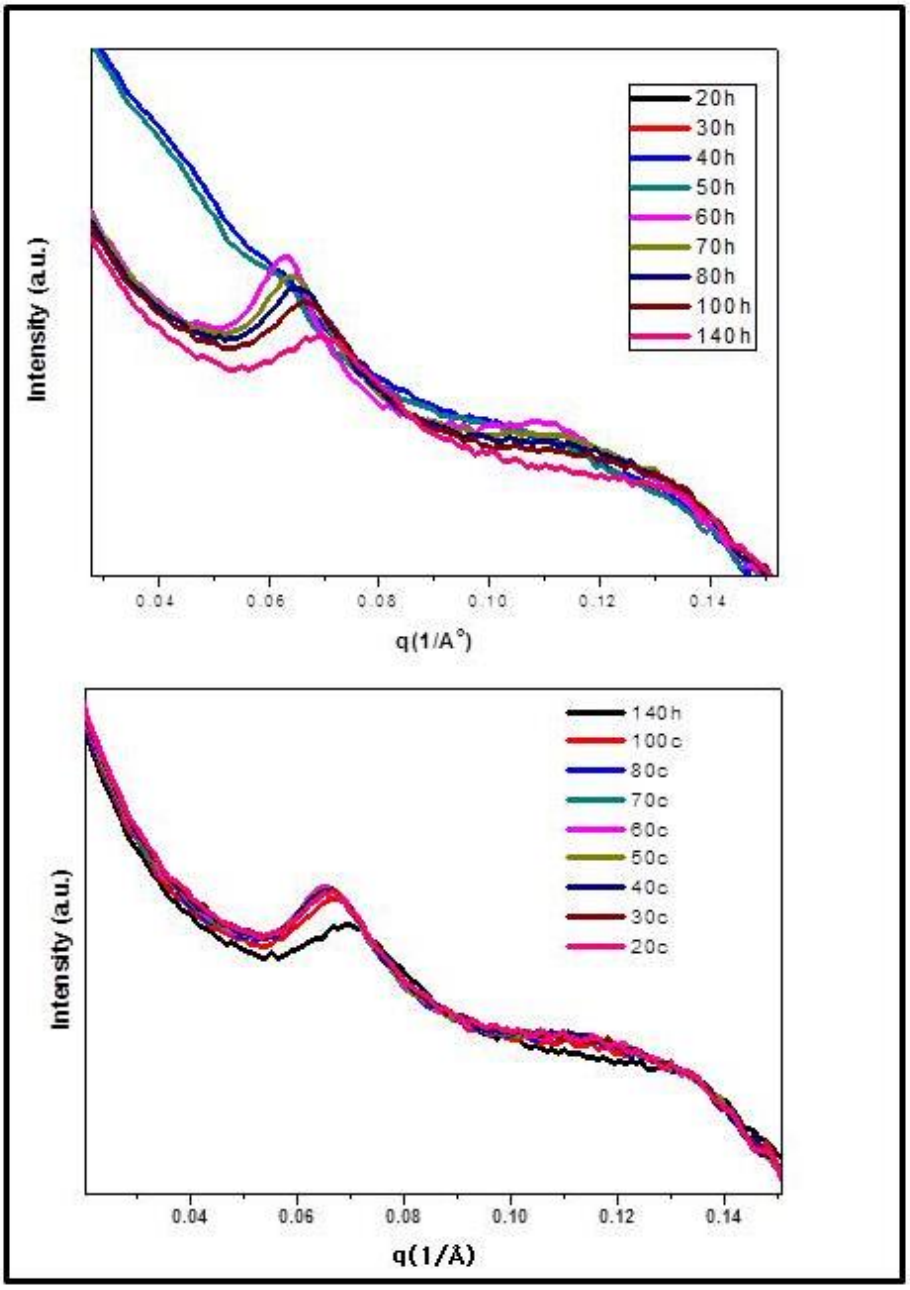


**Figure 4: SAXS analysis of S(PCL-6K-PIB 8K)$_4$ (Upper-heating, lower-cooling)**

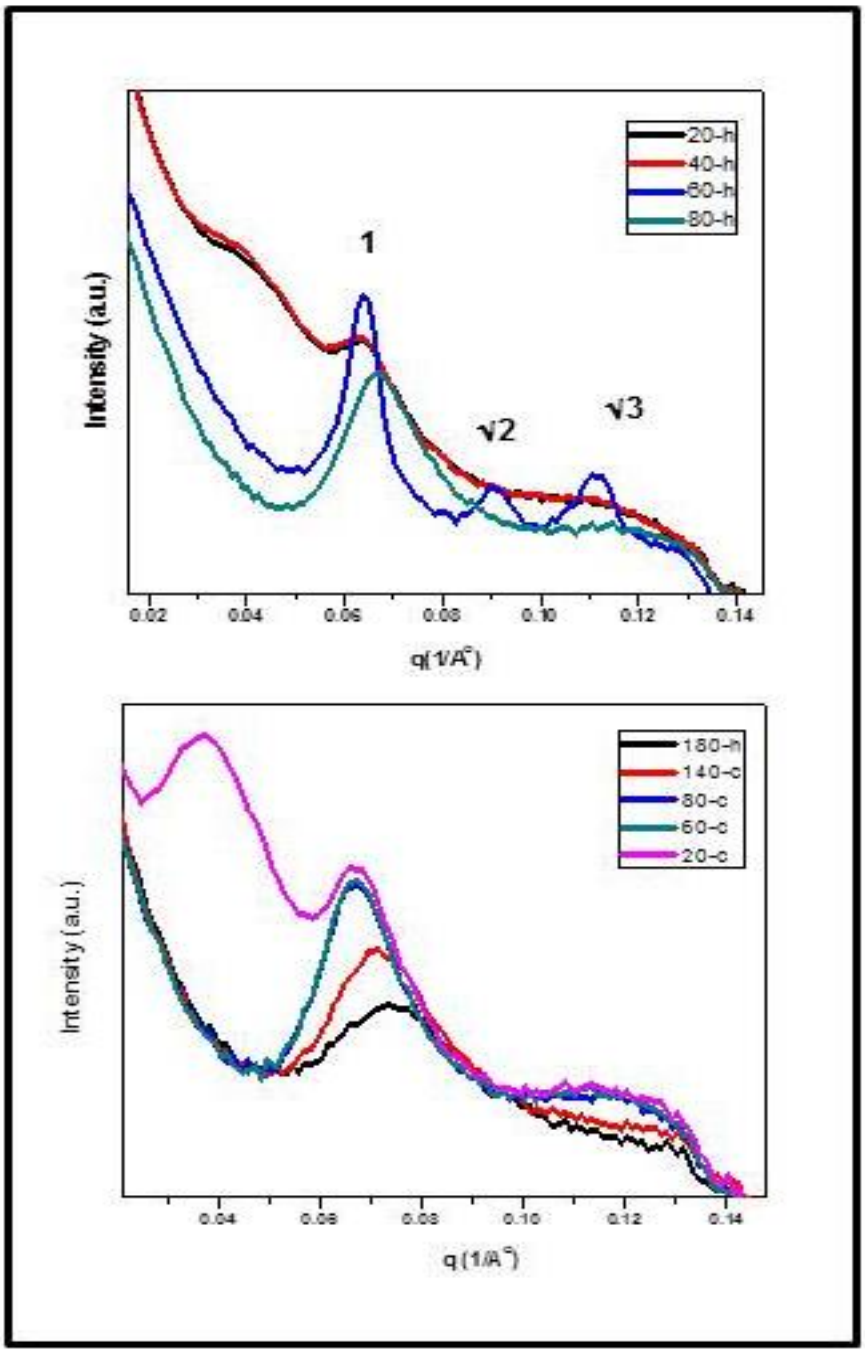


**Figure 5: SAXS analysis of S(PCL-13K-PIB 8K)$_4$ (Upper-heating, lower-cooling)**

**IR analysis of SPCL-PIB supramolecular block copolymer**

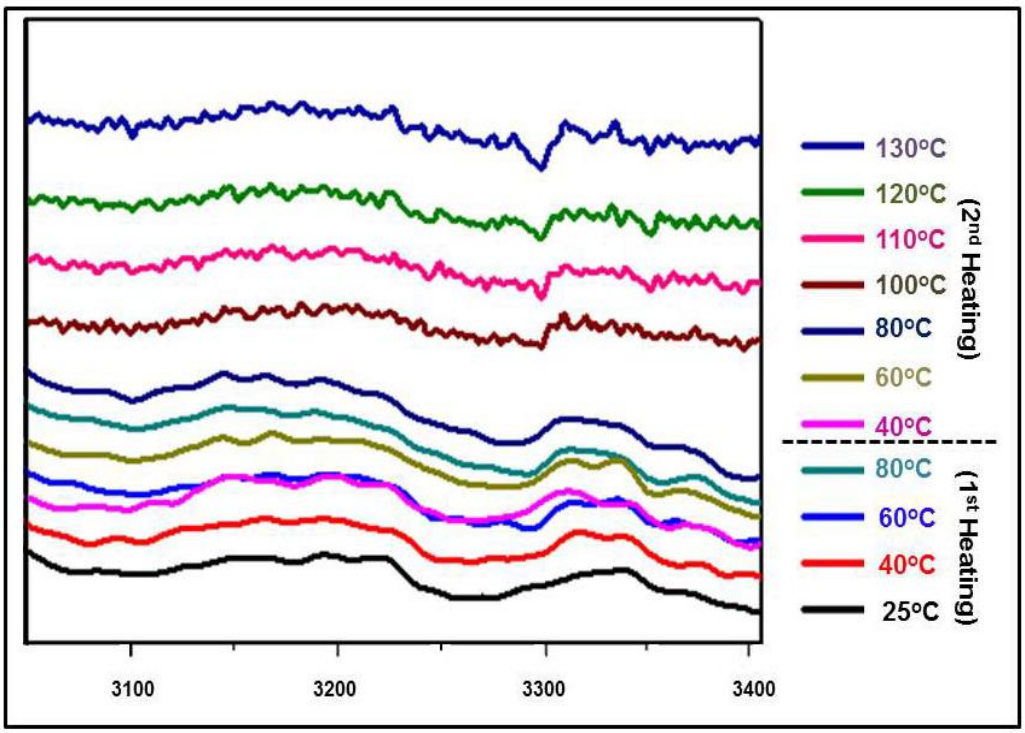


**Figure 6: Temperature dependent IR spectrum of SPCL-PIB supramolecular block copolymer**

The state of supramolecular bond of s(PCL-b-PIB)$_4$ block copolymer was studied via FTIR spectroscopy in crystalline and molten state at various temperatures between 25$^o$C and 130$^o$ C.

The block copolymer SPCL-PIB shows, the broad absorption bands in the range between 3100 and 3400 cm$^{-1}$ indicate associated -NH stretching vibrations (hydrogen bonds between thymine and 2,6-diaminotriazine).

On heating from 25$^o$C to 130$^o$C, the peak shape flattened out and the main broad signal shifted toward higher wavenumbers, indicating the opening of the hydrogen bonds.

## Synthesis of trivalent initiator

In the thesis the successful synthesis of trivalent photocleavable initiator from cynuric chloride and 2-nitro,5-hydroxy benzaldehyde is discussed. Prior to this we had attempted the trivalent initiator synthesis from trimesoyl chloride and 2-nitro,5-hydroxy benzaldehyde in presence of triethyl amine. As a first step trialdehyde was successfully synthesized as shown in the reaction below. But due to insolubility of the trialdehyde in number of solvents (partially soluble only in DMSO-$d_6$), the aldehyde groups couldn't reduce in to alcohol groups.

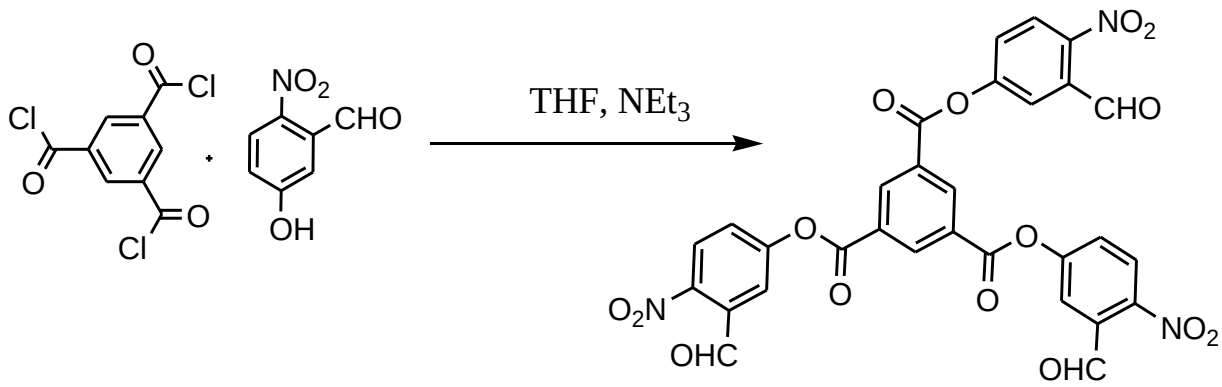


**Scheme: Synthesis of trimesoyl chloride based trialdehyde**

| Sr. No. | Trimesoyl chloride | 5-hydroxy, 2-nitro benzaldehyde | Temp. | Yield | remark |
|---|---|---|---|---|---|
| 1 | 1mmol | 6mmol | rt | -- | No reaction |
| 2 | 1mmol | 3.2mmol | 65°C | 200mg | 85% pure |

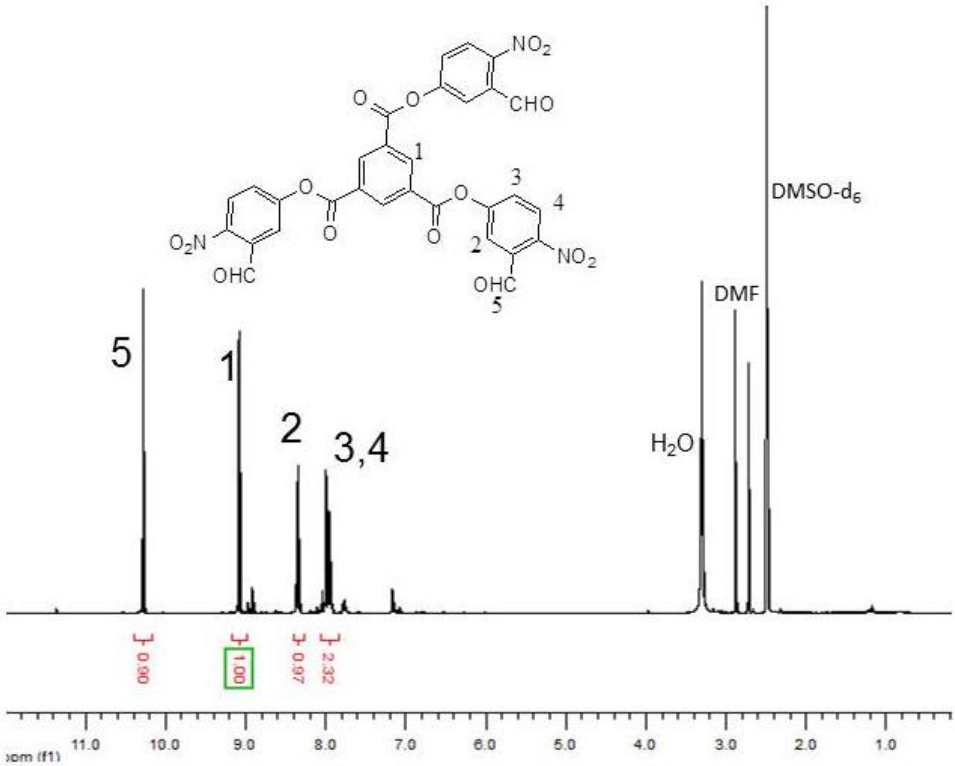


**Figure 7: $^{1}$H NMR of trialdehyde**

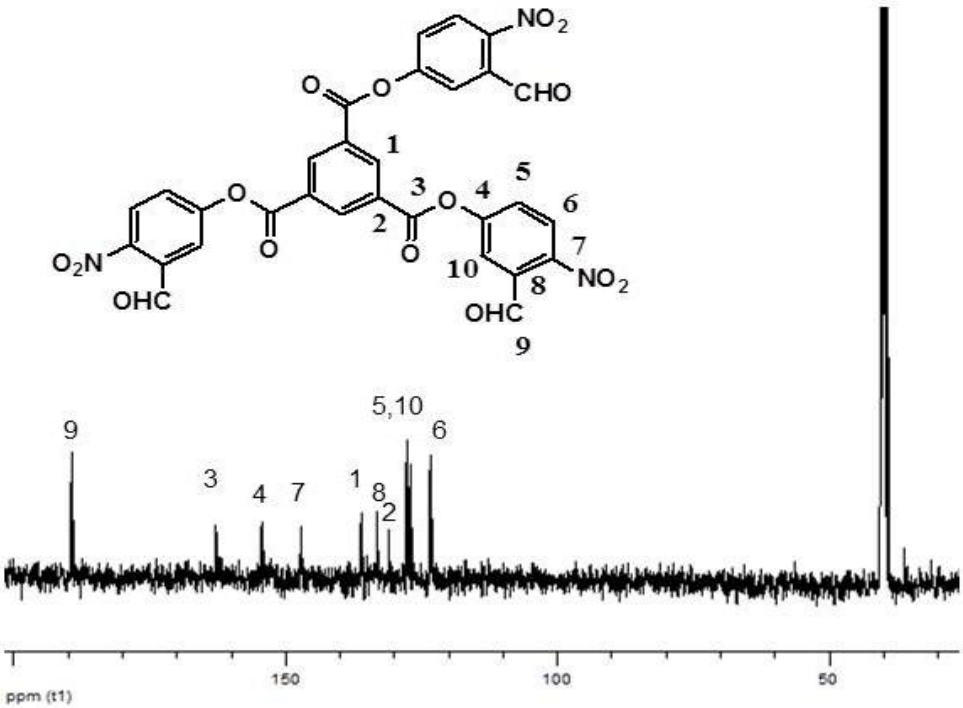


**Figure 8: $^{13}$C NMR of trialdehyde**

**TABLE-1** ESI-TOF data of the photocleavable polymer PC-sPCL-1

| Entry | species | Formula | charge state | imulated (g/mol) | measured (g/mol) | Error (ppm) |
|---|---|---|---|---|---|---|
| 1 | $[M+H+H]^{+2}$ | $C_{97}H_{146}N_6O_{38}$ | +2 | 1001.48 | 1001.55 | 69 |
| 2 | $[M+Na_2]^{2+}$ | $C_{92}H_{137}Li_2N_6Na_3O_{38}$ | +2 | 1008.49 | 1008.55 | 59 |
| 3 | $[M+H+Na]^{+2}$ | $C_{97}H_{145}N_6Na_1O_{38}$ | +2 | 1012.47 | 1012.54 | 69 |
| 4 | $[M+H+K]^{+3}$ | $C_{97}H_{145}K_1N_6O_{38}$ | +2 | 1020.46 | 1020.03 | 421 |
| 5 | $[M+Na+Na+H]^{+3}$ | $C_{145}H_{225}N_6Na_2O_{54}$ | +3 | 986.83 | 986.86 | 30 |
| 6 | $[M+Na_3]^{+3}$ | $C_{144}H_{217}Li_1N_6Na_3O_{52}$ | +3 | 979.50 | 979.53 | 30 |
| 7 | $[M+H+K+Na]^{+3}$ | $C_{139}H_{212}K_4N_6Na_1O_{52}$ | +3 | 992.08 | 991.85 | 231 |
| 8 | $[M+Na_5]^{+5}$ | $C_{252}H_{398}N_6Na_5O_{88}$ | +5 | 1006.32 | 1006.30 | 19 |

**TABLE-2** Species observed in ESI analysis of the photocleaved polymer

| entry | species | Formula | charge state | simulated (g/mol) | measured (g/mol) | error (ppm) |
|---|---|---|---|---|---|---|
| 1 | $[C_6H_{10}O_2]_{11}OHNa^{+1}$ | $C_{66}H_{112}Na_1O_{23}$ | +1 | 1295.74 | 1295.73 | 7.7 |
| 2 | $[C_6H_{10}O_2]_{23}OHNa_2^{+2}$ | $C_{138}H_{232}Na_2O_{47}$ | +2 | 1344.27 | 1344.30 | 22.3 |
| 3 | $[C_6H_{10}O_2]_{35}OHNa_3^{+3}$ | $C_{210}H_{352}Na_3O_{71}$ | +3 | 1360.45 | 1360.45 | 5 |
| 4 | $C_6H_{10}O_2]_{45}OH\ Na_4^{+4}$ | $C_{270}H_{452}Na_4O_{91}$ | +4 | 1311.51 | 1311.48 | 22.8 |
| 5 | $C_6H_{10}O_2]_{59}OH\ Na_5^{+5}$ | $C_{354}H_{592}Na_5O_{119}$ | +5 | 1373.39 | 1373.37 | 14.5 |
| 6 | $C_6H_{10}O_2]_{71}OH\ Na_6^{+6}$ | $C_{426}H_{712}Na_6O_{143}$ | +6 | 1376.63 | 1376.60 | 21.7 |
| 7 | $C_6H_{10}O_2]_{84}OH\ Na_7^{+7}$ | $C_{504}H_{842}Na_7O_{169}$ | +7 | 1395.23 | 1395.25 | 14.3 |
| 8 | $C_6H_{10}O_2]_{90}OH\ Na_8^{+8}$ | $C_{540}H_{902}Na_8O_{181}$ | +8 | 1309.25 | 1309.26 | 7.6 |

## Acknowledgements

First of all, I would like to express my sincere appreciation to my Ph.D. supervisor Prof. Dr. Wolfgang H. Binder for his support, encouragement and personal guidance throughout my thesis, without which this work would not have been possible. There is no doubt that I have learned a lot from him and for that, I will always be grateful.

I am grateful to project partners of my Ph.D. topic, Prof. Dr. Kay Saalwaechter and Prof. Thomas Thurn Albrecht from Physics Department for their support towards successful completion of my PhD work. I would also like to express my gratitude to Dr. Haitham Barqawi for his help in HPLC and ESI-TOF-MS measurements/ analysis and Dr. Tingzi Yan for his help in SAXS measurements and analysis.

I would also like to express my gratitude to Dr. Steffen Kurzhals, Dr. Elena Ostas, Dr. Sravendra Rana and Clement Appiah and all my colleagues for the convenient atmosphere they have provided for me and for their valuable advices and friendly help in a variety of ways in the course of this thesis. I also owe my gratitude to Ms. Anke Hassi, for the support and help about organizational issues.

I also owe my gratitude to my friends in Germany, India and elsewhere for their support and encouragement throughout.

# List of Publications

**Synthesis and crystallization of star-shaped photocleavable poly(ε-caprolactone)s.**

Ajay S. Kasegaonkar, Haitham Barqawi and Wolfgang H. Binder

*Journal of Polymer Science Part A: Polymer Chemistry* 52 (2015) 642-649.

**Poster Presentations:**

**Synthesis of metal complexes as catalysts for synthesis of star shaped poly(ε-caprolactone)s.**

Ajay S. Kasegaonkar, Haitham Barqawi and Wolfgang H. Binder

P2012, Halle (Saale), Germany.

**Lecture Presentation:**

**'Synthesis and crystallization of star shaped sPCL-PIB pseudo block copolymers'**

Ajay S. Kasegaonkar, Tingzi Yan, Haitham Barqawi, Thomas Thurn-Albrecht and Wolfgang H. Binder

European Polymer Congress 2015, Dresden, Germany.

**Curriculum Vitae**

**Personal:**

Name: **Ajay Kasegaonkar**

Date of Birth: 20/10/1983

Marital Status: Married

Nationality: Indian

Address:

Osmanabad, Maharashtra, India.

e-mail: as.kasegaonkar@gmail.com

**Education:**

2011- Present: **Martin Luther University, Halle-Wittenberg**

Macromolecular Chemistry (PhD Candidate)

2005- 2007: **S.R.T.M. University***,* Nanded, INDIA

Organic Chemistry (Master Degree)

2001–2004: **Dr. B.A.M.University,** Aurangabad, INDIA.

Bachelor Degree

**Research Experience:**

2011-Present: **Martin Luther University, Halle-Wittenberg, Germany**

*PhD Thesis* "Synthesis of complex polyster(PCL)-Architectures and their Crystallization." under supervision of Prof. Dr. Wolfgang Binder

2008-2011: **National Chemical Laboratory, Pune, India**

*Research work "synthesis* and characterization of different aliphatic copolyesters (PLLA)" under supervision of Dr. Bhaskar Idage.

2007 March: **S.R.T.M. University***,* Nanded, INDIA

*Project Work* "Simple and efficient synthesis of esters from nitriles" under supervision of Prof. Dr. B. P. Bandgar.

**Publications:**

Synthesis and crystallization of star-shaped photocleavable poly(ε-caprolactone)s.

Ajay S. Kasegaonkar, Haitham Barqawi and Wolfgang H. Binder

*Journal of Polymer Science Part A: Polymer Chemistry* 52 (2015) 642-649.

Ring opening polymerization of dilactide using salen complex as catalyst.

B.B.Idage, S.B.Idage, A.S.Kasegaonkar**,** R.V.Jadhav

*Material Science and Engineering: Part B* 168 (2010) 193-198.

**Presentations:**

Presented a poster with the title **'Synthesis of metal complexes as catalysts for synthesis of star shaped Poly(Ɛ-caprolactone)s'** in polymeric materials P2012, Halle (Saale), Germany.

Presented a **lecture** with the title **'Synthesis and crystallization of star shaped sPCL-PIB pseudo block copolymers'** in the European Polymer Congress 2015, Dresden, Germany.

**Instrumental Skills:**

• Thermo Gravimetric Analysis (TGA)

• Differential Scanning Calorimetry (DSC)

• High Pressure Liquid Chromatography (HPLC)

• Nuclear Magnetic Resonance Spectroscopy (NMR)

• Gel Permeation Chromatography (GPC)

• Dynamic Light Scattering (DLS)

• Infrared (IR) Spectroscopy

**Language Skills:**

• Marathi & Hindi (Native)

• English (Fluent)

• German (Basic)

**Computer Knowledge:**

• MS Office

• Origin

• Mestre-C

01.12.2016 Ajay Kasegaonkar

India

**Eidesstattliche Erklärung**

Hiermit erkläre ich, dass ich die vorliegende Dissertation selbständig und ohne fremde Hilfe verfasst, keine andere als die angegebenen Quellen und Hilfsmittel benutzt sowie wörtliche und sinngemäße Zitate als solche gekennzeichnet habe. Die vorliegende Dissertation bzw. Teile daraus habe ich keiner anderen wissenschaftlichen Einrichtung vorgelegt. Weiterhin bestätige ich, keine anderweitigen Promotionsversuche unternommen zu haben.

01.12.2016 Ajay Kasegaonkar

Osmanabad, India.